NAVAL POSTGRADUATE SCHOOL

MONTEREY, CALIFORNIA

THESIS

THE EFFECT OF FRICTION STIR PROCESSING ON THE MICROSTRUCTURE AND MECHANICAL PROPERTIES OF AF/C458 ALUMINUM LITHIUM ALLOY

by

Tanya L. Giles

September 2005

Thesis Advisor: Terry McNelley

Approved for public release: distribution is unlimited

THIS PAGE INTENTIONALLY LEFT BLANK

REPORT DOCUMENTATION PAGE			Form Approved OMB No. 0704-0188
Public reporting burden for this collection of information is estimated to average 1 hour per response, including the time for reviewing instruction, searching existing data sources, gathering and maintaining the data needed, and completing and reviewing the collection of information. Send comments regarding this burden estimate or any other aspect of this collection of information, including suggestions for reducing this burden, to Washington headquarters Services, Directorate for Information Operations and Reports, 1215 Jefferson Davis Highway, Suite 1204, Arlington, VA 22202-4302, and to the Office of Management and Budget, Paperwork Reduction Project (0704-0188) Washington DC 20503.			
1. AGENCY USE ONLY ***(Leave blank)***	**2. REPORT DATE** September 2005	**3. REPORT TYPE AND DATES COVERED** Master's Thesis	
4. TITLE AND SUBTITLE: The Effect of Friction Stir Processing on the Microstructure and Mechanical Properties of AF/C458 Aluminum Lithium Alloy			**5. FUNDING NUMBERS**
6. AUTHOR(S) Giles, Tanya L.			
7. PERFORMING ORGANIZATION NAME(S) AND ADDRESS(ES) Naval Postgraduate School Monterey, CA 93943-5000			**8. PERFORMING ORGANIZATION REPORT NUMBER**
9. SPONSORING /MONITORING AGENCY NAME(S) AND ADDRESS(ES) N/A			**10. SPONSORING/MONITORING AGENCY REPORT NUMBER**
11. SUPPLEMENTARY NOTES The views expressed in this thesis are those of the author and do not reflect the official policy or position of the Department of Defense or the U.S. Government.			
12a. DISTRIBUTION / AVAILABILITY STATEMENT Approved for Public Release: Distribution is Unlimited			**12b. DISTRIBUTION CODE**

13. ABSTRACT (maximum 200 words)

Aluminum-lithium alloys have been under development for lightweight - high strength aerospace structures but implementation has been slowed significantly because of poor short transverse fracture toughness and brittle intergranular delamination cracking. The alloy AF/C458 (now designated AA 2099) has been designed to exhibit decreased mechanical anisotropy and improved fracture toughness while maintaining ductility and strength levels. This thesis examines the application of Friction Stir Processing (FSP) of AF/C458 as an approach to refine and homogenize the grain structure and enhance mechanical properties. FSP of peak-aged material results in refined, equiaxed grains but with reduced hardness due to the heat input of the process. The effect of post-FSP heat treatment has been established and the influence of FSP on tensile and fatigue properties has been determined.

14. SUBJECT TERMS Aluminum Lithium Alloy, Friction Stir Processing, AF/C458 Alloy, 2099 Aluminum Lithium Alloy, Anticlastic Bend Testing, Orientation Imaging Microscopy, Optical Microscopy, Tensile Testing, Microstructure, Mechanical Properties, Fatigue, Fracture Mode			**15. NUMBER OF PAGES** 87
			16. PRICE CODE
17. SECURITY CLASSIFICATION OF REPORT Unclassified	**18. SECURITY CLASSIFICATION OF THIS PAGE** Unclassified	**19. SECURITY CLASSIFICATION OF ABSTRACT** Unclassified	**20. LIMITATION OF ABSTRACT** UL

NSN 7540-01-280-5500

Standard Form 298 (Rev. 2-89)
Prescribed by ANSI Std. 239-18

THIS PAGE INTENTIONALLY LEFT BLANK

Approved for public release: distribution is unlimited

THE EFFECT OF FRICTION STIR PROCESSING ON THE MICROSTRUCTURE AND MECHANICAL PROPERTIES OF AF/C458 ALUMINUM LITHIUM ALLOY

Tanya L. Giles
Lieutenant, United States Coast Guard
B.S. Biology/Anatomy and Physiology, California State University, Sacramento, 1993

Submitted in partial fulfillment of the
requirements for the degree of

MASTER OF SCIENCE IN MECHANICAL ENGINEERING

from the

NAVAL POSTGRADUATE SCHOOL
September 2005

Author: Tanya L. Giles

Approved by: Terry R. McNelley
Thesis Advisor

Anthony J. Healey
Chairman, Department of Mechanical and Astronautical Engineering

THIS PAGE INTENTIONALLY LEFT BLANK

ABSTRACT

Aluminum-lithium alloys have been under development for lightweight - high strength aerospace structures but implementation has been slowed significantly because of poor short transverse fracture toughness and brittle intergranular delamination cracking. The alloy AF/C458 (now designated AA 2099) has been designed to exhibit decreased mechanical anisotropy and improved fracture toughness while maintaining ductility and strength levels. This thesis examines the application of Friction Stir Processing (FSP) of AF/C458 as an approach to refine and homogenize the grain structure and enhance mechanical properties. FSP of peak-aged material results in refined, equiaxed grains but with reduced hardness due to the heat input of the process. The effect of post-FSP heat treatment has been established and the influence of FSP on tensile and fatigue properties has been determined.

THIS PAGE INTENTIONALLY LEFT BLANK

TABLE OF CONTENTS

LIST OF FIGURES

ACKNOWLEDGMENTS

The author would like to thank Rockwell Scientific Center at Thousand Oaks, CA and Mr. Murray Mahoney for their material and technical support.

Special thanks to Professor Terry McNelley for sharing his knowledge and providing insight throughout this research project.

Many thanks to Dr. Alex Zhilyaev, Dr. Keiichiro Oishi, and Dr. Chanman Park for all the knowledge and technical support/assistance you provided. I greatly appreciate it.

Finally, a special thanks to my friends and family for the support and motivation needed to accomplish this course of work.

THIS PAGE INTENTIONALLY LEFT BLANK

I. INTRODUCTION

Aluminum lithium alloys were primarily developed to provide weight reduction while maintaining high strength for structural implementation in the aerospace industry. However, these alloys often exhibit poor short-transverse (S-T) and unpredictable fatigue crack growth behavior. Specifically, low S-T fracture toughness produces brittle intergranular fracture leading to delamination at stress concentrators like holes and rivets making failure assessments difficult. Research and development by Alcoa under U.S. Air Force contract have resulted in the aluminum lithium alloy (AF/C458), now designated AA 2099, that exhibits decreased mechanical anisotropy and improved fracture toughness while maintaining ductility and strength levels. Friction Stir Processing (FSP) of AF/C458 was studied as a possible approach to enhance the microstructural and mechanical properties of the material by producing high local strains, strain rates, and temperatures below melting producing a refined, homogenized grain structure. This thesis examines a comparison of the microstructural and mechanical properties of AF/C458 aluminum lithium alloy prior to and following FSP.

A. BACKGROUND OF ALUMINUM LITHIUM ALLOY

Aluminum lithium (Al-Li) alloys were primarily developed with the goal of reducing weight thus increasing payload and fuel efficiency. Additions of lithium in aluminum alloys increase elastic modulus and decrease density. To date, limited success in replacing conventional aluminum alloys such as the 7xxx series with Al-Li alloys has been achieved. Unfortunately, some of the major roadblocks to the addition of lithium as a major alloying element have been lower thermal stability with a high lithium content, greater anisotropy, and greater cost. In some instances, fracture toughness is lower due to a greater tendency for low-energy intergranular fracture [1].

1. Age Hardening

Heat treatable materials derive much of their strength from precipitates. Age hardened alloys are typically solution heat treated in the single phase α region then quenched to room temperature to obtain a supersaturated single phase solid solution. Follow-on aging is completed at some intermediate temperature greater than room temperature to allow precipitates to form. The peak aged condition will have an optimal

fine dispersion of second phase, while in overaging, precipitates continue to grow i.e. small precipitates are consumed and large precipitates grow at their expense.

2. Physical Metallurgy and Properties

Lithium (Li) is the lightest metallic element and has an atomic mass of about 7g/mol. For each 1% of lithium a 3% reduction in density and a 5-6% increase in strength in Al-Li alloys. Solubility of Li in aluminum has a limit of about 4.2% although contents this high are rarely used in practice despite the inclination to maximize the strength and density benefits of lithium addition [2-5]. Li content in commercial alloys is usually within the 1.6 –2.4 range. The effect of Li will be discussed later but includes detrimental effects to the facture toughness and mechanical properties.

The properties of Al-Li depend on its alloy composition and its microstructure. High strength is obtained by manipulating the microstructure through solution heat treatment, mechanical working, and aging. The strength is related to the resistance dislocation motion. Al-Li alloys achieve precipitation strengthening by thermal aging after solution heat treatment. Li in small amounts leads to homogenous distribution of the intragranular coherent, spherical $\delta'(Al_3Li)$ precipitates. There is a coprecipitation of the metastable strengthening phases $T_1(Al_2CuLi)$, $T_2(Al_6Cu(LiMg)_3)$, and $\theta'(Al_2Cu)$ along with the $\delta'(Al_3Li)$ during aging up to peak strength conditions [3-4]. Each of the possible strengthening precipitates are in competition for nucleation sites and solute, namely Cu and Li [5]. The formation of $\delta'(Al_3Li)$ precipitates hardens the alloy but decreases ductility because they are easily sheared by moving dislocations.

The equilibrium phase δ is believed to nucleate independently of δ' and grows by dissolution of the surrounding metastable δ'. The δ nucleates heterogeneously after relatively long aging times at the expense of the δ' whereas the δ' forms rapidly and homogeneously [6]. Aluminum and lithium in the δ' precipitates are positioned at specific locations on the $L1_2$ lattice. The close match of lattice parameters with the FCC α lattice results in small misfit strains and, consequently, when solution heat treated and aged for short times below the δ' solvus line, produces a homogeneous distribution of coherent δ' precipitates [7-8]. Other intragranular metastable phases such as, $T_1(Al_2CuLi)$, and

$\beta'(Al_3Zr)$ can also occur in addition to intergranular equilibrium phases such as $T_2(Al_6CuLi_3)$ and $\delta(AlLi)$.

Typical alloying elements include Cu, Mg, and Zn. Cu and Mg have been shown to reduce the solubility of Li and enhance the precipitation of Al_2Cu and Al_2CuMg phases that are more resistant to shearing producing an effective strengthening element to the alloy [8, 9-10]. The Zr is added in combination with Mg to produce a very strong age-hardening response, high toughness, and considerable corrosion resistance [9]. Mn and Zr alloying elements have shown evidence of affecting the kinetics of the precipitation process. Zr additions lead to the formation of the intermetallic dispersoid $\beta'(Al_3Zr)$, which acts to inhibit recrystallization during hot rolling but also affects the pancake-like grain structure formation and texture. Mn results in a larger, incoherent dispersoid that may act as nucleation sites for recrystallization [8, 10].

3. Fracture Toughness and Anisotropy

The susceptibility of Al-Li alloys to brittle intergranular fracture (BIF) is mainly in the short transverse (S-T) direction. Macroscopically, this can be seen as delaminations occurring at stress concentrations such as holes or rivets. The tendency of BIF seems to increase with higher concentrations of lithium but alloys with a lower concentration are not immune. Several studies have proposed numerous mechanisms leading to BIF: (i) planar slip resulting in high stresses where slip bands impinge on grain boundaries; (ii) embrittlement due to alkali metal impurity phases; (iii) grain boundary structural changes associated with segregation of lithium; (iv) strain localization at the soft δ' precipitate free zones; (v) presence of coarse equilibrium grain boundary precipitates; and (vi), high hydrogen content [1, 10-12]. Lynch *et al*. [1] arguably suggests lithium segregation at the grain boundaries as the prime cause for BIF although little is known on the exact cause.

Although $\delta'(Al_3Li)$ is one of the major strengthening agents in Al-Li alloys, it is also key in loss of fracture toughness. In fabrication, lithium produces a homogeneous distribution of intragranular coherent, spherical, $\delta'(Al_3Li)$ precipitates in the microstructure. Plastic deformation in aluminum and most of its alloys occurs by motion of unit dislocations moving on the {111} close packed planes and in the <110> close

packed directions [7]. Existing research that crack extension in aluminum alloys essentially occur along δ' precipitate shear bands (PSB), high angle grain boundaries, and low angle grain boundaries with low angle grain boundaries being the most difficult. The PSBs form primarily due to the shearing of δ' precipitates along the {111} crystallographic planes which are oriented ~ 55^{o} to the rolling direction [12]. The presence of other metastable and equilibrium precipitates increases fracture resistance by making PSB formation more difficult.

In-plane anisotropy of yield strength has been attributed to crystallographic textures, grain morphologies, and directional precipitates. Additionally, hot-rolled Al-Li alloys exhibit a minimum yield strength near 45^{o} to the rolling direction due to rolling textures and elongated grain morphologies. Yield strength anisotropy can be reduced by thermomechanical processing consisting of overaging, warm rolling and recrystallization treatment which weakens the sharp rolling texture and refines grain shape. The shearable δ' precipitates discussed above tend to increase yield strength anisotropy by encouraging planar slip while non-shearable precipitates tend to inhibit it [11]. The distribution and size of these precipitates can be influenced by thermomechanical processing ultimately dictating the mechanical properties of the material [5].

4. AF/C458

Significant improvements have been accomplished by changes to the alloy chemistry and thermo-mechanical treatments to increase fracture toughness. Investigations have focused on controlling microstructural evolution to reduce grain boundary precipitation and limiting inhomogeneities such as coarse constituents or precipitate free zones (PFZs) [5]. AF/C458 was developed using a combination of compositional elements and proper processing techniques and represents a third generation of aluminum lithium alloy. It is believed to have resolved or mitigated many of the shortcomings encountered with the previous Al-Li generations [13].

B. FRICTION STIR PROCESSING

Some high strength aluminum alloys have notoriously poor weldability using conventional joining techniques. Friction Stir welding (FSW) is a solid state joining process developed by The Welding Institute in 1991 that uses a rapidly rotating, non-consumable tool to produce plastic deformation and frictional heating to join materials

[14-15]. Friction stir processing (FSP) is a metal working technology adapted from FSW using the same basic principles. However, unlike FSW that is used to as a joining process, FSP is employed on a monolithic material in order to provide localized modification and control of microstructures. FSP often results in homogenization and refinement of the microstructure leading to improved mechanical properties [15-16]. This technology allows for the distinct opportunity to selectively improve desired mechanical properties in key areas.

In FSP, a cylindrical, wear-resistant, rotating tool is brought into contact with the surface of the constrained material. The tool is designed to have a pin used to "stir" and shoulder that prevents the upward flow of the softened material. Friction-induced heating softens the metal and tool is able to penetrate until the shoulder comes into contact with the work piece surface. The tool is then traversed along the surface in the desired direction or patterns. The process is illustrated in Figure 1-1 below. Tool design (depending on the material), tool rotational speed (revolutions per minute or rpm), and/or traversing speed (inches per minute or ipm) may vary to produce the desired microstructure.

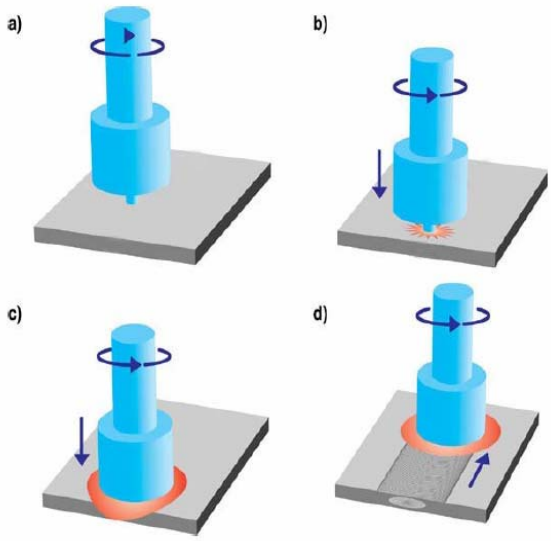

Figure 1-1. Schematic Illustration of FSP (Courtesy of M. W. Mahoney, RSC).

FSP is considered a severe hot working process that produces intense plastic deformation brought on by the rotating tool with extreme localized strain and strain rates as well as elevated temperatures up to 0.8-0.9 of the melting point of the material. FSP is an adiabatic process and since the parent material is not melted, no solidification problems occur as the processed zone cools. However, temperatures are often high enough to cause precipitate dissolution and re-precipitation. Cooling rates can be affected by the ipm and rpm of the tool along with the degree of overlapping during processing and have a prevailing influence on the subsequent microstructural features. Prior investigations with alloy constitution and phase relationship data of the stir zone provide insight into the thermomechanical history of the material [15-16].

C. OBJECTIVE OF THIS RESEARCH

The main objective of this research is to establish a baseline assessment on the S-T fracture toughness of the newly developed AF/C458 alloy using a specially developed fatigue test simulating cyclic stresses occurring in aerospace operations. This will allow a comparative examination on the effect of friction stir processing on the short transverse properties. With this analysis and a comprehensive look at the microstructural and mechanical properties, it may be possible to adopt friction stir processing of plates at critical areas during construction applications avoiding the possibility of undetected delaminating failures.

II. EXPERIMENTAL PROCEDURES AND TESTING

A. MATERIAL & COMPOSITION

Two plates manufactured by Alcoa for Boeing of AF/C458 plate in a T8 condition were provided for this research as shown in Figure 2-1. They are each approximately 58 x 38 x 1.2 cm in size. Chemical analysis on the material was conducted by Anamet Inc, Hayward, CA with the results tabulated below.

Element	Concentration (wt %)
Al	Bal.
Cu	2.30
Li	1.66
Zn	0.56
Mg	0.20
Mn	0.30
Zr	0.08

Figure 2-1. As Received (AR) and Friction Stir Processed (FSP) plate provided along with composition by weight percent of AF/C458

Friction stir processing was completed on one plate by Rockwell Scientific Corporation, Thousand Oaks, CA, in the spiral raster pattern illustrated in Figure 2-2 below. The material was processed using a stepped spiral tool similar to those shown as an inset picture of the tool in Figure 2-2. Spiral raster patterns were completed having an overlapping of advancing and retreating sides improving the likelihood of isotropy, and processed at a tool speed of 400 revolutions per minute (rpm) at a traversing speed of 5 inches per minute (ipm). Due to the constraint effects and the thermomechanical cycles

experienced by the plate during friction stir processing, some tearing occurred at the outer edges. All subsequent specimens were carefully chosen to avoid any visible defects.

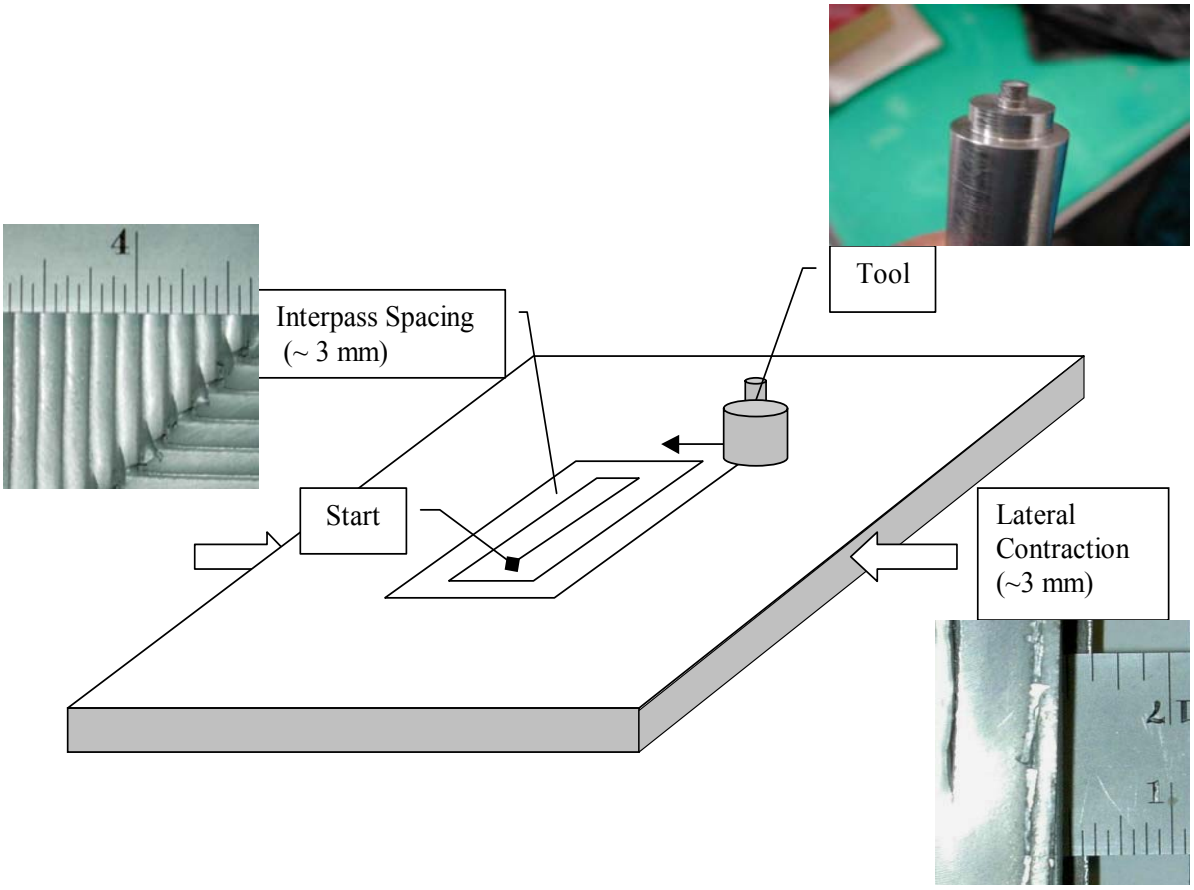

Figure 2-2. Spiral raster pattern of FSP plate with inset photos of actual materials

B. MICROSCOPY

1. Sample Preparation

Samples were sectioned using a Charmilles Andrew EF630 electric discharge machine (EDM) employing a consumable 0.3 mm diameter brass cutting wire. For optical microscopy (OM), 10x10x12 mm sections in the longitudinal (L), long transverse (LT), and short transverse (ST) directions were then mounted in 1.25-inch diameter premold-red phenolic using a Buehler SIMPLIMET 2 mounting press. Mechanical polishing of the mounted As Received (AR) and FSP plate samples was completed following the schedule outlined in Table 2-1 using Buehler ECOMET 3 & 4 polishing wheels. Water was used as a lubricant for steps 1-4. Each sample was ultrasonically cleaned in methanol for 15 minutes in between each step (4-7). Samples were then etched

using Keller's reagent. Samples for Optical Imaging Microscopy (OIM) were prepared following the OM procedures then electropolished as described in the OIM section.

Step	Abrasive	Time	RPM
1	500 Grit SiC Paper	1 minute	120
2	1000 Grit SiC Paper	1 minute	120
3	2400 Grit SiC Paper	1 minute	120
4	4000 Grit SiC Paper	1 minute	120
5	3 μm Metadi Diamond Suspension	10 minutes	40
6	1 μm Metadi Diamond Suspension	10 minutes	40
7	0.05 μm Colloidal Silica	15 minutes	20

Table 2-1. Polishing procedure for microscopy

2. Optical Microscopy (OM)

Optical microscopy was conducted using a JENAPHOT 2000 reflected light photomicroscope. Digital output via a PULNIX TMC-74-CCD camera was captured and processed using SEMICAPS software. Micrographs of AR and FSP samples were obtained for short-transverse (ST), long transverse (LT), and longitudinal (L) plate planes with respect to the rolling direction (RD) for comparison.

3. Scanning Electron Microscopy (SEM)

A Topcon SM-510 Scanning Electron Microscope (SEM) operating with a tungsten filament at an accelerating voltage of 20kV was used for tensile and anticlastic testing fractographs.

4. Orientation Imaging Microscopy (OIM)

A Topcon SM-510 Scanning Electron Microscope (SEM) operating with a tungsten filament at an accelerating voltage of 20kV in conjunction with Orientation Imaging Microscopy (OIM) hardware and TSL software was used for OIM data collection and analysis. Reference axes were defined as the reference direction (RD) in

line with the rolling direction of the AR plate, the normal direction (ND) coincident to the through thickness of the plate, and transverse direction (TD) parallel to the horizontal. Samples were cut from a plane having a normal direction parallel to the transverse direction: i.e. the ND-RD plane. Samples were polished following the procedure in Table 2-1 and finished by electropolishing with a 33% nitric acid-67% methanol solution initially cooled to -25ºC. The electron beam was operated in spot mode with a beam diameter of $0.2\,\mu m$. Software provided grain orientation maps, pole figures, misorientation angles, and grain size data for selected areas.

5. Transmission Electron Microscopy (TEM)

Transmission electron microscopy (TEM) was accomplished with a Topcon 002B instrument operating at 200kV. Samples for TEM examination were obtained by first sectioning with a low-speed diamond saw to obtain a transverse slice of the ND-RD plane for both the FSP and AR material. Then, disks 3 mm in diameter were thinned to perforation by electro-polishing using a 33 pct. nitric acid – 67 pct. methanol solution initially cooled to -25ºC.

C. ROCKWELL B HARDNESS TESTING

1. Sample Preparation & Testing Procedures

Hardness data was obtained from 10x10x12 mm samples sectioned using EDM. Hardness was measured using the 'B' scale with 100 kg weight. Data was averaged from 3 data points for each position.

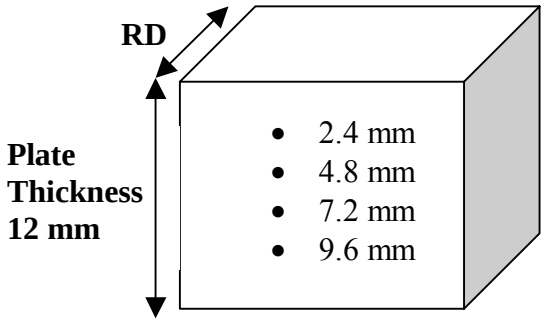

Figure 2-3. Testing positions for Rockwell B hardness data

D. TENSILE TESTING

1. Sample Design, Preparation, and Dimensions

Tensile samples were sectioned from the selected material using EDM then polished with 1000 grit SiC paper and checked for macro defects under OM prior to testing. Several sample designs conforming to ASTM E-8 standards were employed

a)

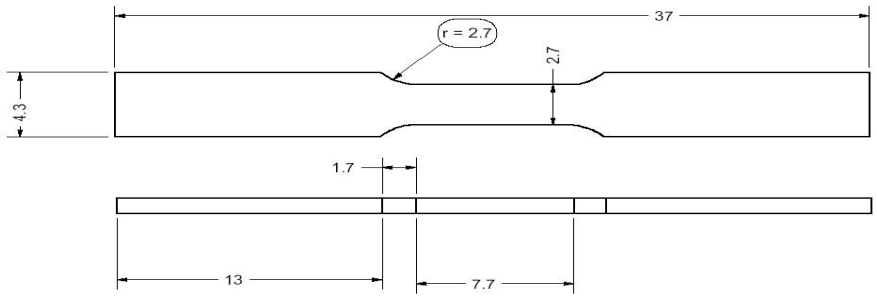

b)

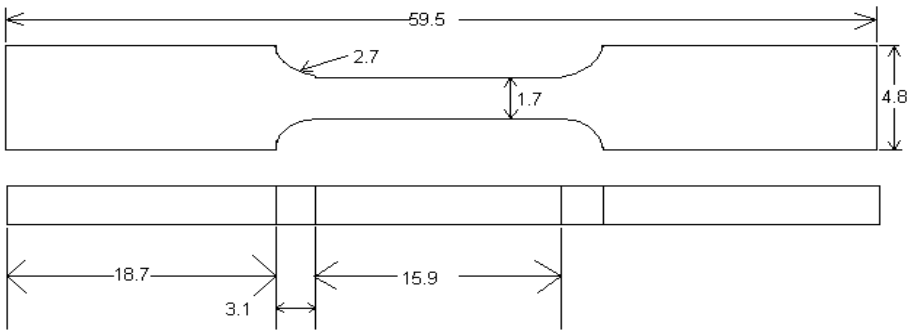

c)

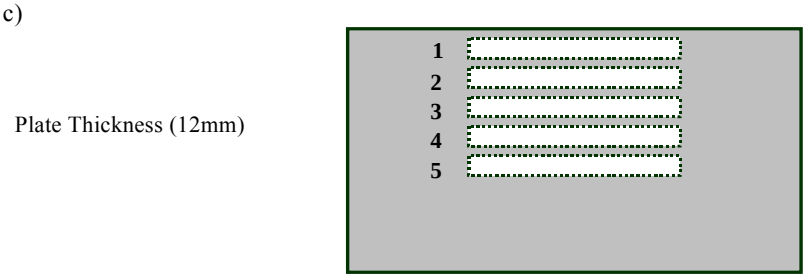

Sampling Label Example:
21-T-AR-blank 2, position 1, transverse direction, as received plate

Figure 2-4. Dimensions (mm) of longitudinal and transverse tensile samples for a) FSP b) As-Received (After Ref. 25) c) sample positioning of AR L and T series

depending on the material and need. Midplane samples of the FSP in the longitudinal and transverse directions were tested using the sample design shown in Figure 2-4 a). Due to plastic deformation occurring outside the gage length in the AR samples, a modified design with an increased gage length and decreased gage width, as shown in Figure 2-4 b), was used for the AR plate. A transverse and longitudinal series of the AR plate from the surface past the midplane, as illustrated in Figure 2-4 c), were completed to test for variations in mechanical properties through the thickness.

In order to examine the through thickness mechanical properties, a special micro design was created in order to fit the thickness of the 12 mm plate. Figure 2-5 illustrates the size and positioning of the sample relative to the plate. Specimens were cut perpendicular to the rolling direction using the EDM machine and prepared as discussed above.

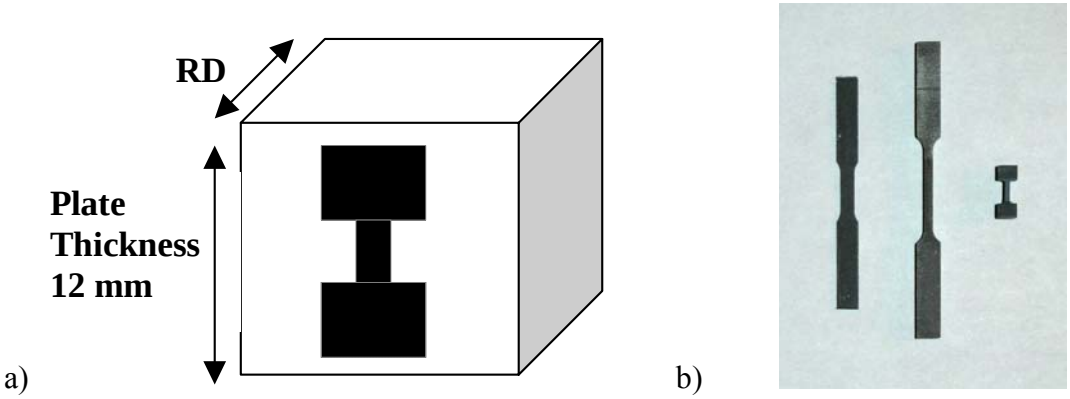

Figure 2-5. a) Positioning of micro specimen tensile samples b) visual comparison of sizes of tensile samples (left to right) FSP for L & T orientations, AR for L & T series, Micro specimens for through thickness testing

2. Testing Apparatus and Procedures

All tensile testing except the micro specimens was performed using a computer controlled Instron Model 4507 machine. Specimens were loaded at a constant cross head speed until failure. Load and displacement data was collected using Series IX software. The gage width, thickness, and length were measured and recorded prior to testing. An extensometer was not used due to the small sample size. As a result, a locally prepared MATLAB m-file was developed to adjust for the elastic response due to the machine

frame and grips and determine stress/strain information. Due to lack of adequate equipment locally, all micro specimens were tested at the Institute for Metals Superplasticity Problems in Ufa, Russia at constant strain rates using a lab constructed bench top tensile machine.

E. ANTICLASTIC BEND TESTING

1. Background

Anticlastic testing is a severe fatigue testing procedure designed to simulate the types of loading encountered by wing/fuselage structures at critical locations, and pressure vessels for cryogen containment. Utilizing opposite bending moments, reversed normal stresses at the surface of the plate and reversed shear stresses at the midplane or neutral surface are produced. This results in maximum normal stresses at the plate surface and maximum shear stresses at the midplane as illustrated in Figure 2-6. This should give a qualitative determination of the inherent S-T weakness often exhibited by aluminum lithium alloys and useful comparison to the effect of friction stir processing.

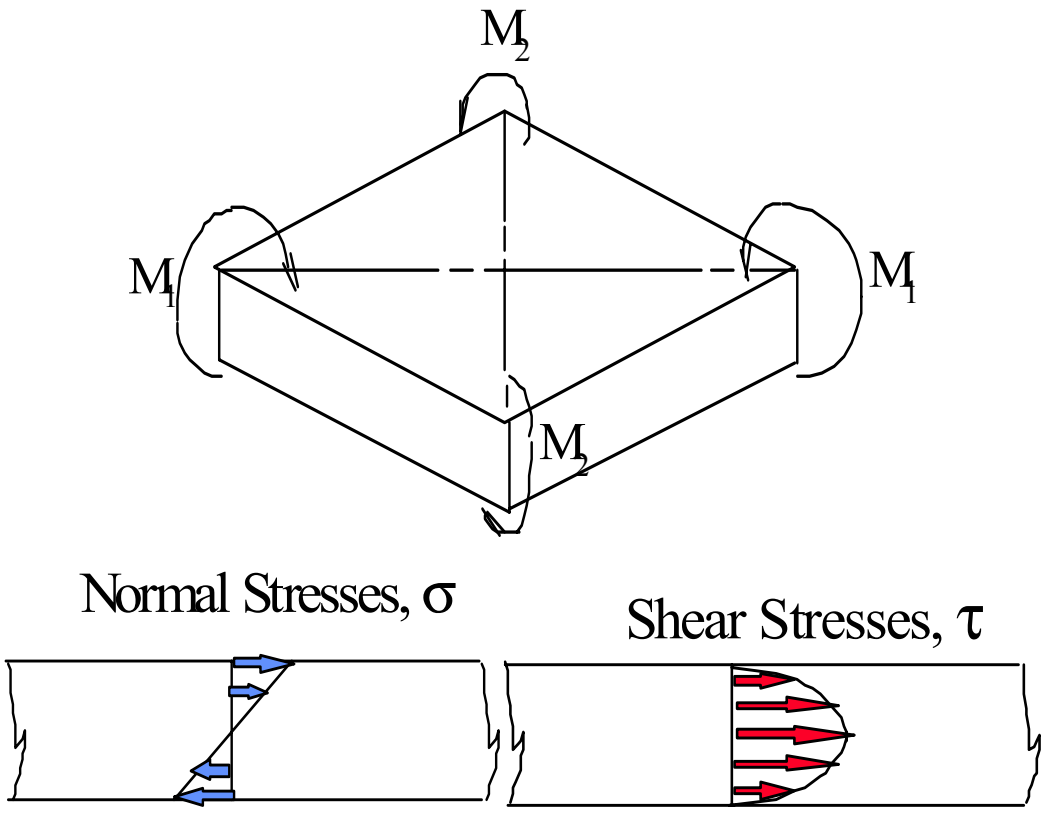

Figure 2-6. Stress and moments produced in anticlastic testing (Courtesy of M. Mahoney, RSC)

2. Sample Design and Dimensions

Sample design and dimensions were provided by Rockwell Scientific with basic schematic provided in Figure 2-7. A full blueprint is provided in Appendix D.

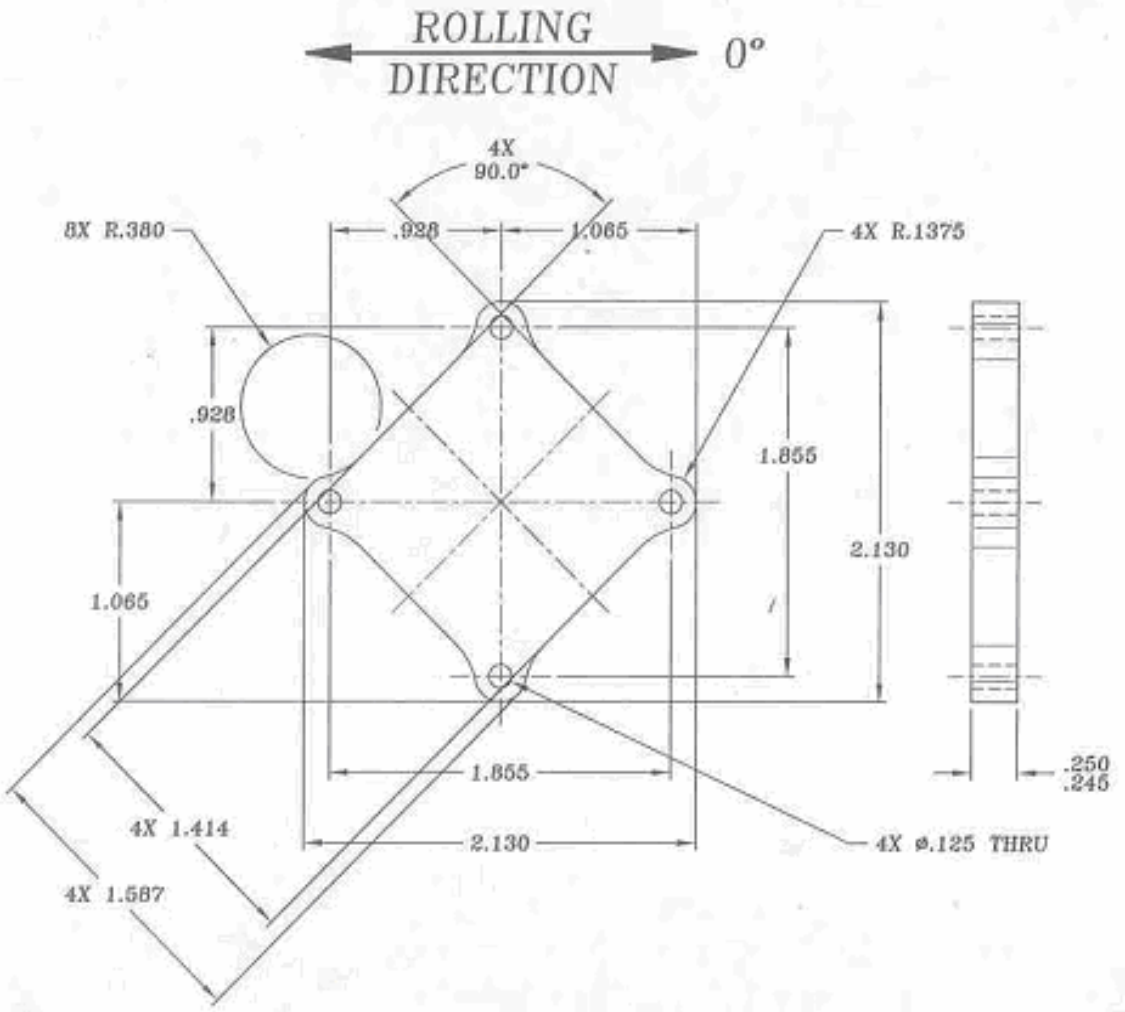

Figure 2-7. Sample design and dimensions (Courtesy of M. Mahoney, RSC)

3. Sample Preparation

Anticlastic specimens blanks were cut by EDM machining using a computer code developed locally. Samples were oriented specifically with the bending moments to be perpendicular and parallel to the rolling direction then machined from both sides with the specimen being obtained from the mid-thickness. Holes were then drilled and samples

polished with 1000 grit SiC paper. All samples were checked for macroscopic defects prior to testing.

4. Testing Apparatus

All anticlastic bend testing was performed using an Instron Model 4507 machine. Specimens were mounted in the testing apparatus shown in Figure 2-8 designed and manufactured by Rockwell Scientific. Testing was conducted under grip control set to cycle under +/- 1500, 1000, and 750-pound loads at a crosshead speed of 2.5 in per minute until failure. The number of cycles to failure and fracture mode was then recorded for each specimen.

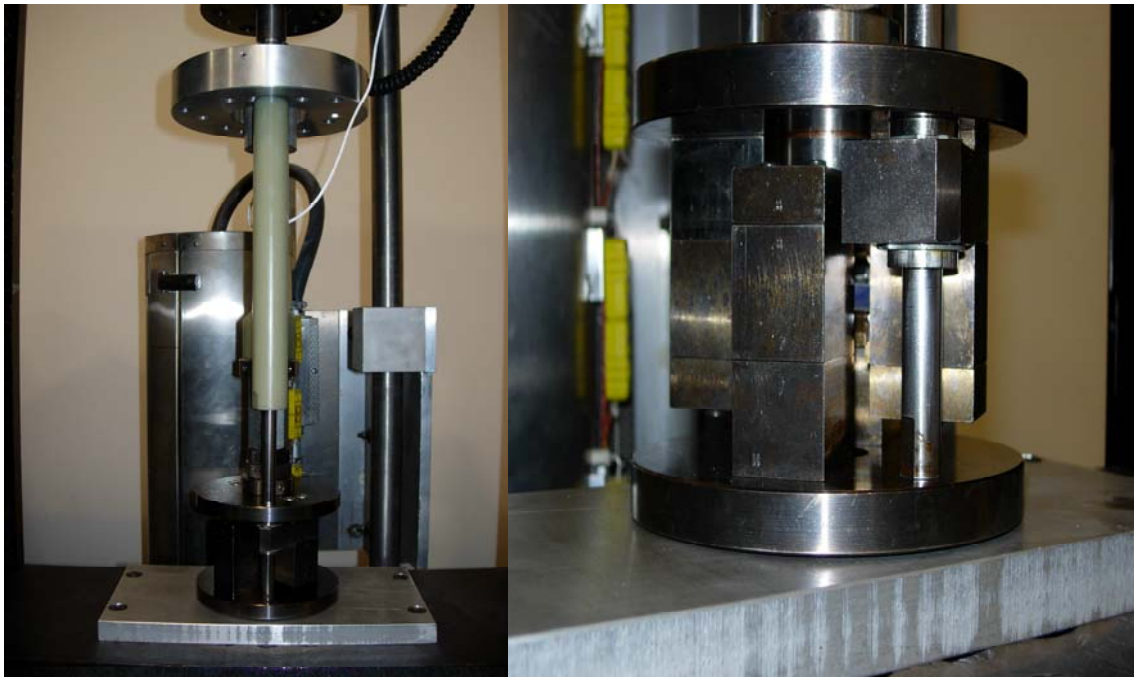

Figure 2-8. Anticlastic bend testing apparatus.

F. HEAT TREATMENT

All material used to determine the effect of aging was subjected to the prescribed temperature of $148 \pm 1^{o}C$ for the prescribed time then air cooled at room temperature.

THIS PAGE INTENTIONALLY LEFT BLANK

III. RESULTS

. Representative results will be presented and analyzed in this chapter while all experimental data is included in Appendix A-C for reference

A. AS RECEIVED (AR) PLATE

1. As-Received Material Microstructure

OM results for the as received plate indicated a highly elongated, pancake shaped grain structure with a wide variation in grain width and grain aspect ratio typical of a rolled material. A 3-D OM representation of the microstructure is given in Figure 3-1 a).

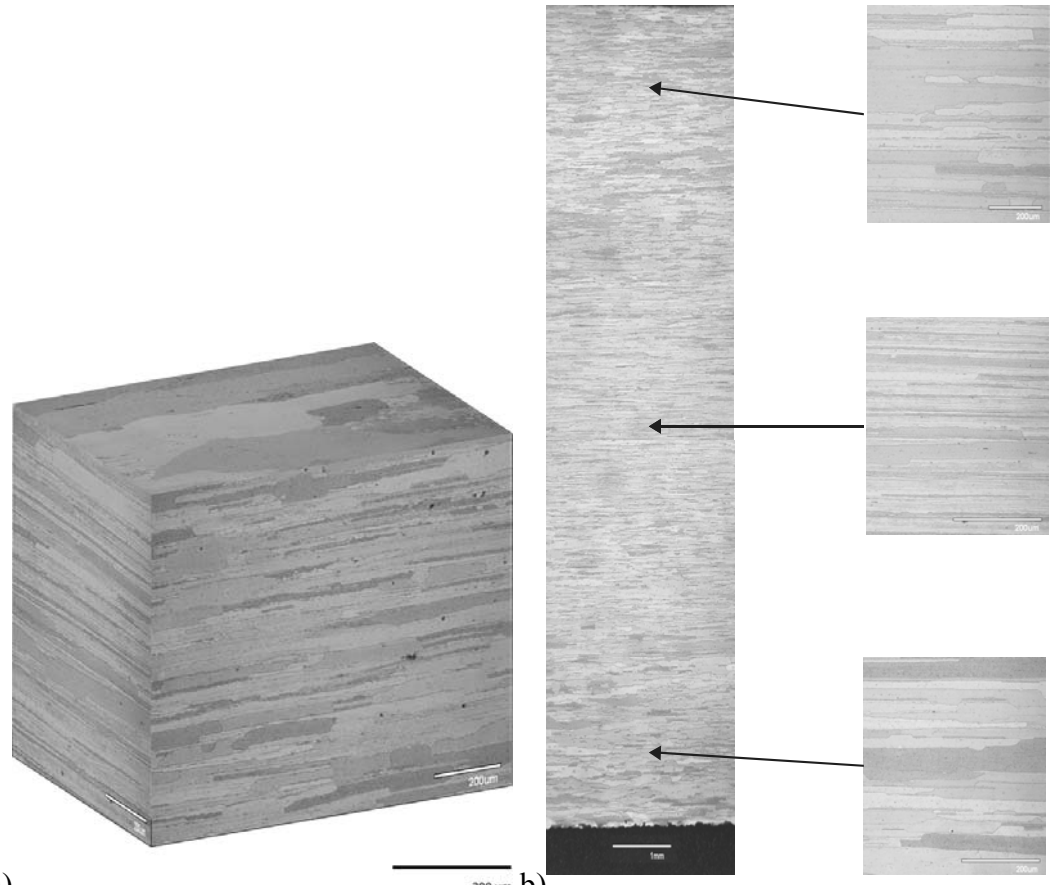

a) b)

Figure 3-1. Micrographs showing a) orthogonal representation of the microstructure b) variation in grain thickness in the ST direction.

A decrease in average grain thickness from the surface to the midplane was observed through the thickness of the plate (Figure 3-1 b)). Bright field (BF) TEM

revealed the grains included subgrains in the size range of 2-10 microns. Dark field (DF) imaging revealed β' and fine δ' precipitation in this material.

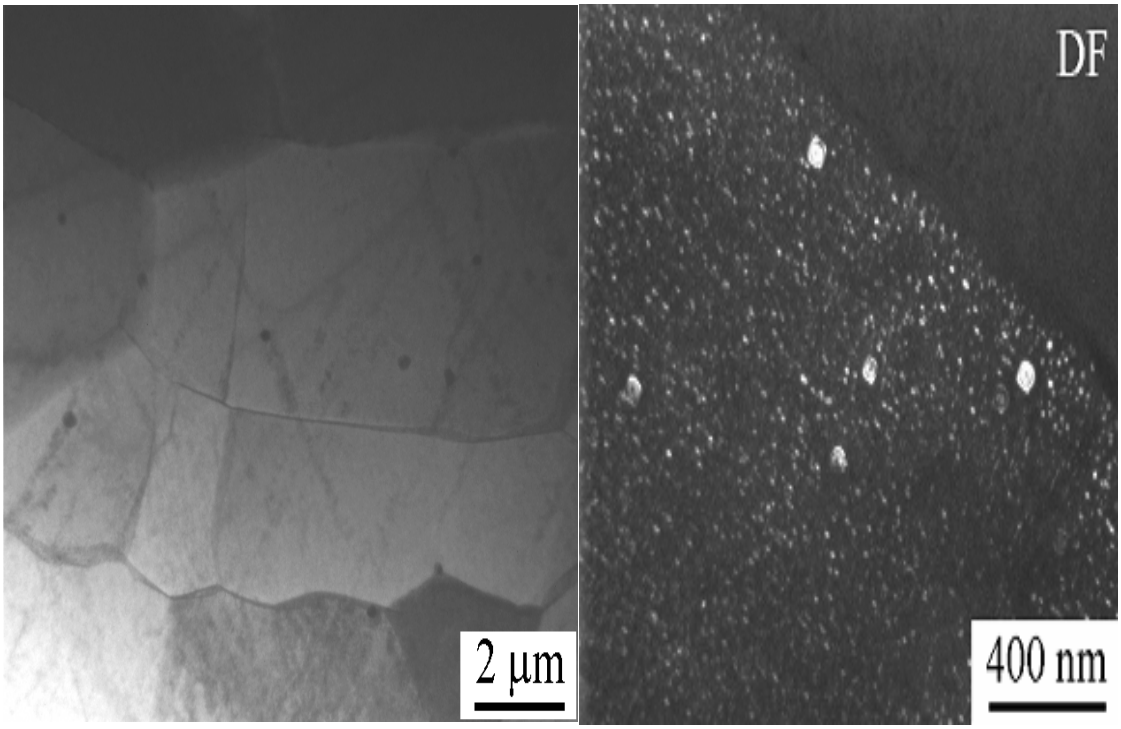

Figure 3-2. a) TEM micrograph illustrating the pancake grain structure for AF/C458 alloys. b) Precipitation of spherical β', and a fine homogeneous distribution of δ'.

OIM data agreed with the OM/TEM results and provided grain-to-grain misorientation angles of the grains. An increased number of low angle grain boundaries ($<10^{o}$ rotation) correlates with TEM micrographs showing the presence of subgrains. In addition, misorientation distribution showed a large number of 50-60^{o} rotations. Full OIM results are given in Appendix A. Reference axes were defined as follows: the reference direction (RD) was assigned as positive downward; the normal direction (ND) was directed toward the screen, and the transverse direction (TD) was parallel to the horizontal. For sample orientation, the TD direction is parallel to the rolling direction of the AR plate. Pole Figure (PF) and Inverse Pole Figure (IPF) analysis in standard RD, TD, and ND axes showed a similar deformation texture indicative of rolled FCC materials.

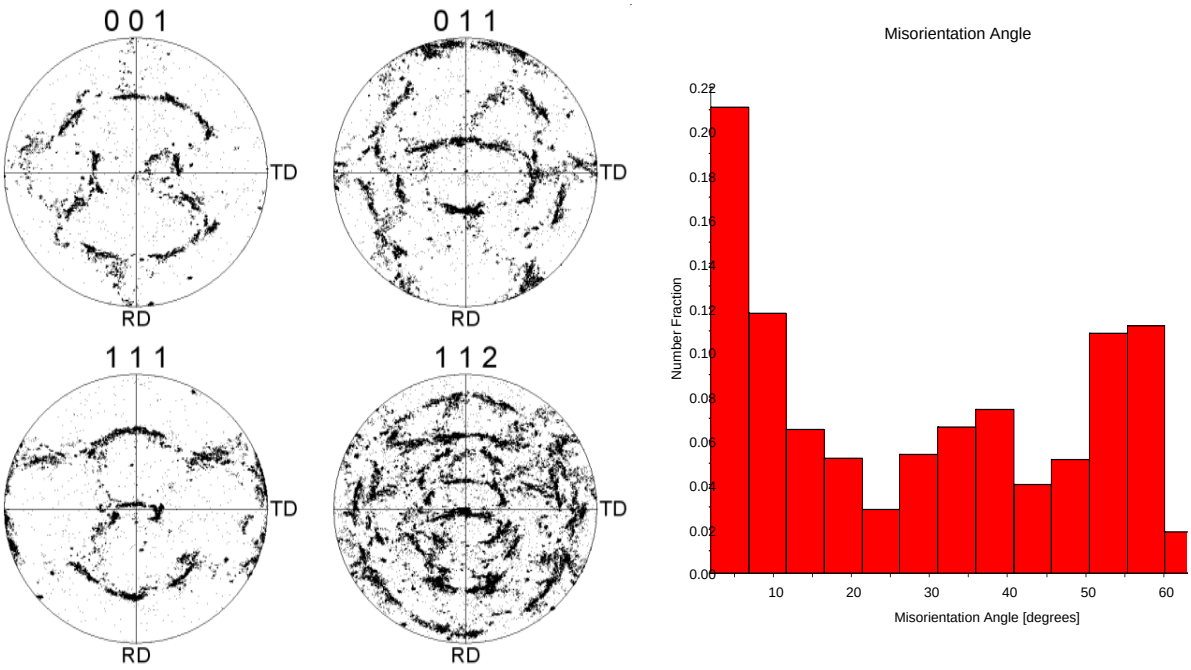

a) b)

Figure 3-3. OIM results for AR plate; a) PF diagram b) Misorientation angles.

2. As-Received Material Mechanical Properties

Hardness testing through the thickness of the plate indicated a slight variation through the depth; the greatest hardness values were observed along the centerline (Figure 3-4). Standard deviation in hardness measurements for the AR plate was approximately +/- 1.5 HRB. Tensile testing later confirmed variations in mechanical properties and is discussed below.

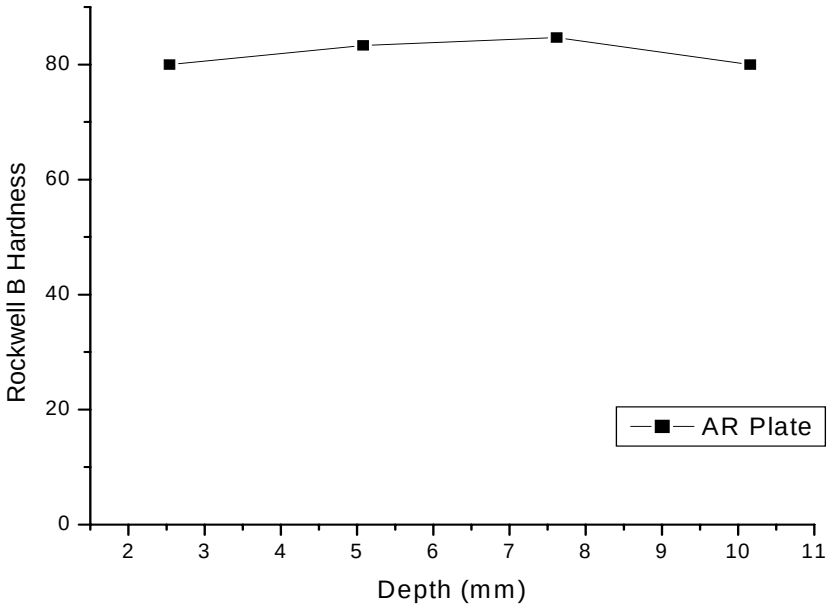

Figure 3-4. Hardness results as a function of depth in the AR plate.

Stress/strain curves (SSC) for the longitudinal and transverse series of the AR plate were plotted and included in Appendix B. Results show a general increase in strength and decrease in ductility from the surface to the midplane in both the transverse and longitudinal orientations. The midplane in the longitudinal direction exhibited yield strength of about 500 MPa and tensile strength of about 540 MPa. Midplane ductility was the lowest at ~5.5%. Transverse samples followed the same mechanical trends but were slightly lower in all regards. Short transverse testing revealed an extremely low ductility of 2.5% and, as expected, had the lowest strength. The anisotropic mechanical behavior is illustrated in Figure 3-5 a)-c).

Fracture surfaces were nominally oriented 45^{o} with respect to the load axis with the fracture path through the thickness of the gage area. All micro-specimens exhibited a flat fracture surface perpendicular to the load axis. Some necking was observed. Fractography revealed facets with some microvoid formation and secondary cracking suggesting a mixture of intergranular and transgranular fracture. SEM fractographs of tensile samples are included in Appendix C.

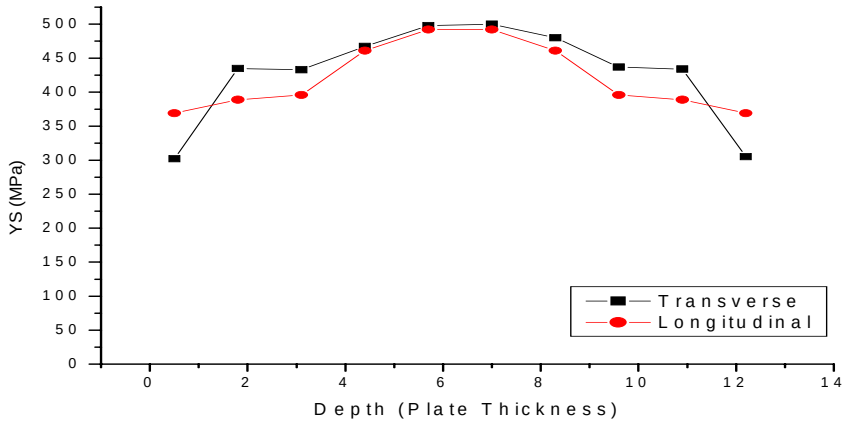

a)

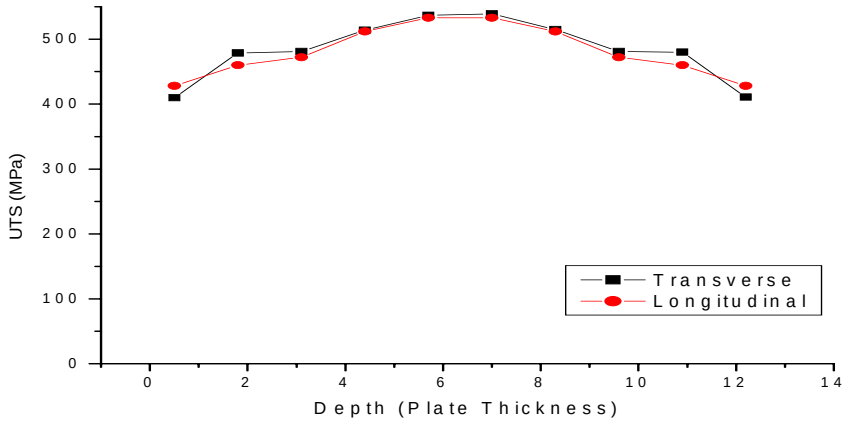

b)

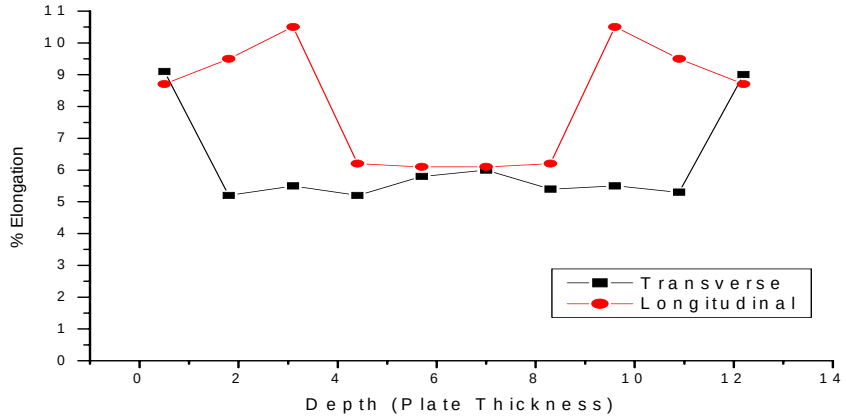

c)

Figure 3-5. Selected mechanical properties of AR plate in both longitudinal and transverse directions a) yield strength b) tensile strength c) % elongation.

Anticlastic bend testing results are shown in Figure 3-6. Fracturing occurred in the plane normal to the plate surface in a delaminating manner. All specimens tested at the various loads failed by the same mode with the lowest stress showing the largest degree of delamination (Figure 3-7). Specimen failure did not occur instantaneously but required numerous cycles and fracture paths to develop. Failure was mainly intergranular separation along the L-T plane with some evidence of intragranular micro-fracturing (Figure 3-8).

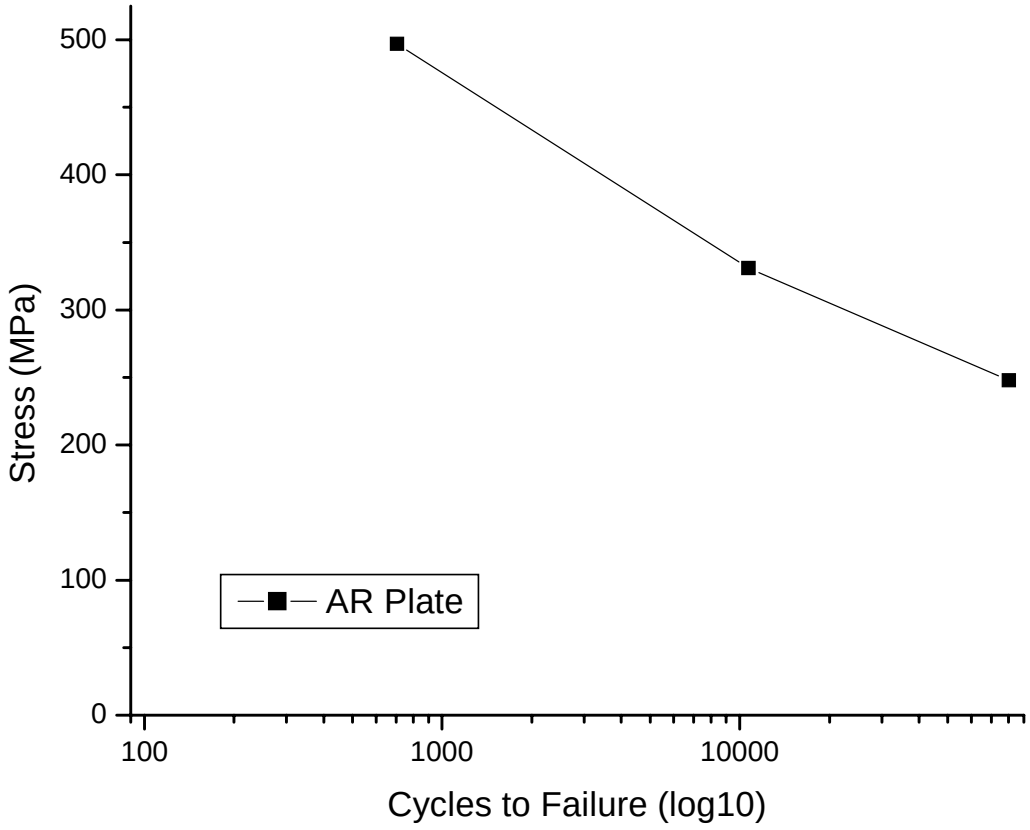

Figure 3-6. Anticlastic fatigue testing results for the AR plate.

Figure 3-7. Delaminating behavior of AR plate at lowest tested cyclic load.

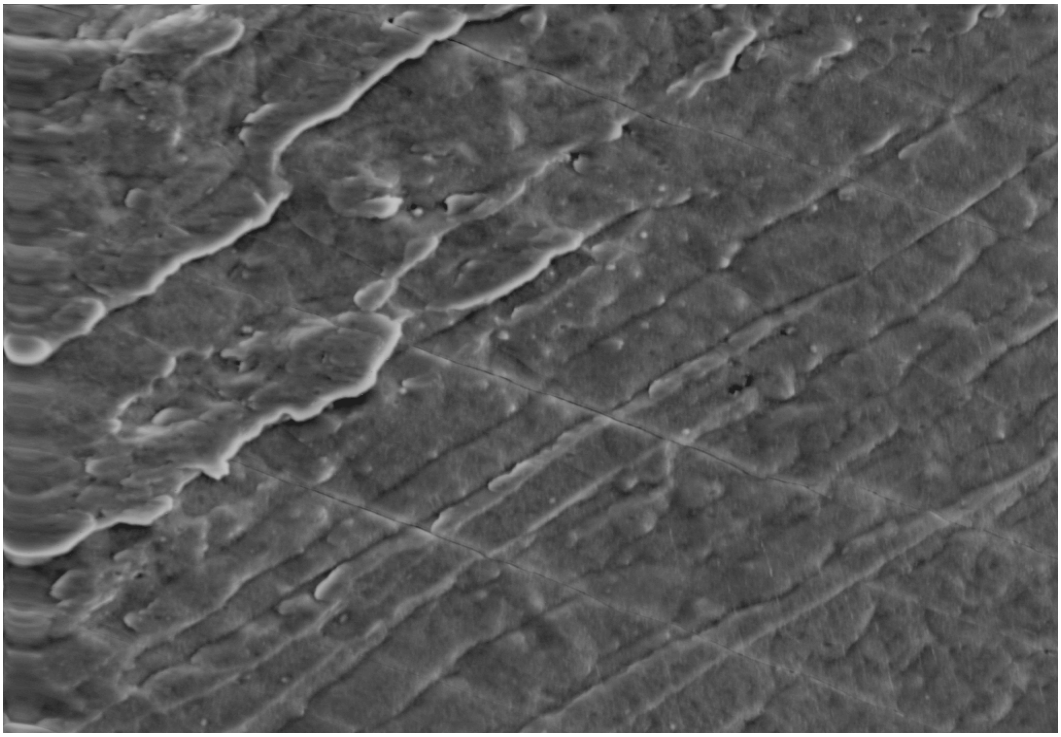

Figure 3-8. SEM fractograph (500x) of anticlastic AR test sample showing intergranular microfractures.

B. FRICTION STIR PROCESSED PLATE

1. FSP Material Microstructure

The intense plastic deformation associated with the frictional and adiabatic heating due to the rotating tool resulted in a recrystallized, fine-grained microstructure throughout the volume subjected to FSP. This is shown in Figure 3-9 a); the flattened, pancake-shape grains of the AR plate have been replaced with equiaxed grains. However, band-like features are evident and the grain size is coarser near the surface in contact with the tool. This is shown by the inset micrographs in Figure 3-9 b). Some band-like patterns were observed at low magnifications indicating the possibility of microstructural variations within the FSP zone.

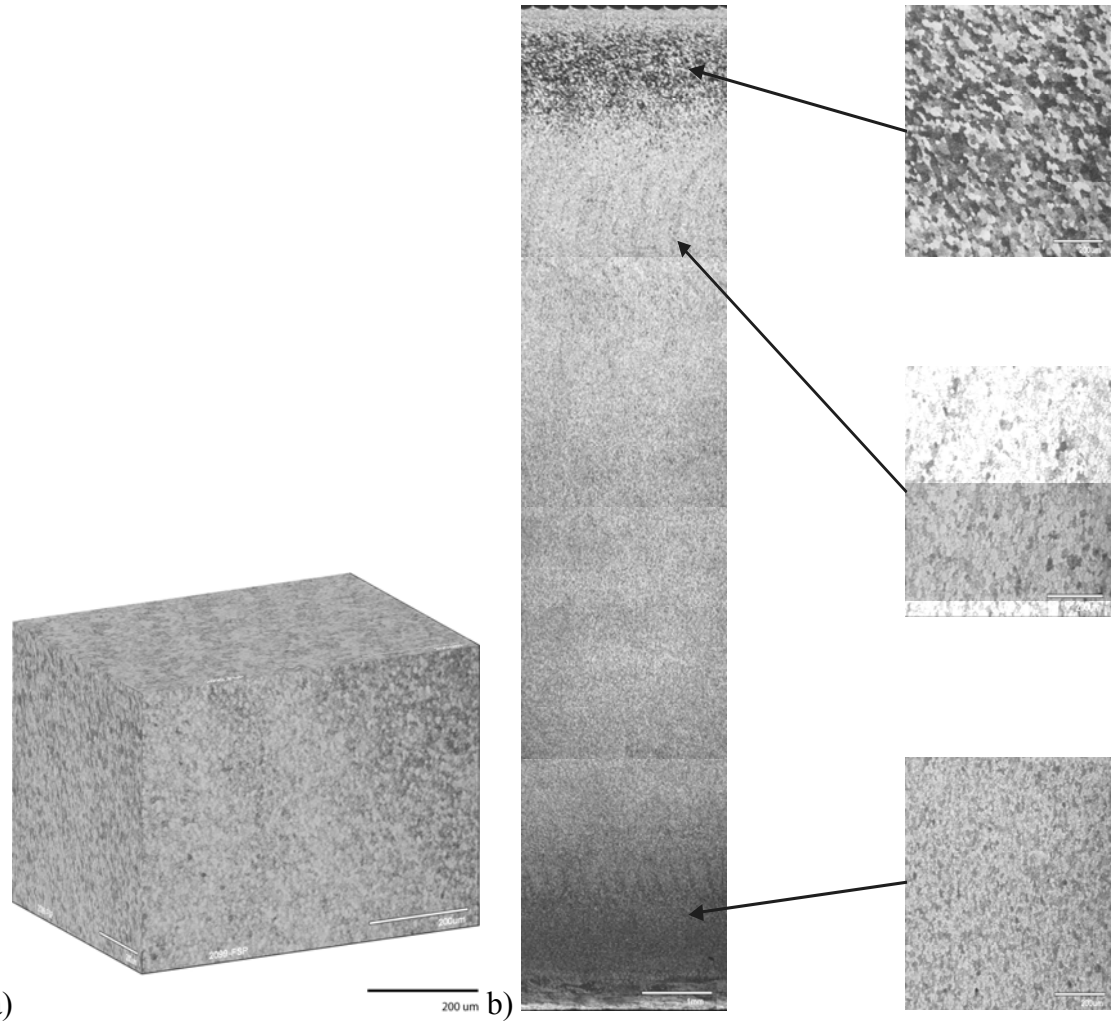

a) b)

Figure 3-9. a) Polished and etched orthogonal sections of 12mm of AF/C458 plate after FSP b) Micrographs showing through-thickness microstructural details.

TEM examination (figure 3-10) revealed coarse precipitates located at the grain boundaries, which were coarser in size and in greater amount when compared to the AR plate. Intergranular precipitates were also larger reflecting overaging due to FSP. Selective area diffraction (SAD) revealed platelet precipitates that had formed on the $\{111\}_{\alpha}$ planes of the matrix lattice. The {110} SAD patterns indicated that the fine δ' had reverted to solution when compared with the AR plate.

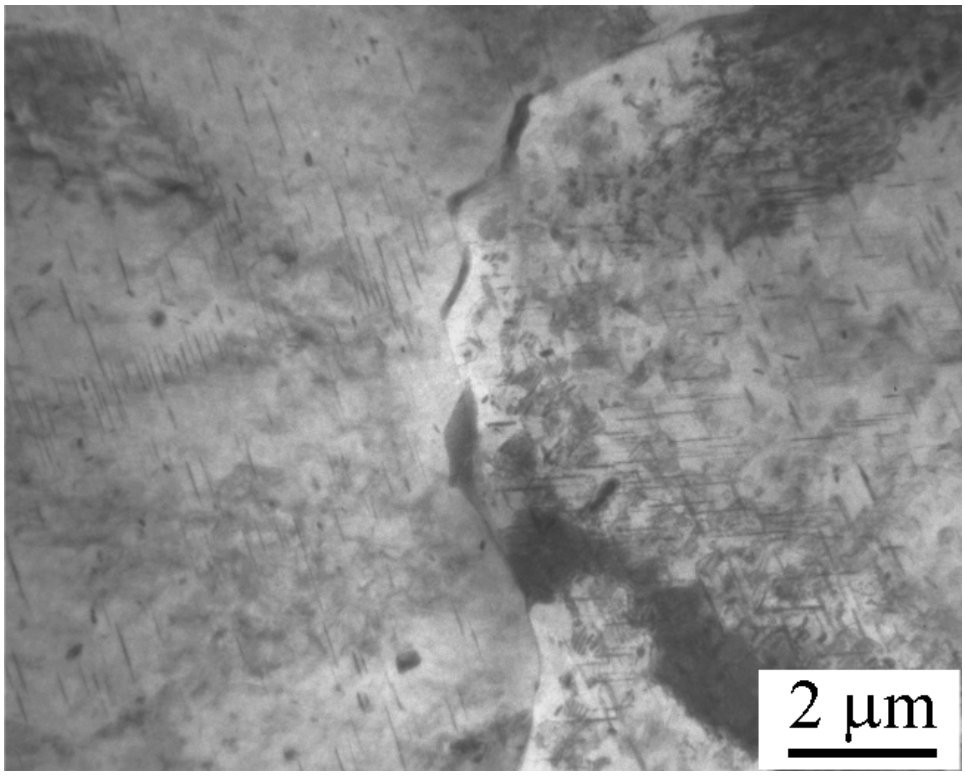

Figure 3-10. TEM micrograph of AF/C458 plate subjected to FSP.

OIM results showed similar grain size to that determined by OM/TEM, with an average grain diameter of 11.5 micrometers. Reference axes remain the same for FSP as the AR sample. The pole figures (PF) and inverse pole figures (IPF) were examined for the top, mid-thickness, and bottom portions of the FSP zone through the thickness of the plate. Analysis revealed an average decrease of approximately 4 micrometers in grain size from the surface to the bottom of the plate as shown in Figure 3-11 a). Overall, the

grain boundary misorientation distributions were flatter than for the AR plate and varied slightly through the thickness with the bottom having the largest number of high angle boundaries. This is illustrated in Figure 3-11 b)-e). Texture also varied, with the top having the most distinct and the bottom a nearly random texture. A sample texture of the mid-thickness rotated 90^{o} by RD showed two <111>//ND fiber components. Such a texture is consistent with shear deformation due to the rotating tool. IPF indicates a continuous dynamically recrystallized grain structure.

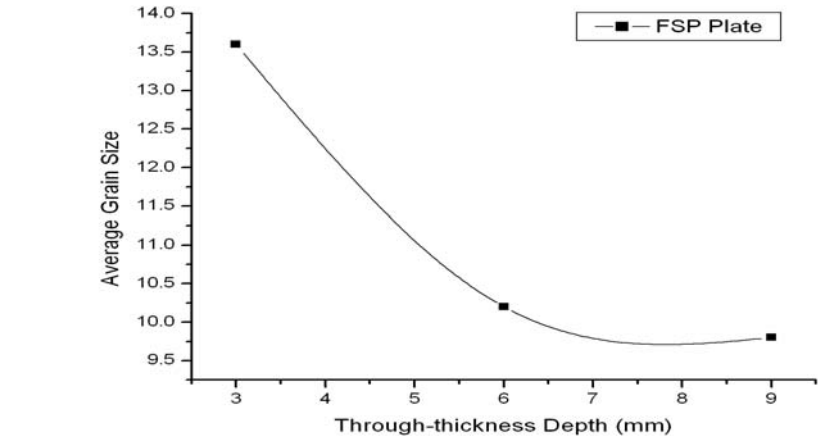

a)

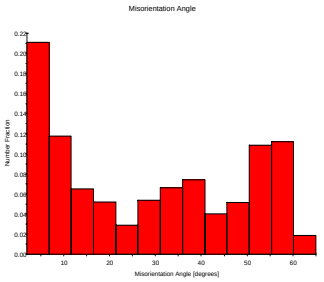

b)

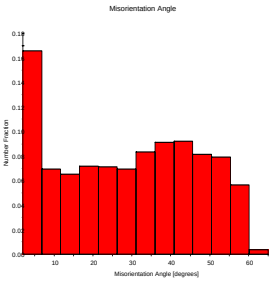

c)

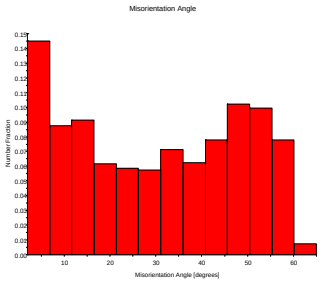

d)

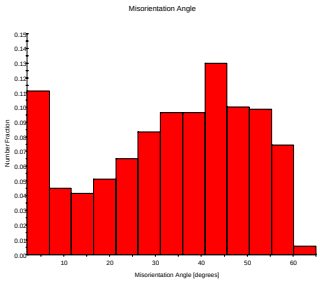

e)

Figure 3-11. OIM results for FSP plate; a) variation in average grain size as a function of depth. Misorientation angles for b) AR plate c) surface d) mid portion e) bottom portion of FSP of plate.

2. FSP Mechanical Properties

All FSP material displayed an apparent loss in yield and tensile strength of the material following friction stir processing as indicated from the tensile and hardness data included in Appendix B. As seen in Figure 3-12, hardness results showed a significant decrease in hardness in through-thickness with an average decrease of approximately 34 HRB from the surface to the bottom of the plate. Standard deviation in hardness measurements for the FSP plate was +/- 2.5 HRB.

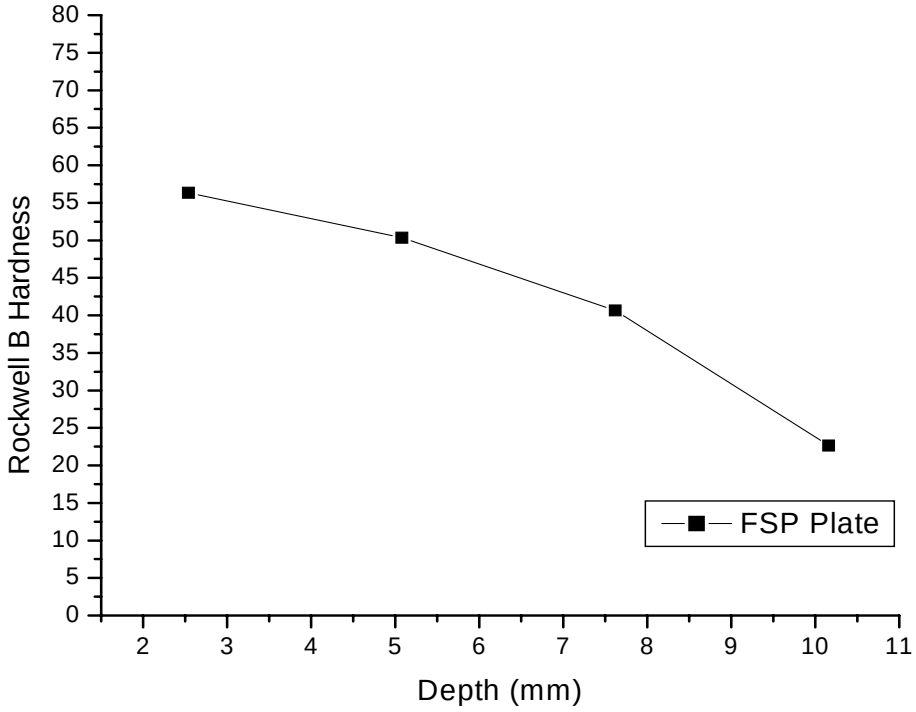

Figure 3-12. HRB as a function of depth of the FSP plate.

Stress/strain curves for the midplane longitudinal and transverse samples of the FSP plate were plotted and included in Appendix B. Results show a midplane yield strength of 271 MPa and a tensile strength of 329 MPa. Transverse properties were slightly lower at 214 MPa (YS) and 308 MPa (UTS). Short transverse tensile testing results revealed an improved ductility S-T direction rendering the material nearly isotropic in ductility with 8.6, 7.1, and 7.0 % in the L, T, and ST directions respectively.

Fracture surfaces were nominally oriented 25-35^{o} with respect to the load axis with the fracture path through the width of the gage area following a 45^{o} angle. Micro-specimens exhibited the same fracture characteristics as the L and T orientations. Some necking was observed. Fractography revealed mostly intergranular fracture with some microvoid formation on the grain surfaces (Figure 3-13).

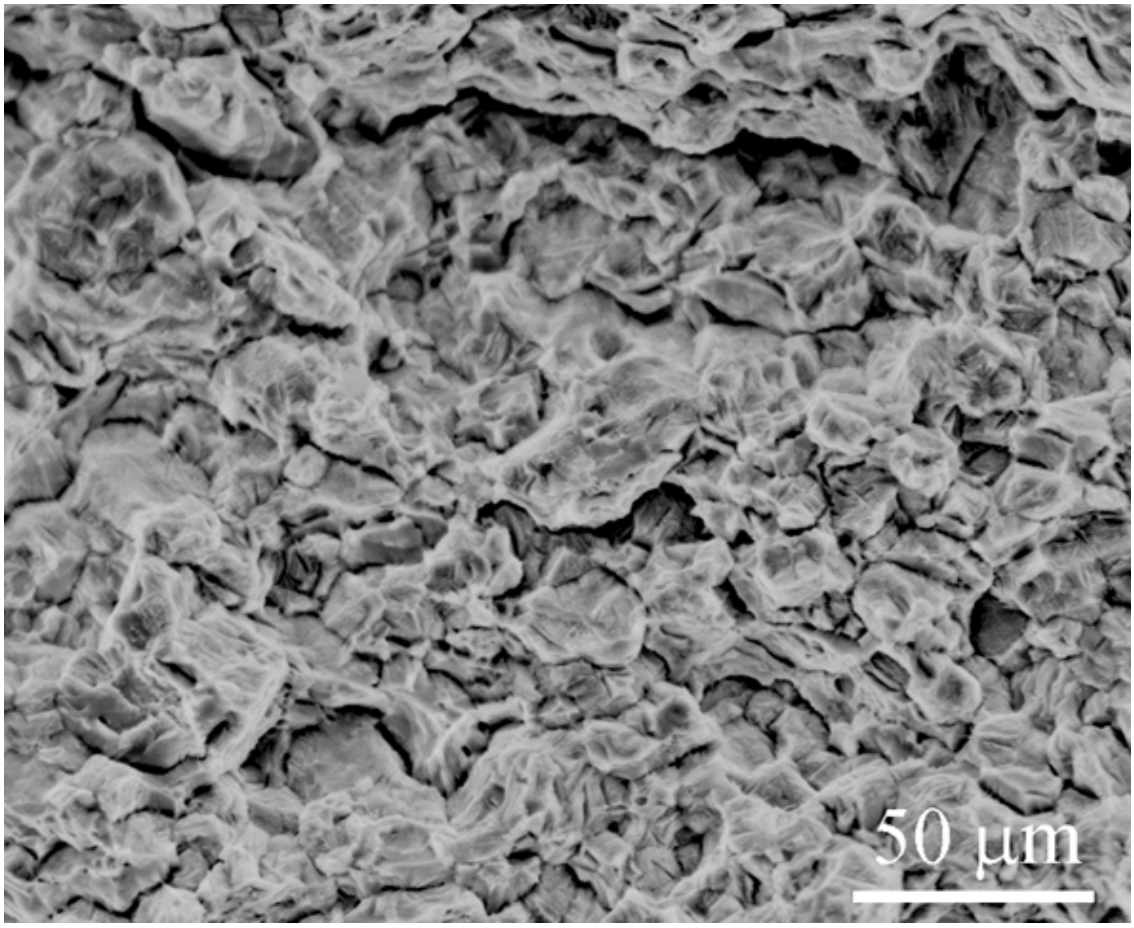

Figure 3-13. SEM fractograph (500x) of FSP tensile sample showing intergranular fracture.

Anticlastic bend testing results are shown in Figure 3-14. Fracturing occurred in the plane parallel to the normal of the plate surface. All specimens tested at the various loads failed by the same mode. Specimen failure did not occur instantaneously but required numerous cycles and fracture paths to develop. Failure was mixed (both ductile and brittle) with fatigue striations visible. Transition from ductile to brittle usually occurred around the midplane of the sample.

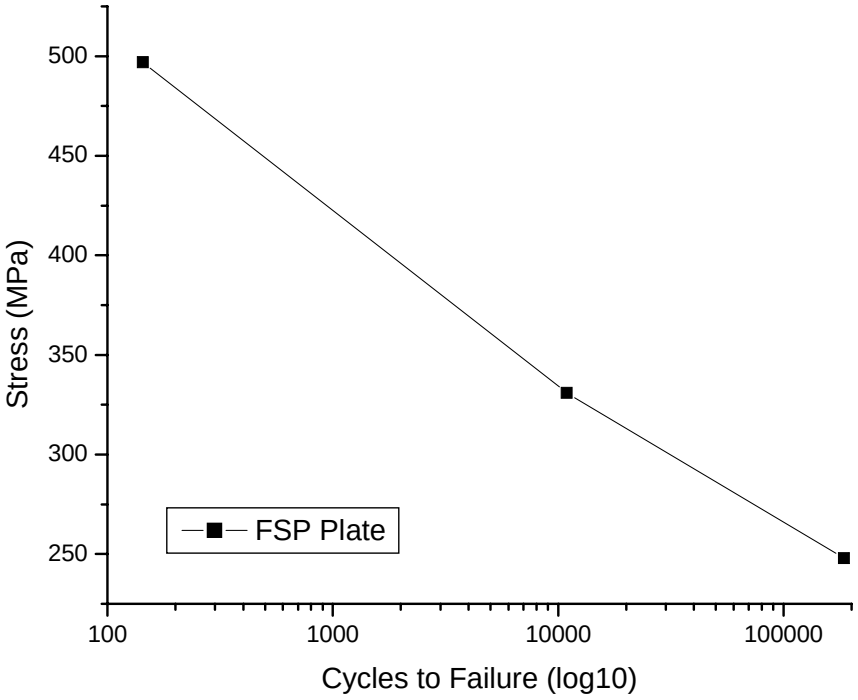

Figure 3-14. Anticlastic fatigue testing results for the FSP plate.

C. HEAT TREATED FSP PLATE

1. Effect on Microstructure

The TEM results indicate that subsequent aging has little effect on the size and amount of coarse precipitates within the matrix and at the grain boundaries. The most significant effect was the re-precipitation of the fine δ' that was absent following FSP. There also seemed to be a greater relative area of grain boundary occupied with precipitates than in the FSP material prior to heat treatment.

2. Effect on Mechanical Properties

Post FSP heat treatment (HT) resulted in a recovery of some lost mechanical properties. As seen in Figure 3-15, there was an initial drop in hardness for heat treatments less than 2 hours followed by a gradual increase in hardness. After about 24 hours, no significant increase in hardness was observed. For this reason, post FSP heat treatments for tensile and anticlastic testing were conducted with a 24 hour post FSP heat treatment @ 148 ^{o}C.

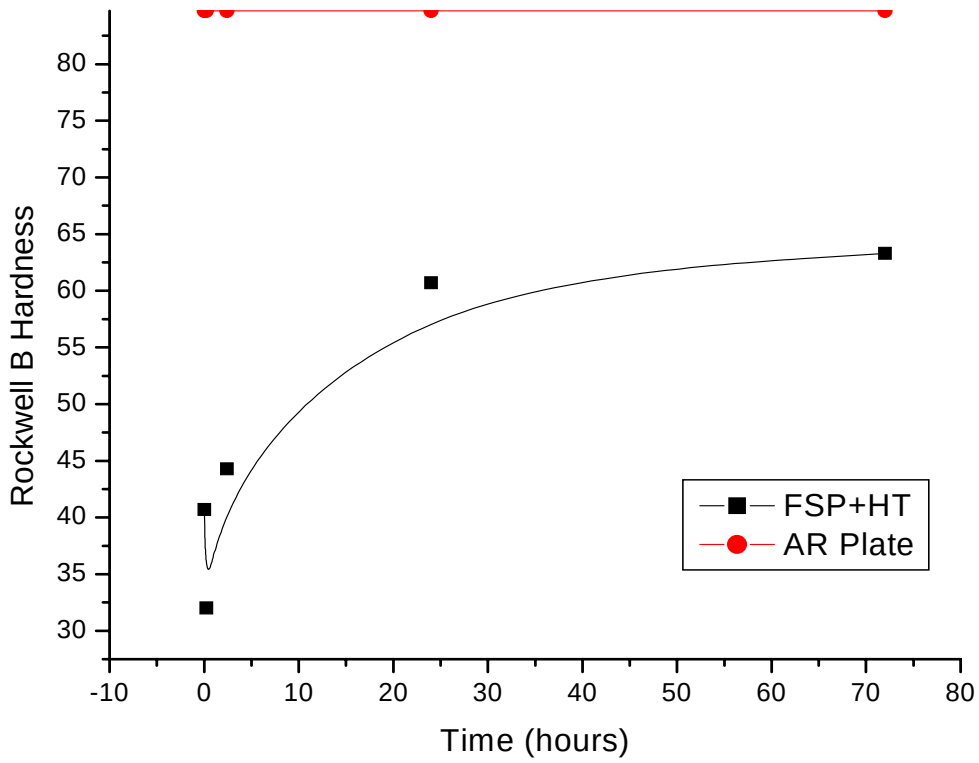

Figure 3-15. Hardness response of FSP plate following heat treatment at 148°C (B-Spline curve fit on FSP+HT data).

SSC for FSP+HT in the longitudinal orientation (midplane sample) is included in Appendix B. Post FSP aging resulted in a yield strength of 295 MPa, tensile strength of 351 MPa, and % elongation of 10%. A second midplane sample using the same heat treatment was allowed to naturally age at room temperature for 30 days prior to testing. No appreciable difference in yield or tensile strength was seen but a 2 % increase in ductility was observed. Fracture morphology of tensile samples for all orientations were the same as FSP specimens without heat treatment. SEM fractographs are included in Appendix C and show no appreciable difference from the FSP samples without post FSP heat treatment.

Anticlastic bend testing results are shown in Figure 3-16. Fracturing occurred in the plane parallel to the normal of the plate surface. All specimens tested at the various loads failed by the same mode. Specimen failure did not occur instantaneously but

required numerous cycles and fracture paths to develop. Failure was mixed (both ductile and brittle) with fatigue striations visible although less area of cyclic fatigue was observed when compared to FSP samples without HT. There were no signs of mixed (normal v. delamination) in any of the heat-treated samples tested. The post FSP heat treatment effect on the microstructural, mechanical, and fatigue properties will discussed in greater detail in the following section.

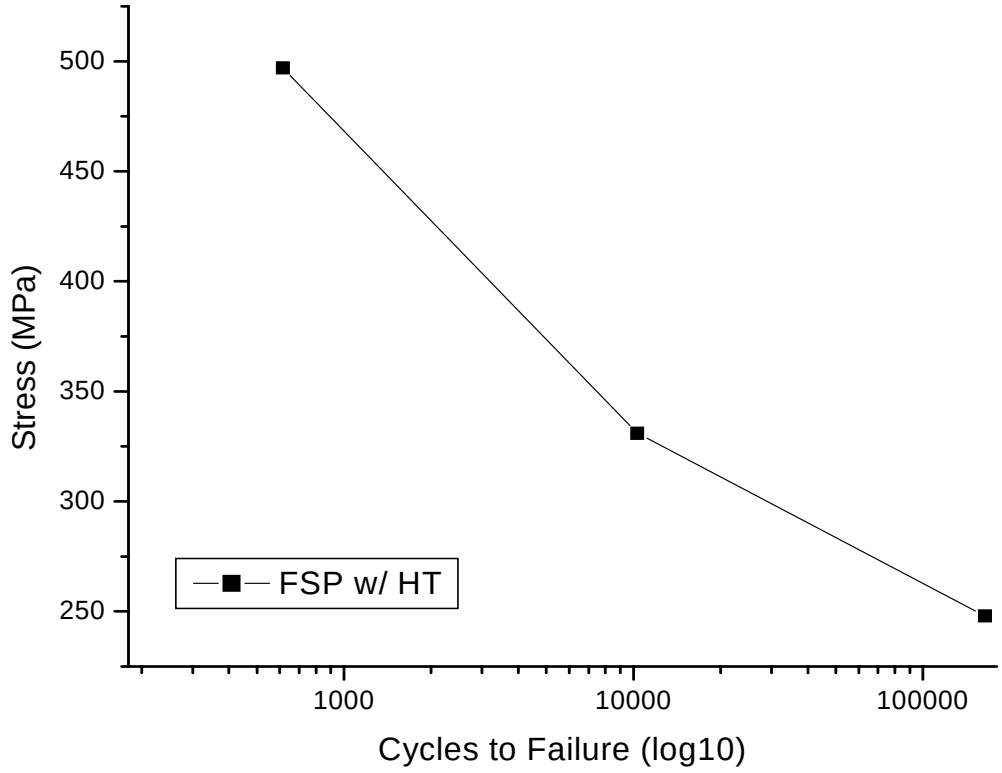

Figure 3-16. Anticlastic fatigue results for FSP following heat treatment @ 148 ^{o}C for 24 hours.

THIS PAGE INTENTIONALLY LEFT BLANK

IV. DISSCUSSION

A. MICROSTRUCTURAL CORRELATION TO MECHANICAL PROPERTIES

The AF/C458 plate is a precipitate hardened material containing several strengthening phases, specifically θ', δ', and T_1. The θ' phase is a semicoherent precipitate with a tetragonal structure that grows as thin plates on the $[001]_\alpha$ planes, whereas the hexagonal T_1 platelets appear on the $\{111\}_\alpha$. The spherical β' phase is typically less than 0.5 micrometers in diameter and is homogenously dispersed in the matrix; however, β' can occasionally be seen at high angle grain boundaries [9]. The δ' phase nucleates and grows on Guinier-Preston (GP-I) zones [5, 17-18].

Prior research has determined that friction stir processing temperatures of aluminum lithium alloys can reach up to 400-550^{o}C within the stir zone. At these temperatures, existing precipitates in aluminum alloys can coarsen or re-dissolve into aluminum matrix depending on the alloy composition and temperatures reached [15]. Recent AF/C458 studies have identified the T_1 solvus boundary at approximately 120^{o}C and determined that T_1 precipitation dominates that of the other phases, θ''/θ' and δ', in competition for solute (Cu and Li) when heterogeneous nucleation are present [5]. In a previous study, Yoshimura *et al.* [18] findings showed that δ' required an incubation period in 1.6wt% Li alloy, suggesting that nucleation of this phase does require an activation energy due to a small but non-zero interfacial energy and the diffusion of Li in the Li-lean alloys [19].

T_1 is an equilibrium phase that grows at the expense of the metastable δ'. As shown in the aluminum lithium phase diagram in Figure 4-1, dissolution of T_1 and δ' most likely occurs in the predicted temperature range for friction stir processing. As previously mentioned, this suggests a competitive reprecipitation of T_1 and δ' occurs and is dictated by precipitation kinetics and availability of nucleation sites.

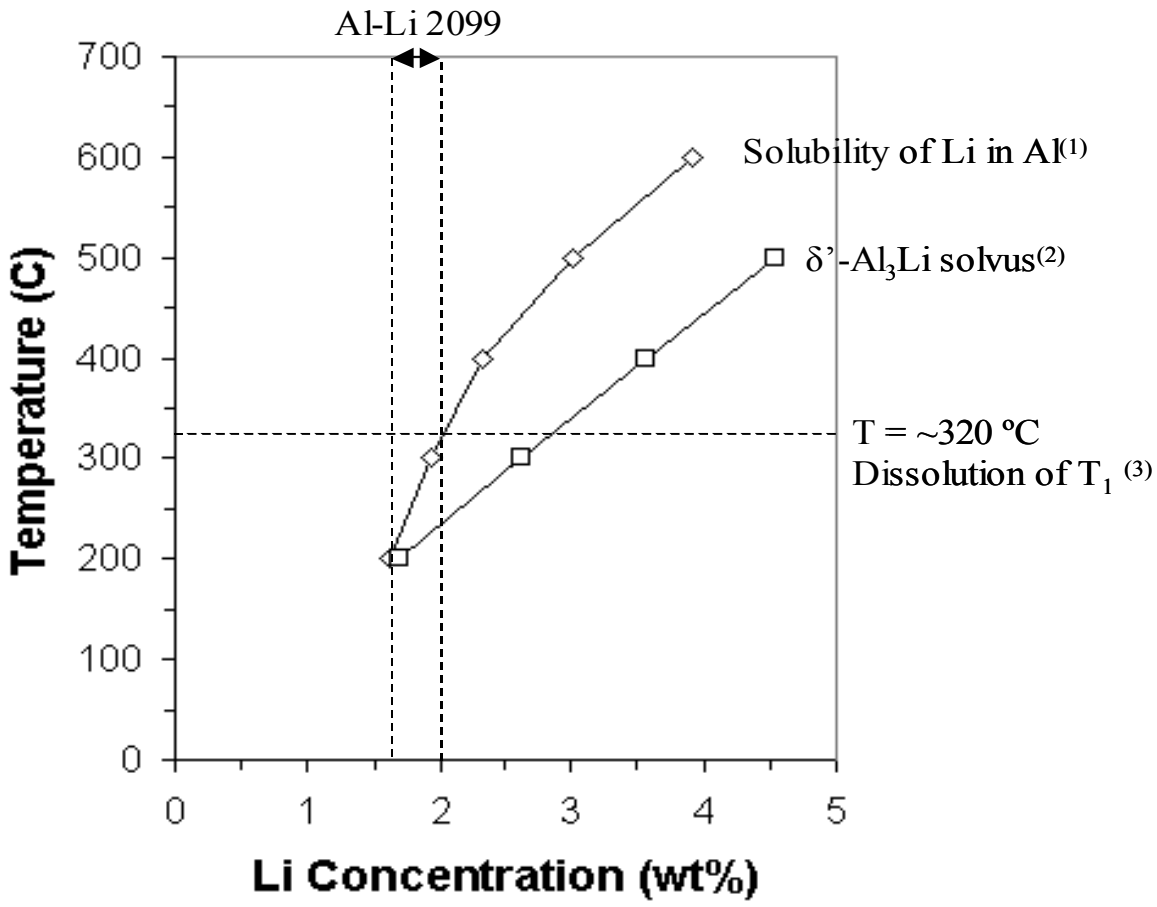

Figure 4-1. Aluminum lithium phase diagram with metastable solvus line with Li range for AF/C458 (AA2099) indicated [From Ref. 3, 20-22].

As seen in TEM results, the AR plate shows $\{111\}_{\alpha}$ platelet precipitate formation along with the spherical β' and fine δ' precipitates within the matrix. Some precipitation is found along grain and subgrain boundaries. Following FSP, several key changes occur in the microstructure; specifically, the dispersion strengthening precipitate δ' reverts to solution. In addition, an increase in size and number of grain/subgrain and the intragranular platelet precipitates occur suggesting dissolution, coarsening, and reprecipitation of the precipitates occurring during FSP. Interestingly, post FSP heat treatment had little effect on the number and size of coarse precipitates.

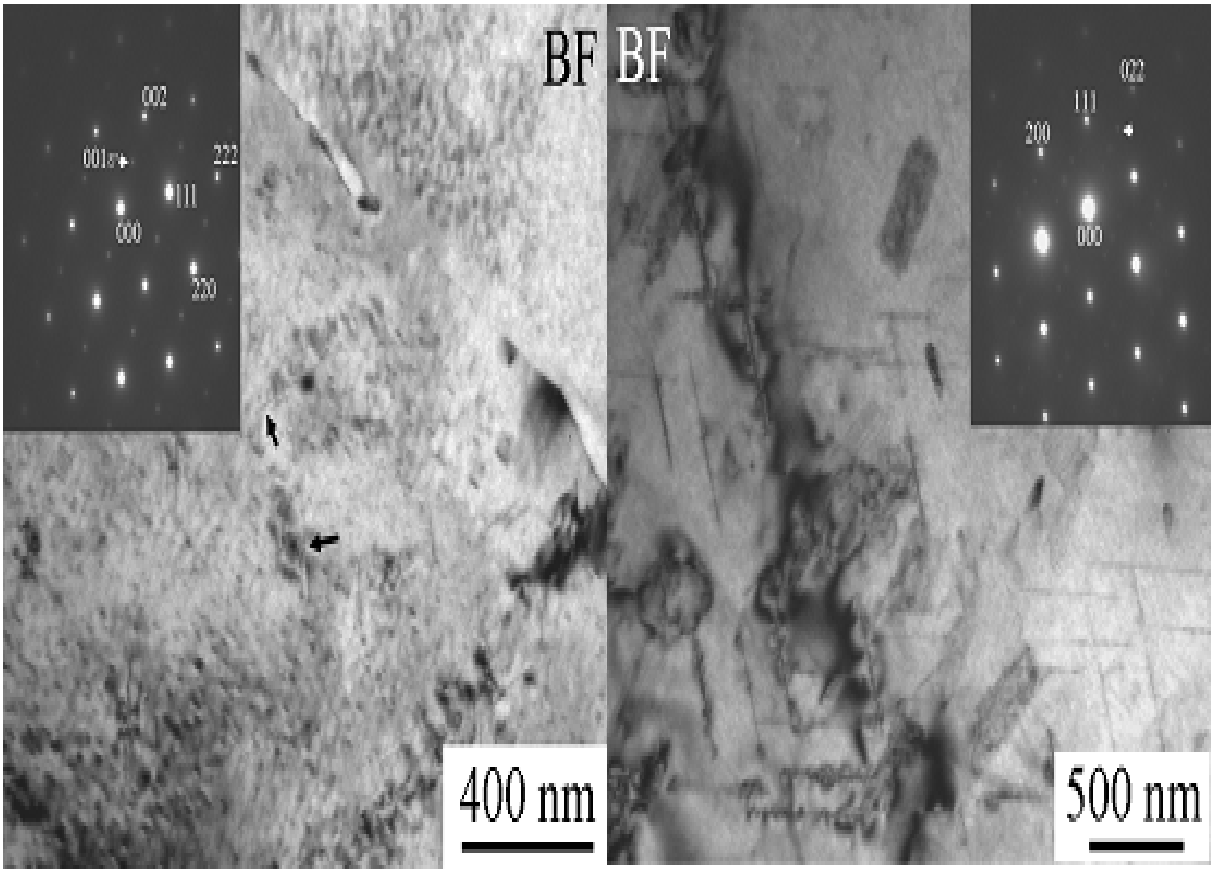

Figure 4-2. BF TEM micrographs of AR and FSP plate with a comparison of (110) SAD patterns.

The OIM data seems to indicate that the original grain and subgrain boundaries appear to be replaced with fine equiaxed recrystallized grains in the processed zone. Prior studies suggest a mechanism of continuous dynamic recrystallization [11,14] and suggest a hardly altered yet severely rotated texture following FSP. During friction stir processing the material undergoes intense shearing and concurrent dynamic recrystallization [14, 19,22]. Texture evolution during FSP is complex and still being studied. Texture data, with a 90^{o} rotation about RD, showed two <111>//ND fiber components comparable to those found in similar Al-Li alloys [19].

Hardness testing following FSP showed a marked decrease in hardness through the thickness of the plate with the bottom portion having the lowest values. This correlates with the area in contact with the bottom portion of the tool. In FSP, full penetration is not achieved and, in this case, the bottom ~1-2 mm was not "stirred." In

FSW, the thermomechanically affected zone (TMAZ) is a transition zone between the stir zone and the heat affected zone (HAZ) of the parent metal where the elongated grains are highly deformed but do not undergo recrystallization. In the HAZ, the parent material experiences a thermal cycle but does not undergo any plastic deformation. There is little or no TMAZ in the through thickness of the FSP material, essentially due to the tool orientation when compared to the grain morphology, i.e. bottom of tool transverses along the "top" of the pancake-shaped grains. It should be noted, however, that the HAZ is present in the last two millimeters of plate since the tool did not achieve full penetration.

Most research in FSW indicates that the peak temperature and extent of deformation dictate the recrystallized grain size achieved during FSW/FSP; larger grain size develops towards the surface in contact with the tool and decreases outwardly from the processed zone, corresponding to temperature variations within the processed zone. In addition, the bottom portion has a lower peak temperature and shorter thermal cycle due to the backing plate (used during processing) that acts as a heat sink, effectively retarding grain growth [15,19,22-24]. OIM data correlates with these findings in the form of ~4 micrometer decrease in grain size from the surface to the bottom of the plate. Usually, an increase in hardness is associated with a decrease in grain size leading to the assumption that the bottom would have the highest value, which was not the case. However, However, AF/C458 is a precipitate hardened material deriving its strength less from grain size and more on allocation and distribution of strengthening precipitates as well as strain hardening. Therefore, the most likely cause for the drop in hardness for the lower portion of the plate is the coarsening and dissolution of precipitates during the subjected thermal cycle. The tool shoulder may also provide strain hardening at the plate surface

A decrease in hardness is directly associated with a decrease in strength. Hence, as explained above, the loss of strength following friction stir processing is most likely due to the change in type, size, and distribution of strengthening precipitates. The UTS_{FSP} / UTS_{AR} ratio between the FSP and AR plate tensile strengths were 0.68, 0.64, 0.68 in the L, T, and S-T orientations respectively. For elongation, the ratios were 1.07, 1.15, and 2.8 in the L, T, and S-T orientations respectively. The ratios obtained in this study are comparable to published results for similar alloys [15].

Figure 4-3 illustrates a comparison of the mechanical properties measured for each sample examined during this study. The anisotropy in ductility is apparent in the as received material. As expected from earlier discussion on the issues with aluminum lithium alloys, the S-T orientation ductility exhibits extremely low ductility. Notably, the ductility becomes nearly isotropic for all orientations following FSP, with a remarkable increase in the S-T direction, nearly 3 times greater than the AR plate as illustrated in the SSC curves shown in Figure 4-4.

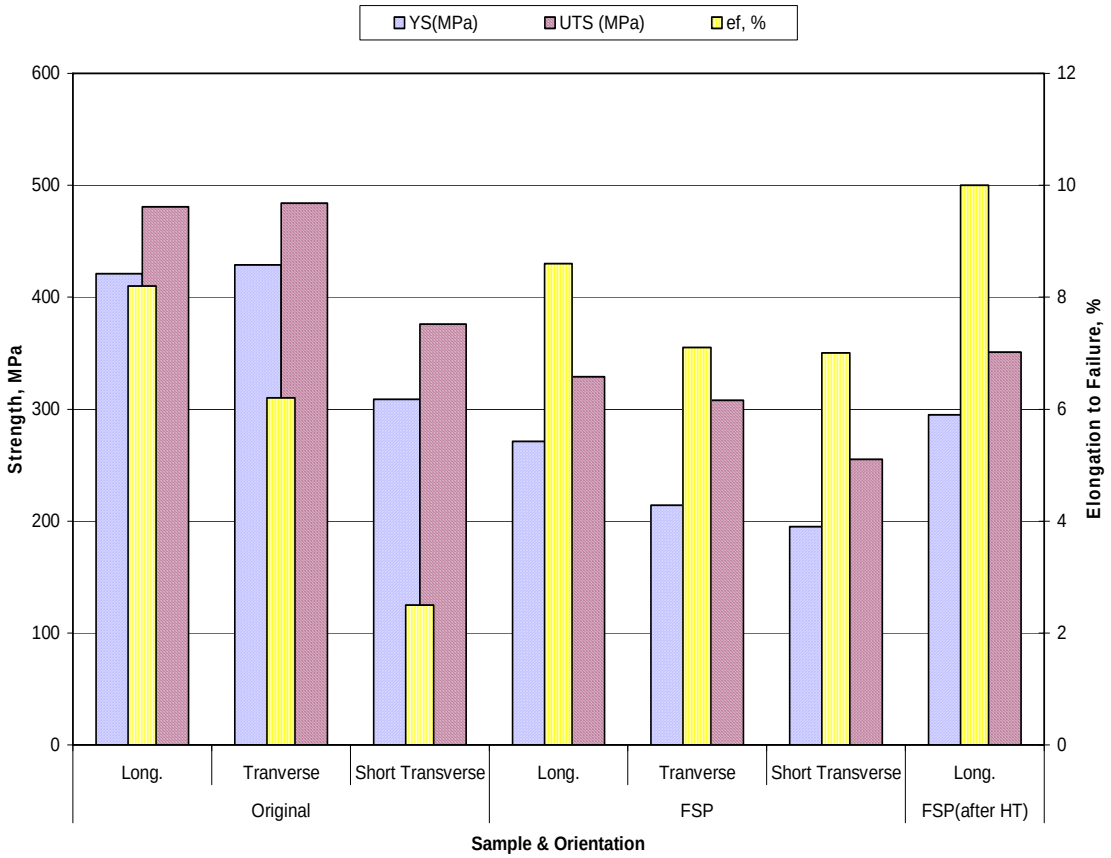

Figure 4-3. Mechanical properties for AR and FSP specimens in the L, T, and S-T orientations. FSP+HT is provided in the L orientation only.

A reduction in ductility has been accounted for by an increase in fine hardening precipitates and the development of PFZs [15,23]. The slight increase in ductility for the L and T orientations following FSP may be attributed to change in grain structure despite the precipitation events. This is supported by the ~2.5% increase in ductility from the

longitudinal FSP sample following post FSP heat treatment. There was little change in the size and number precipitates except the reappearance of δ', which would be expected to reduce ductility. On the other hand, there was a significant change in grain morphology when compared to the AR plate suggesting that the smaller, equiaxed grains increase grain boundary surface area, therefore, inhibit planar slip mechanisms.

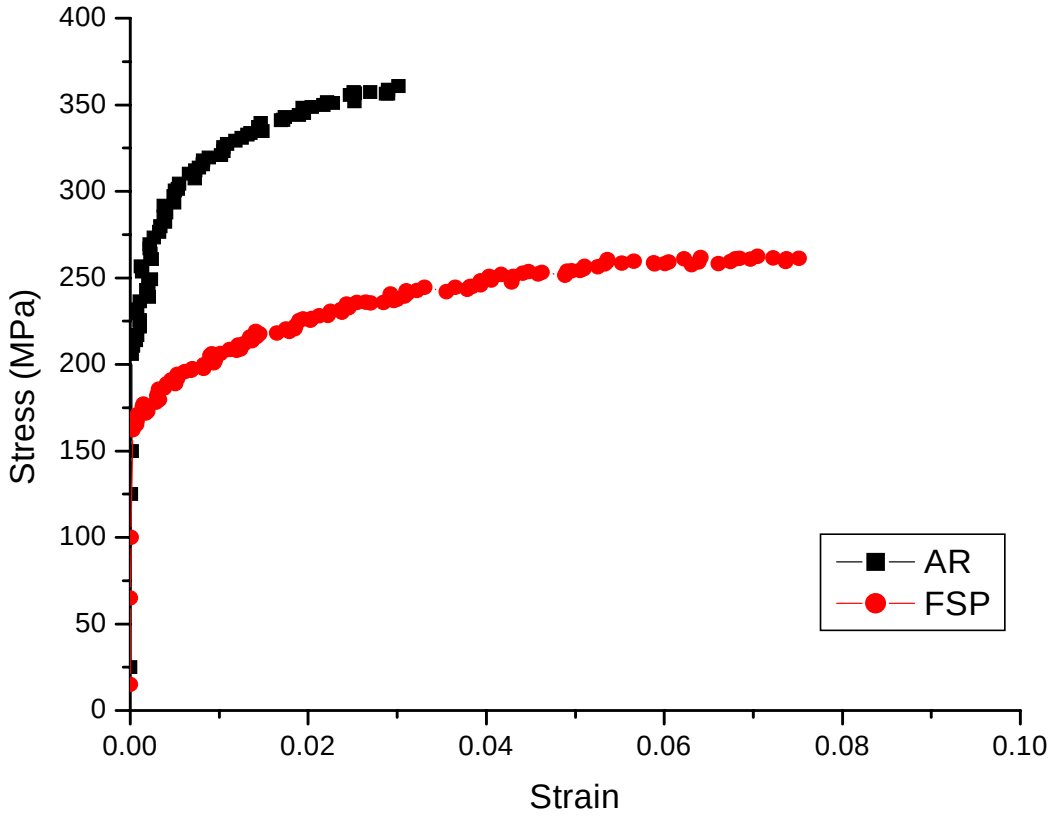

Figure 4-4. Comparison of SSC through-thickness curves for FSP and AR plate.

B. FATIGUE

For aerospace applications, fatigue properties are critical. Evaluation of the fatigue behavior of the AR and FSP plate using anticlastic bend testing revealed some interesting results. Only one sample of the AR, FSP, and FSP (+24 hr HT) was tested at each stress level and, unfortunately, there always exists considerable scatter in fatigue data at the same stress level. For this reason, the data is given as a qualitative assessment illustrating the weaknesses of Al-Li alloys and to note whether friction stir processing hinders the propensity for delamination.

1. Change in Fracture Mode

Without question, friction stir processing eliminates the tendency for delamination in AF/C458 plate (Figure 4-5). As discussed earlier, there are several proposed mechanisms to explain low S-T fracture toughness in Al-Li alloys. Key changes to the as-received plate as a result of FSP were: (i) change in grain structure from elongated, pancake-like grains to fine, equiaxed grains (ii) an increase in coarse precipitation (iii) a change in texture and misorientation of grain boundaries. One of the leading explanations for this behavior is δ'-induced planar slip, which terminates at the grain boundary. Accordingly, the degree of delamination would be directly related to the grain size and aspect in relation to the slip plane. TEM analysis of the FSP plate indicated the disappearance of δ', followed by its reappearance after heat treatment. Both FSP and FSP+HT samples failed parallel to the loading direction and not in a delaminating manner. This suggests that grain morphology plays a key part in delamination. It should be noted though that both FSP and FSP +HT samples had a larger number of coarse precipitates to hinder slip processes compared to the AR plate.

Strong textures and the grain morphology of rolled aluminum lithium alloys play a key role in in-plane anisotropy [11]. The finer and more uniform microstructure after FSP also exhibits a shear deformation texture that varies through the thickness of the plate. In addition, mechanical testing indicated a reduction in anisotropy following FSP. It is unclear if and how these contribute to the change in fracture mode.

Figure 4-5. Anticlastic test specimens (FSP-left, AR-right) illustrating change in fracture mode.

2. Fatigue Life

The FSP and FSP+HT samples were tested under the same loads as the AR plate with 2 of the 3 samples considerably above two thirds of the tensile strength of the material. Despite the high applied to yield strength ratio, the FSP material was similar in fatigue life when compared to the AR plate as seen in Figure 4-6. One exception was at the highest load (6.7 kN) in which the FSP sample with no heat treatment failed fairly quickly (143 cycles) compared to the AR (705 cycles) and FSP+HT (615 cycles) plate. The difference in the FSP and FSP+HT plate cycles to failure at this stress is most likely attributed to the reappearance of δ' precipitates hence increased strength after post FSP heat treatment (Figure 4-8). At the lowest load (3.3 kN), friction stir processing shows a considerable improvement in the fatigue life over the AR plate. In addition, when normalized (Figure 4-6 b)), a significant increase in fatigue strength following FSP occurs. This may be attributed to the increased energy required for the normal fracture mode in contrast to delamination.

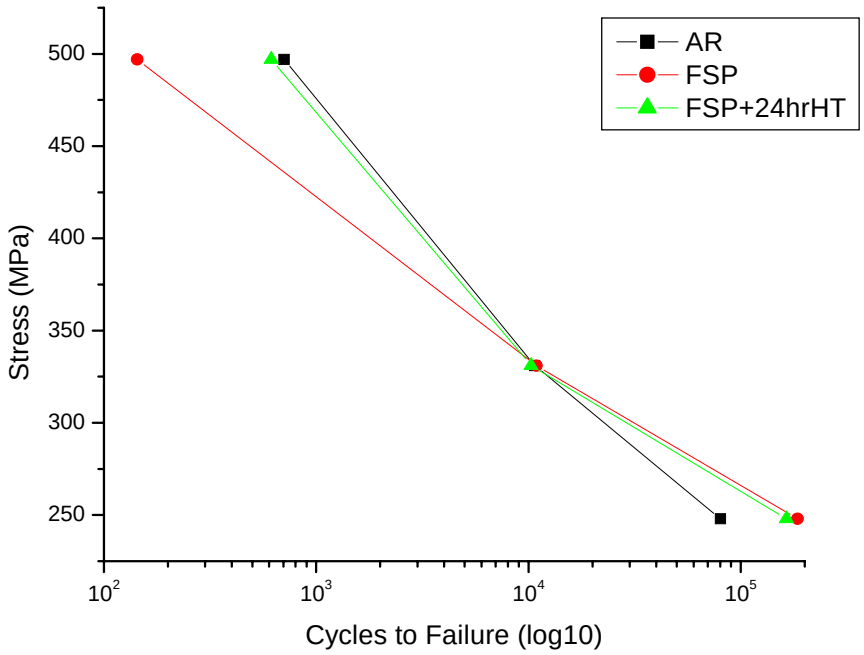

a)

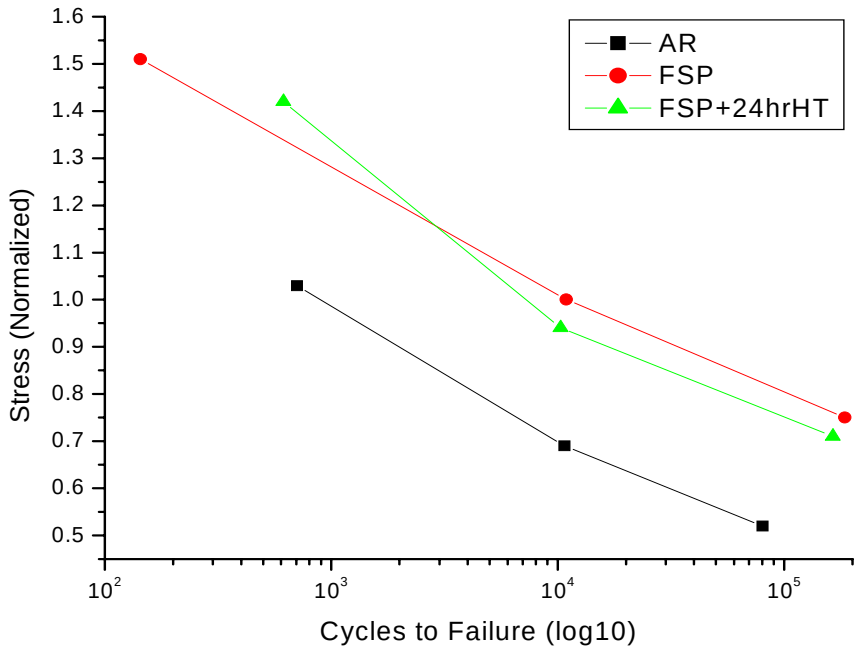

b)

Figure 4-6. a) S-N plot for AR, FSP, and FSP+HT plate b) S-N plot normalized with yield strength.

C. POST FSP HEAT TREATMENT

Post FSP heat treatment results in age hardening of the material. As stated earlier, the major strengthening phases in aluminum lithium co-precipitate and are in competition with each other for solute. Results indicate that during friction stir processing, the T_1 precipitation dominates over δ', leading to its disappearance from FSP TEM results (Figure 4-8). Since there was little difference found in the size or distribution of coarse precipitates in the FSP and FSP followed by aging, it is most likely that the re-precipitation of the fine δ'-phase precipitates in the matrix was the primary contributor to the aging response shown in Figure 4-7 and the recovery of strength as shown in Figure 4-3 and indicated in mechanical testing.

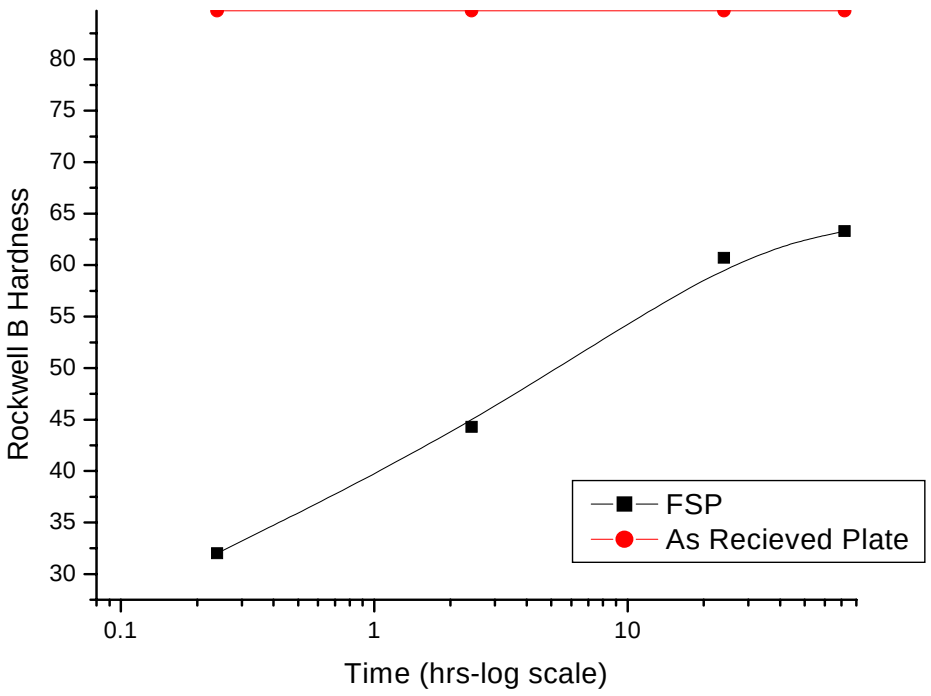

Figure 4-7. Aging response of FSP plate indicating a recovery of strength with post FSP heat treatment.

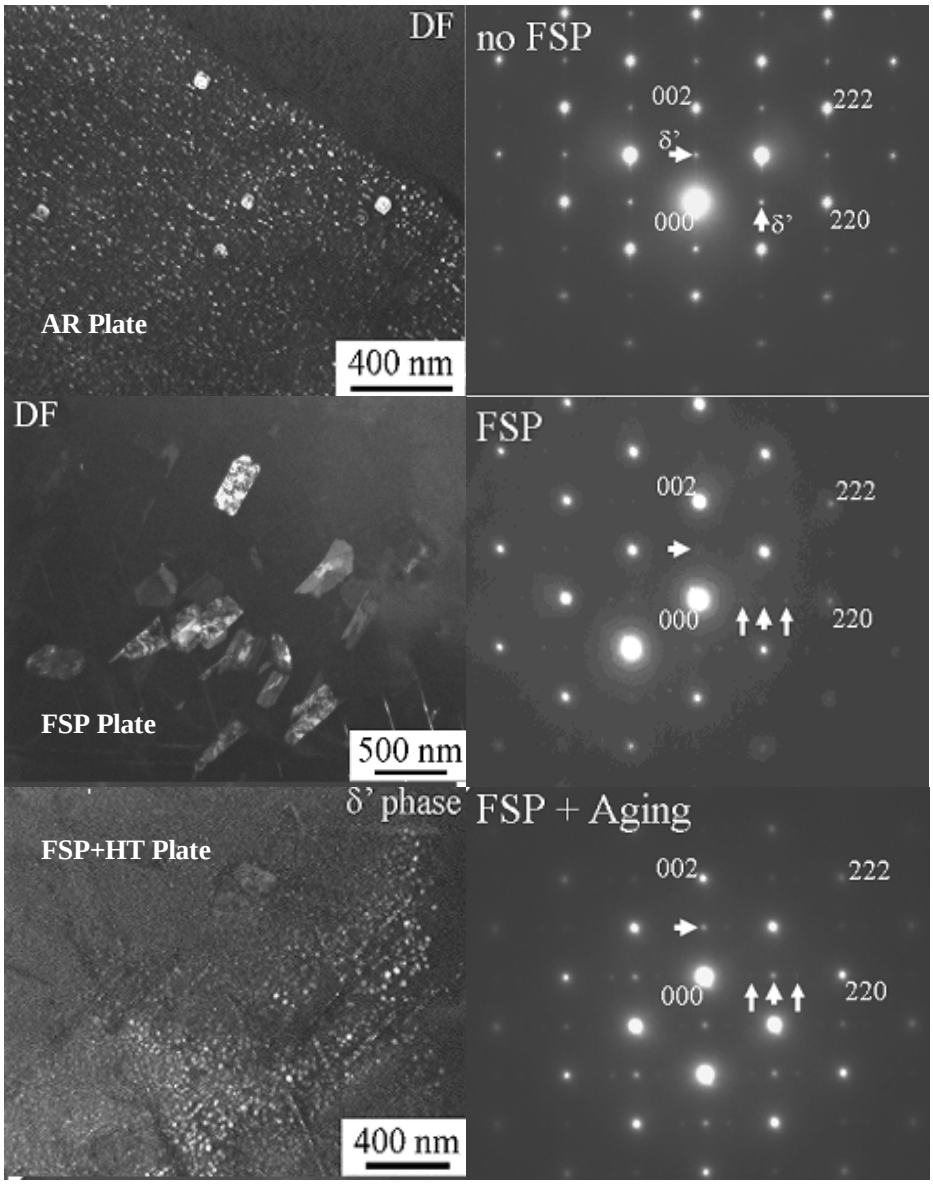

Figure 4-8. DF TEM micrographs with (110) SAD patterns of AR, FSP, and FSP+HT plate showing reappearance of the δ' due to subsequent aging. Before FSP spots of δ' (arrows) are apparent, but after FSP the intensity of the spots are weak. The additional spots (small arrows) appear instead. They may be T_1 phase.

As stated earlier, the FSP material showed a variation in hardness through the thickness of the plate (see Appendix B; Hardness Data), due to strain hardening and the variation in grain size indicated by OIM/OM data. Subsequent heat treatment at the higher aging times showed a gradual shift to a flatter i.e. more isotropic through thickness hardness profile. There are several factors likely involved, including annealing of strain

hardening, various precipitation effects, and changes in grain size. The initial drop in hardness at short aging times (Figure 4-9) was most likely due to a strengthening precipitate returning to solution and recovery effects, as explained above.

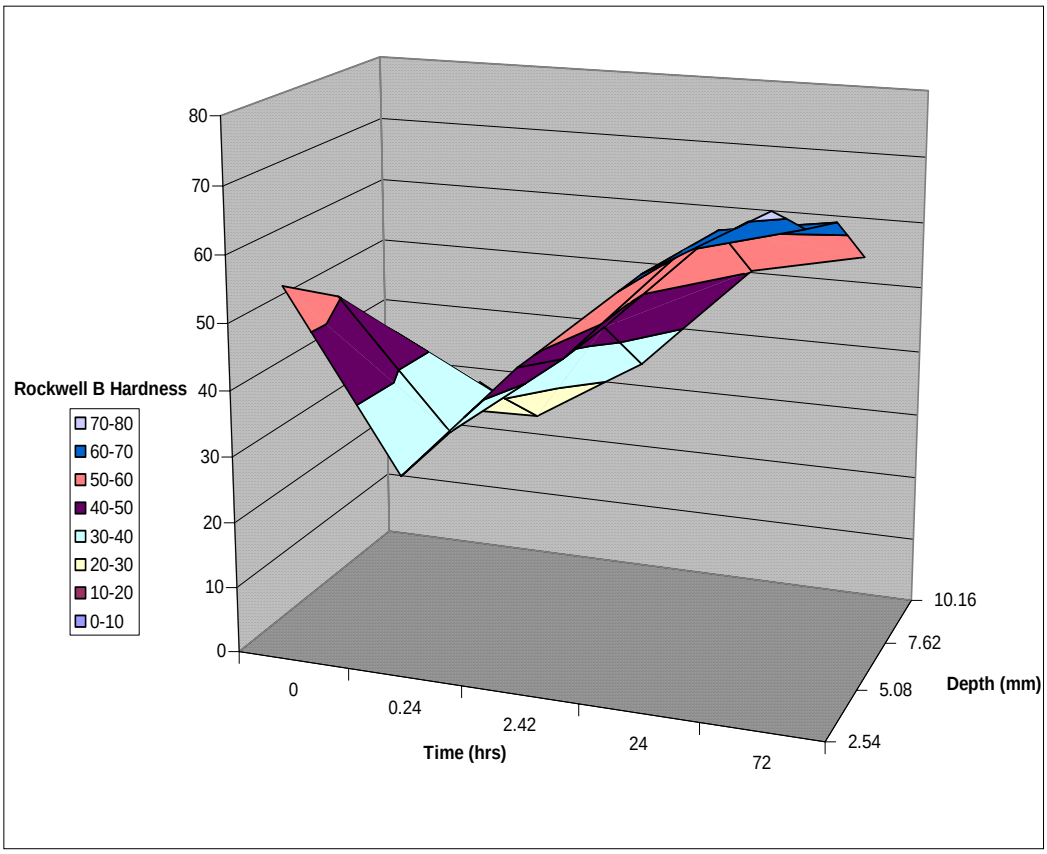

Figure 4-9. Hardness v. aging time profile as a function of through-thickness depth.

V. CONCLUSIONS AND RECOMMENDATIONS

A. CONCLUSIONS

FSP provides the ability to selectively modify the microstructure of a material to achieve desired properties albeit at the expense of others. The following conclusions were drawn from the information and data collected in this study:

1. FSP resulted in a refined, homogenized grain structure.
2. The processed plate exhibited a significant loss in strength.
3. Variations in grain size and subsequent mechanical properties exist through the thickness of the plate.
4. FSP resulted in a nearly isotropic ductility.
5. FSP greatly improved the through thickness ductility of the material.
6. FSP changed the fracture path tendency from perpendicular to parallel with respect to the loading direction.
7. Post FSP heat treatment recovers some strength losses without changing the bend testing fracture mode or sizeable loss of fatigue life.

B. RECOMMENDATIONS

The following areas are recommended for further research:

1. Investigate the effect of ipm/rpm processing combinations along with pattern variations to lessen strength losses following FSP.
2. Investigate the effect of initial temper conditions and post FSP heat treatment/mechanical working combinations for lower strength losses.
3. Examine the effect of friction stir processing both surfaces of the plate as a possible way to mitigate through thickness variations in hardness.
4. In-depth study of FSP variations in the L, T, and S-T orientations.

THIS PAGE INTENTIONALLY LEFT BLANK

APPENDIX A. MICROSTRUCTURAL

A. MICROGRAPHS

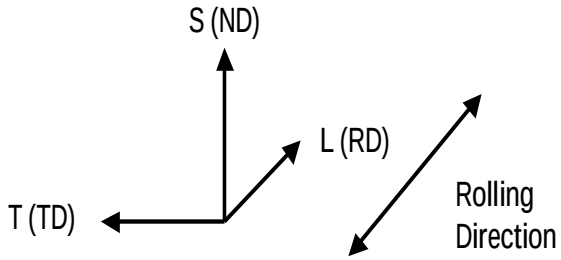

a) b) c)

AR plate at 290x with surface normal to a) S direction b) L direction c) T direction (L direction oriented parallel to the rolling direction)

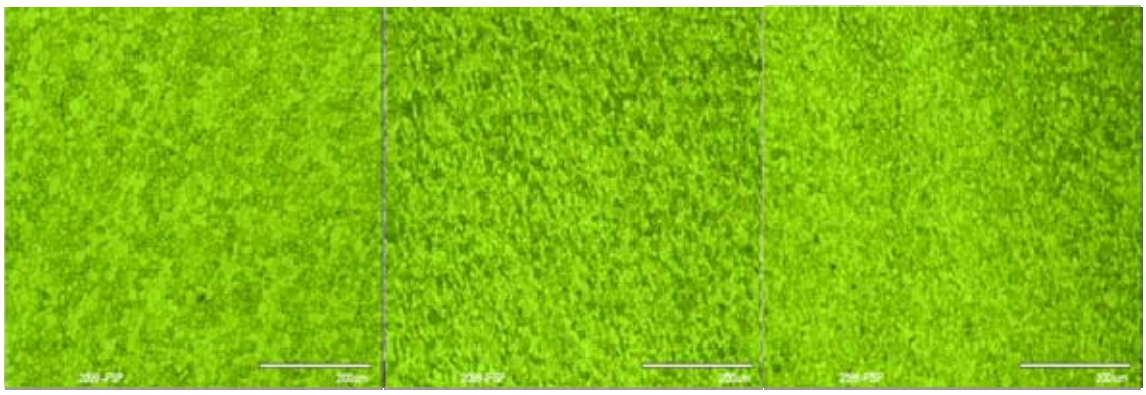

a) b) c)

FSP plate at 290x with surface normal to a) S direction b) L direction c) T direction (L direction oriented parallel to the rolling direction)

B. TEM

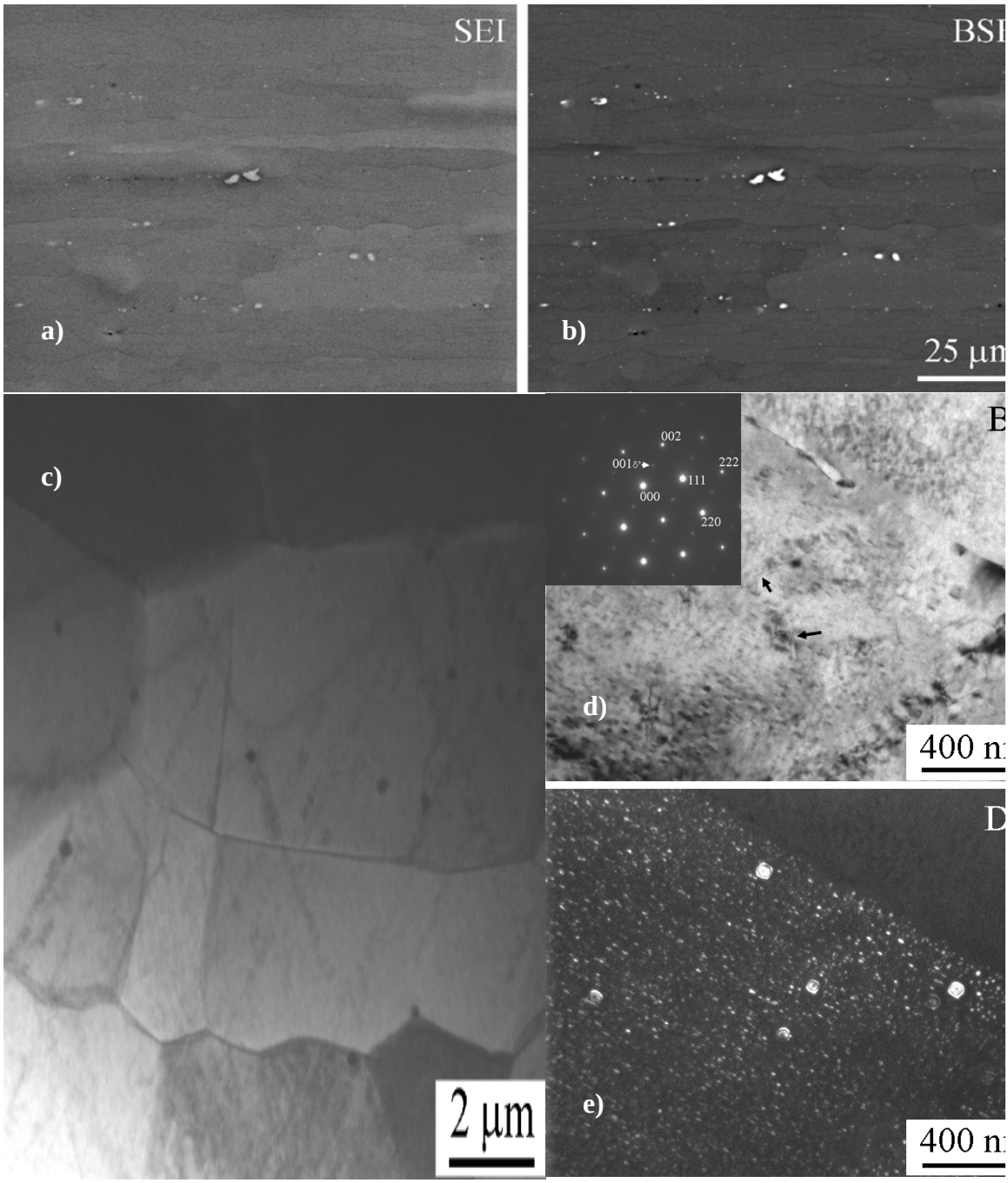

a) SEI and b) BSEI c) and d) BF and e) DF TEM micrographs of AR plate

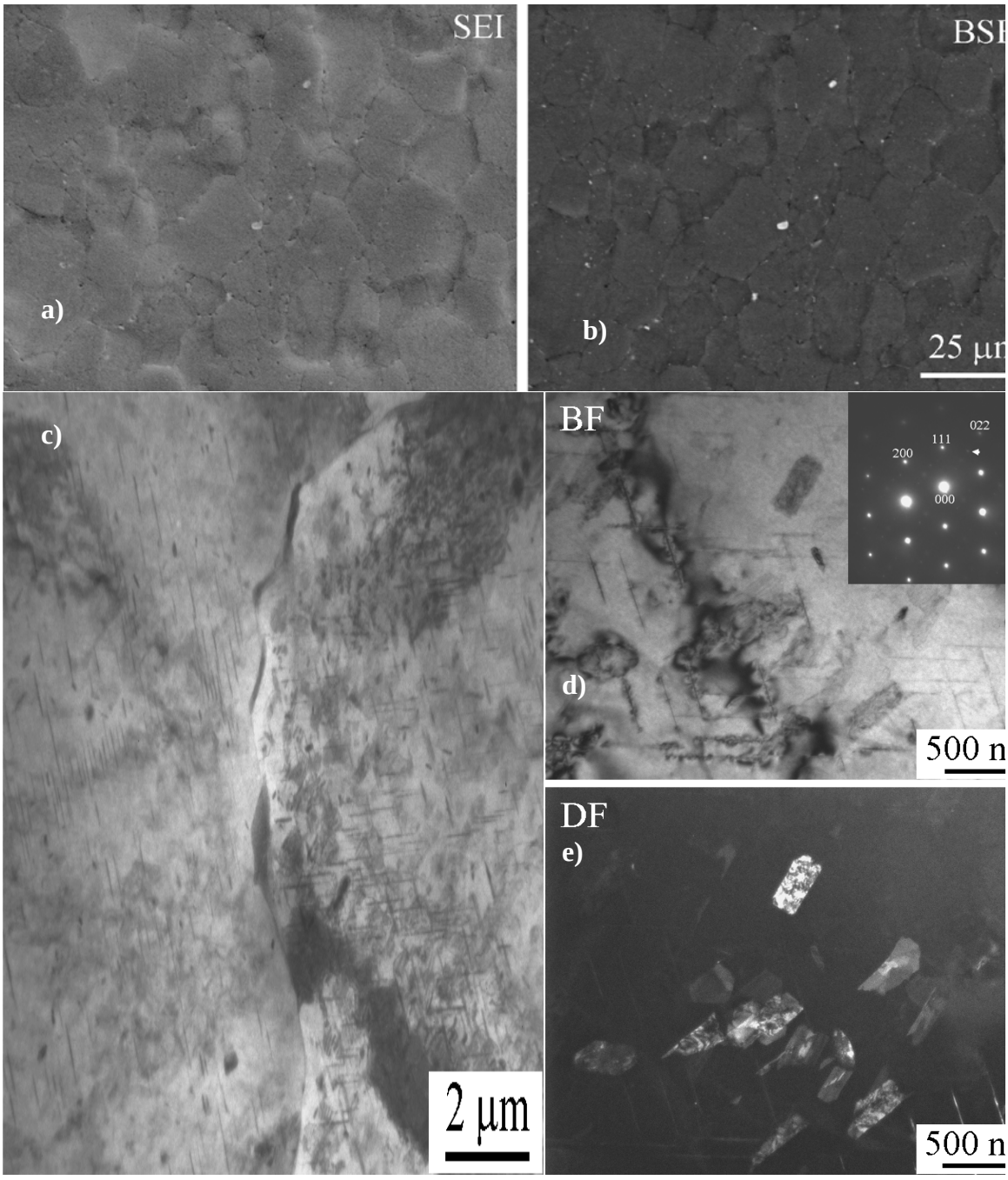

a) SEI and b) BSEI c) and d) BF and e) DF TEM micrographs of FSP plate

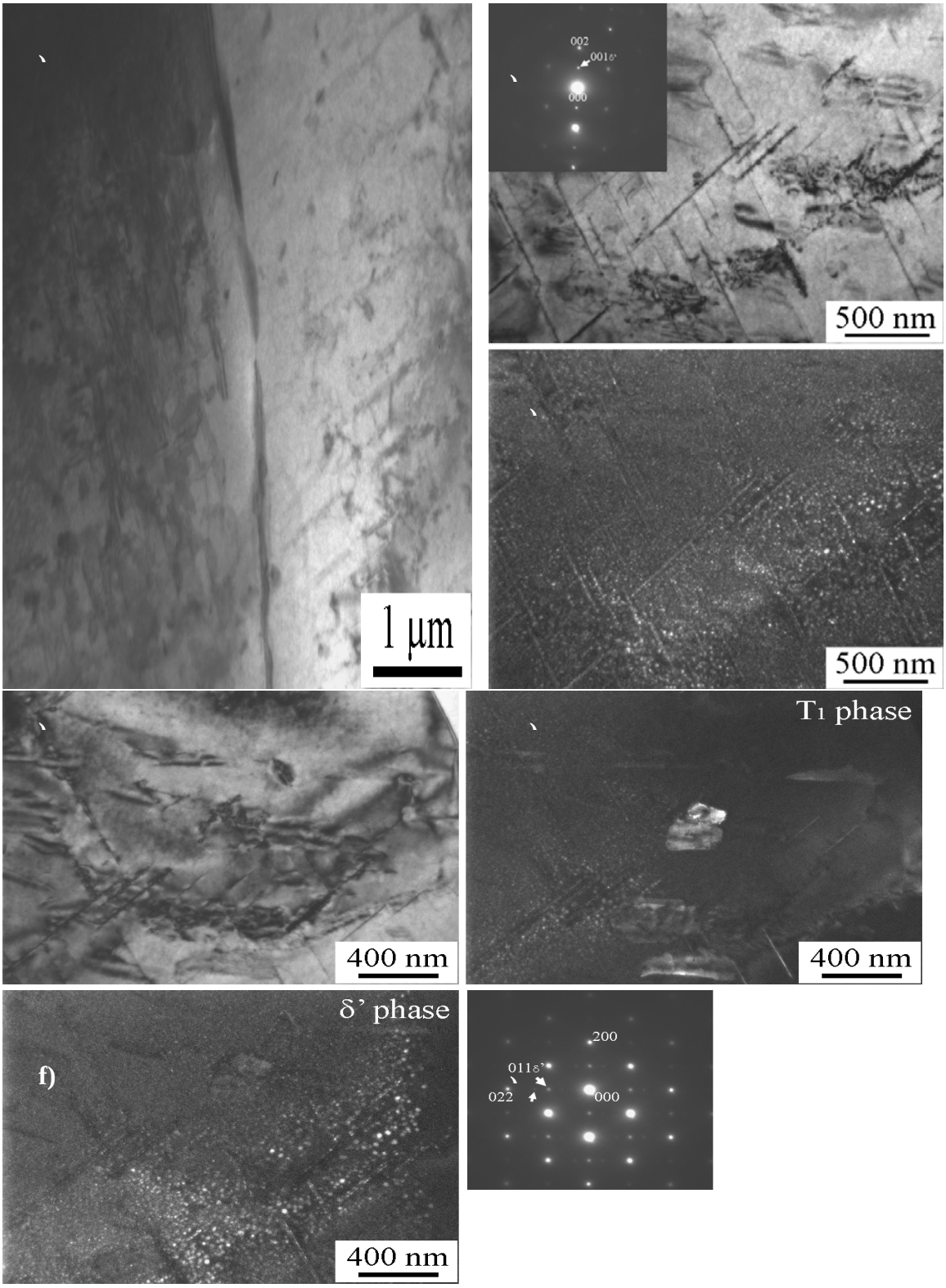

BF (a, b, and d) and DF (c, e, and f) TEM micrographs of FSP plate following aging at 148°C for 24 hours. (e) SAD pattern showing reappearance of δ' phase.

C. OIM

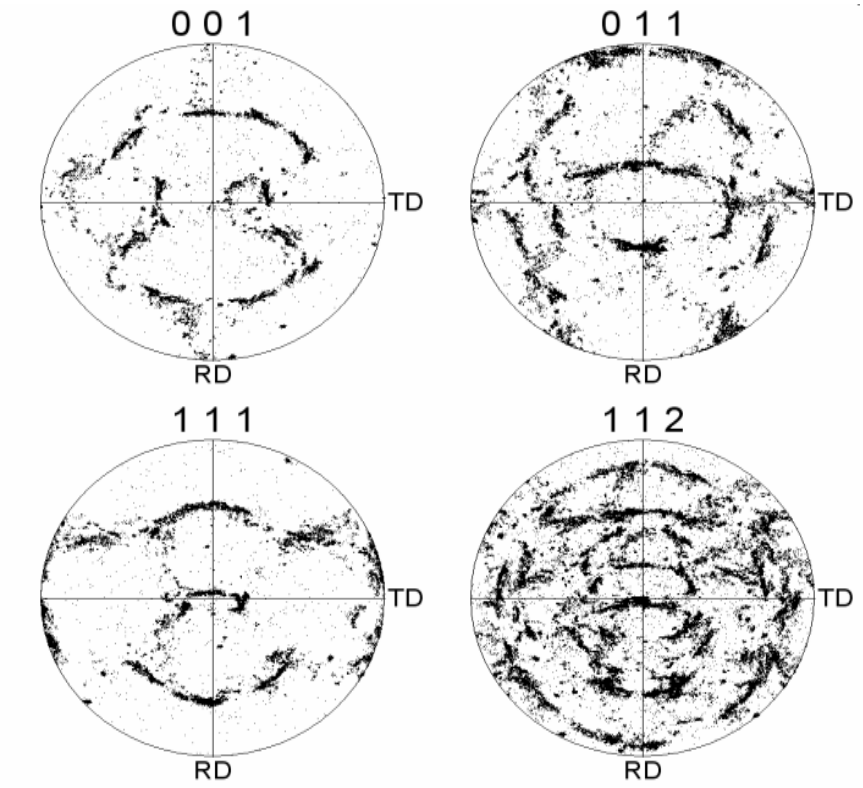
0 0 1
TD
RD
0 1 1
TD
RD
1 1 1
TD
RD
1 1 2
TD
RD

a)

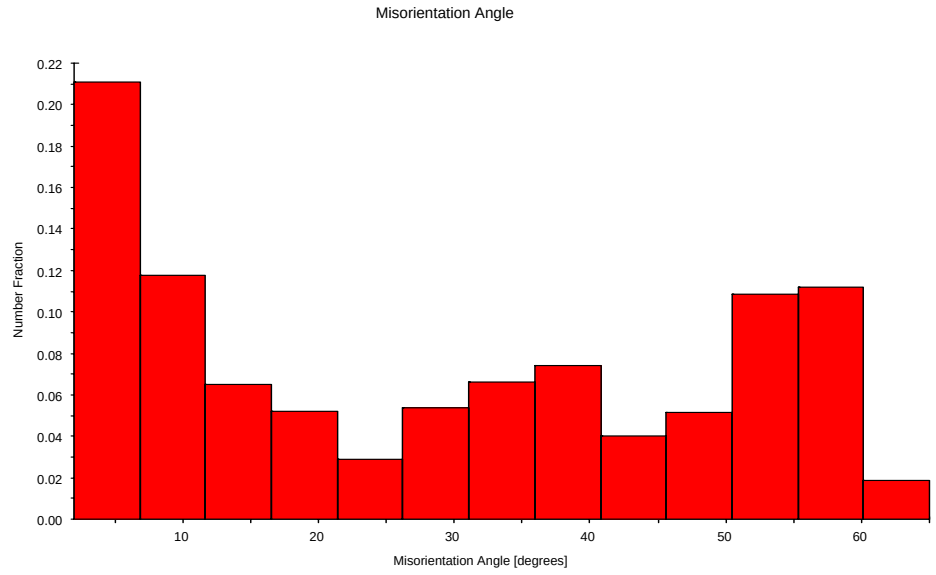
Misorientation Angle
Number Fraction
0.22
0.20
0.18
0.16
0.14
0.12
0.10
0.08
0.06
0.04
0.02
0.00
10
20
30
40
50
60
Misorientation Angle [degrees]

b)

c)

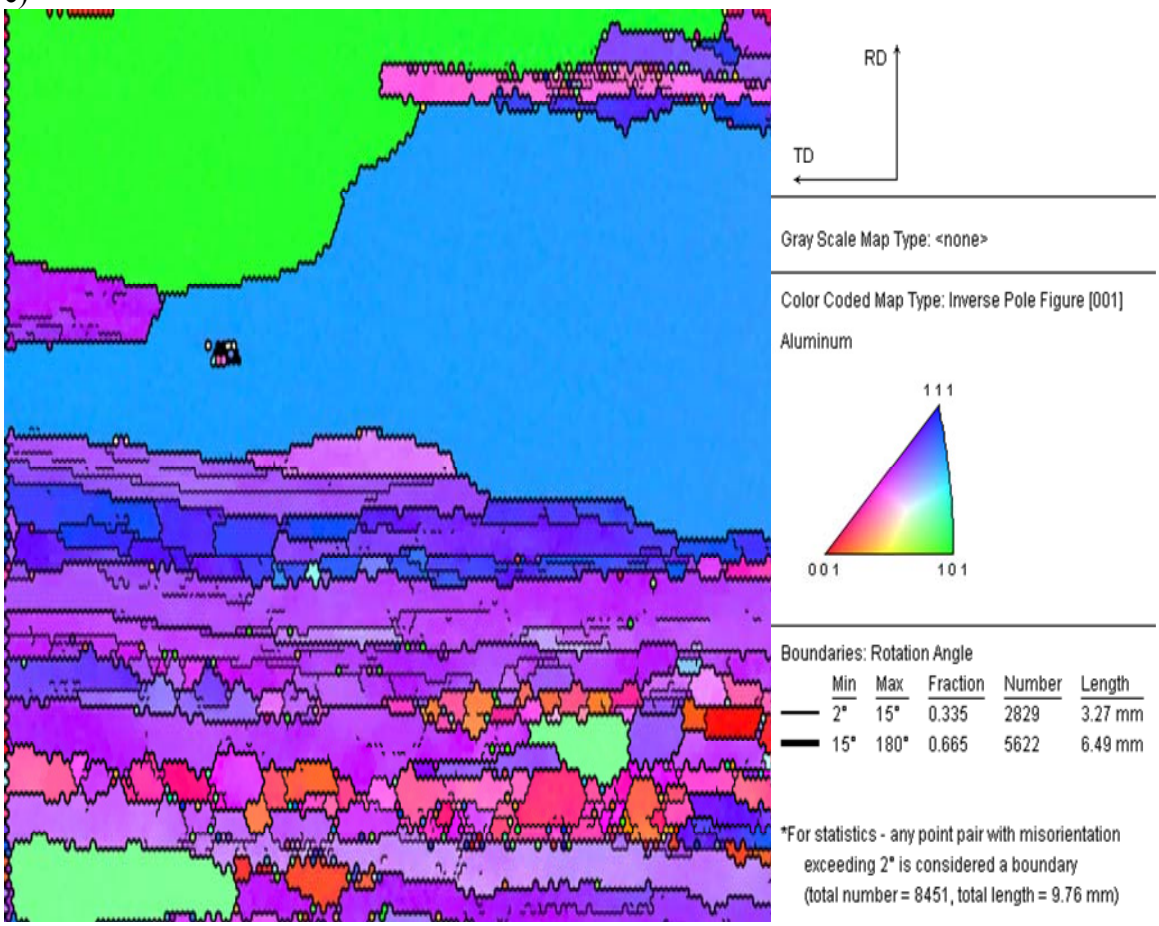

OIM results for AR plate: a) Pole Figure showing texture b) Distribution of misorientation angles c) Inversed Pole Figure (IPF) showing grain and subgrain boundaries (2-15 degrees)

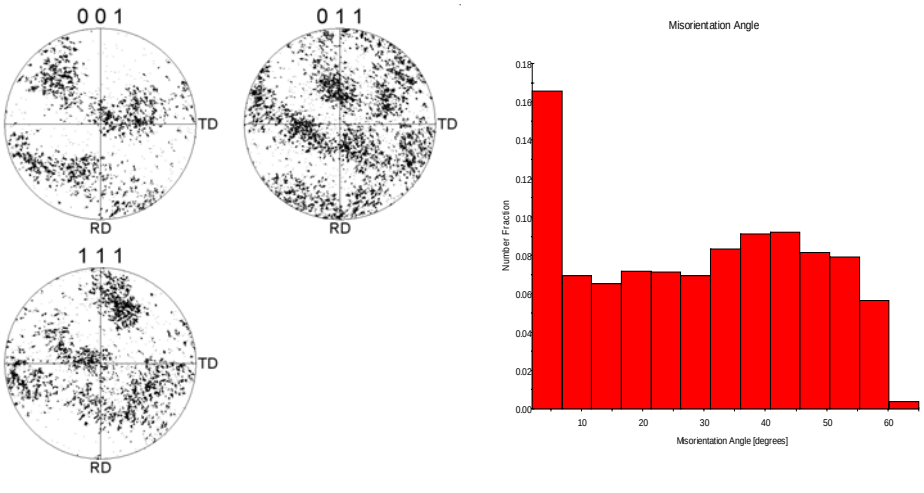

a)

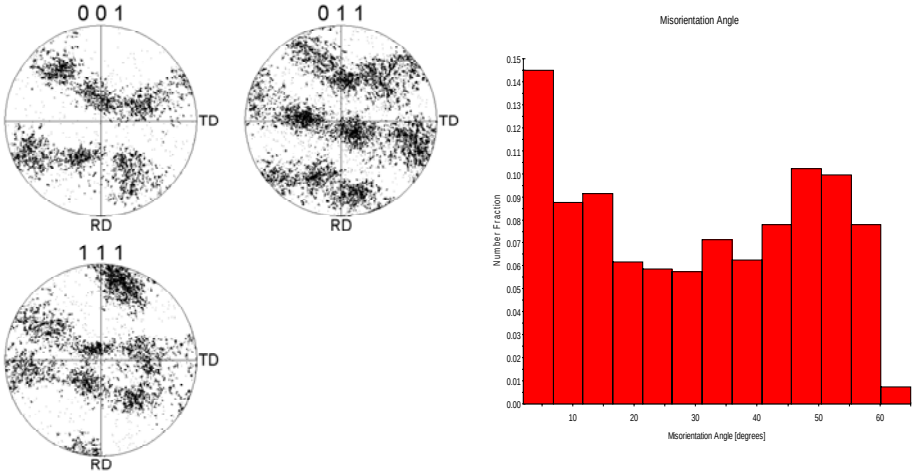

b)

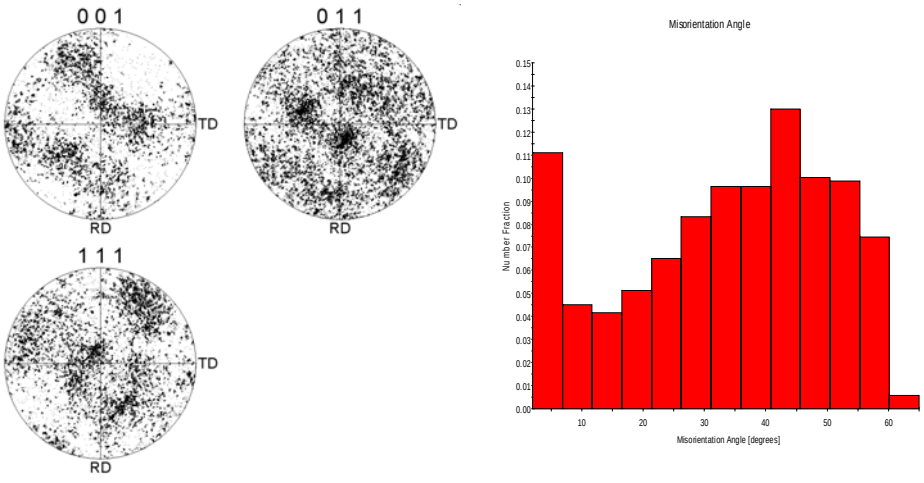

c)

PF and misorientation angle representations for FSP locations a) toward surface b) mid-thickness c) toward bottom of the stir zone in the plate

a)

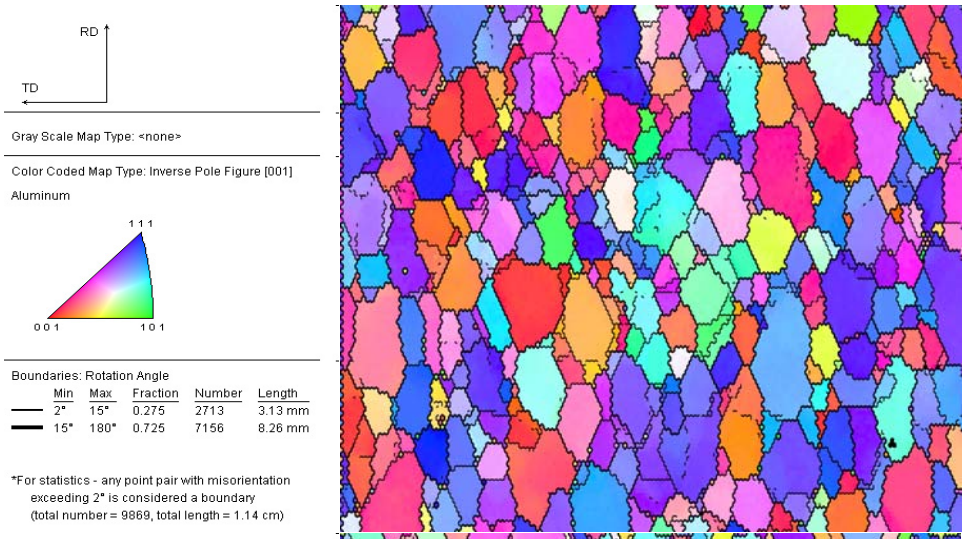

b)

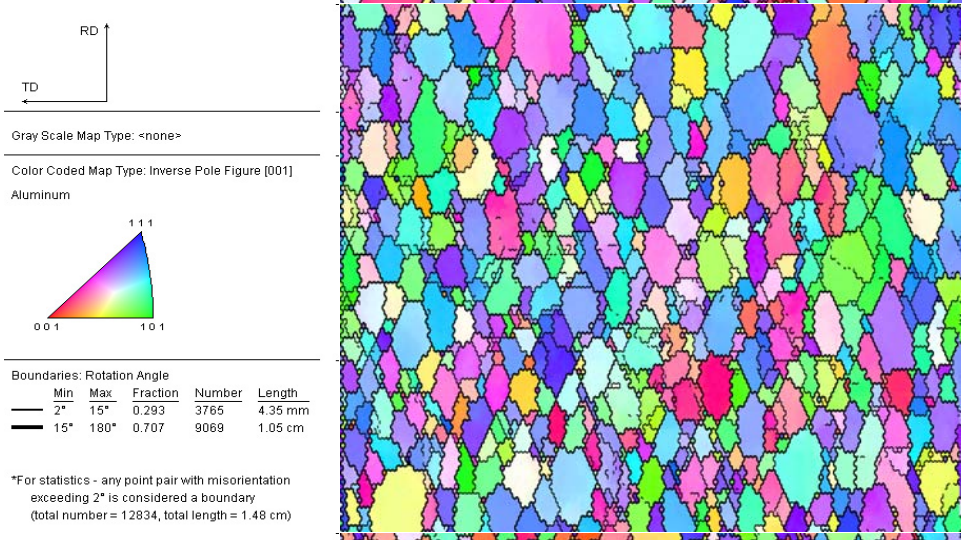

c)

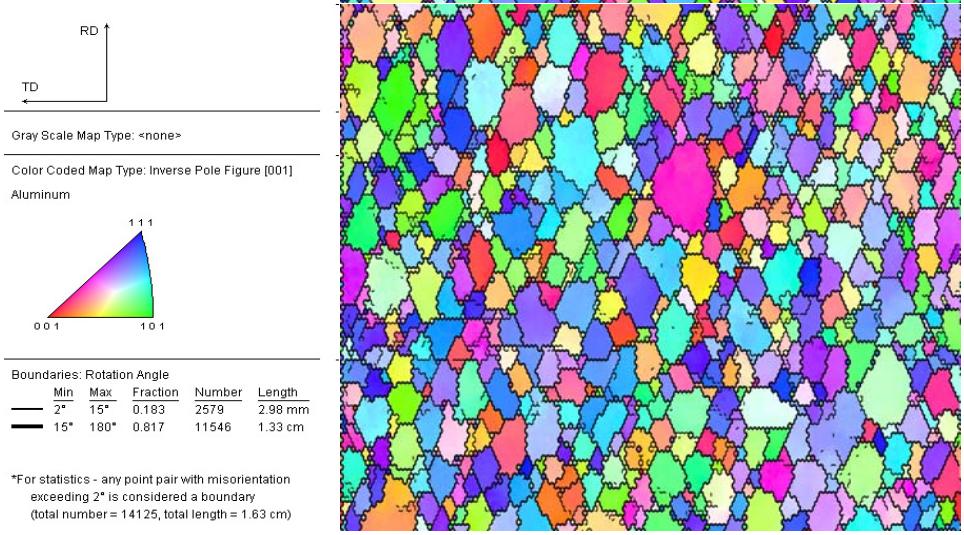

OIM IPF results for FSP plate showing grain and subgrain boundaries (2-15 degrees) variation at locations a) toward surface b) mid-thickness c) toward bottom of the stir zone in the plate.

APPENDIX B. MECHANICAL

A. STRESS-STRAIN PLOTS

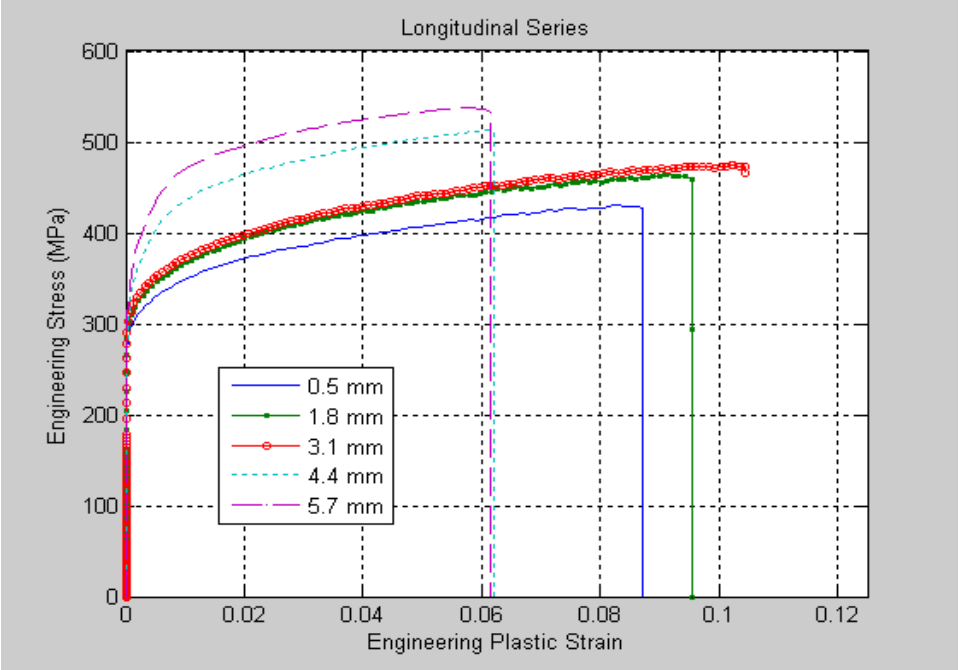

As Rcvd plate-longitudinal series

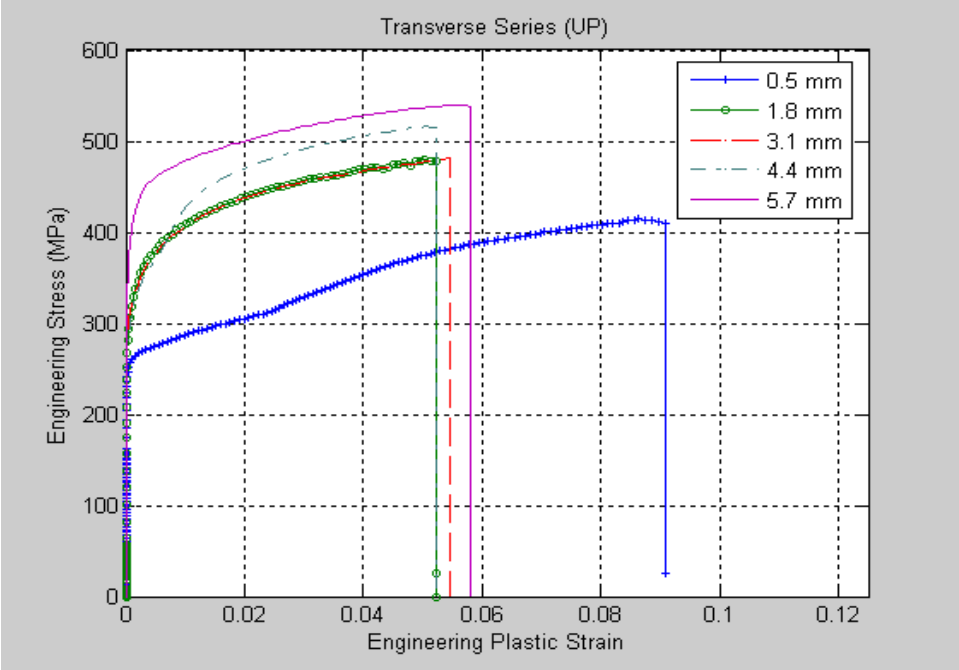

As Rcvd plate-transverse series

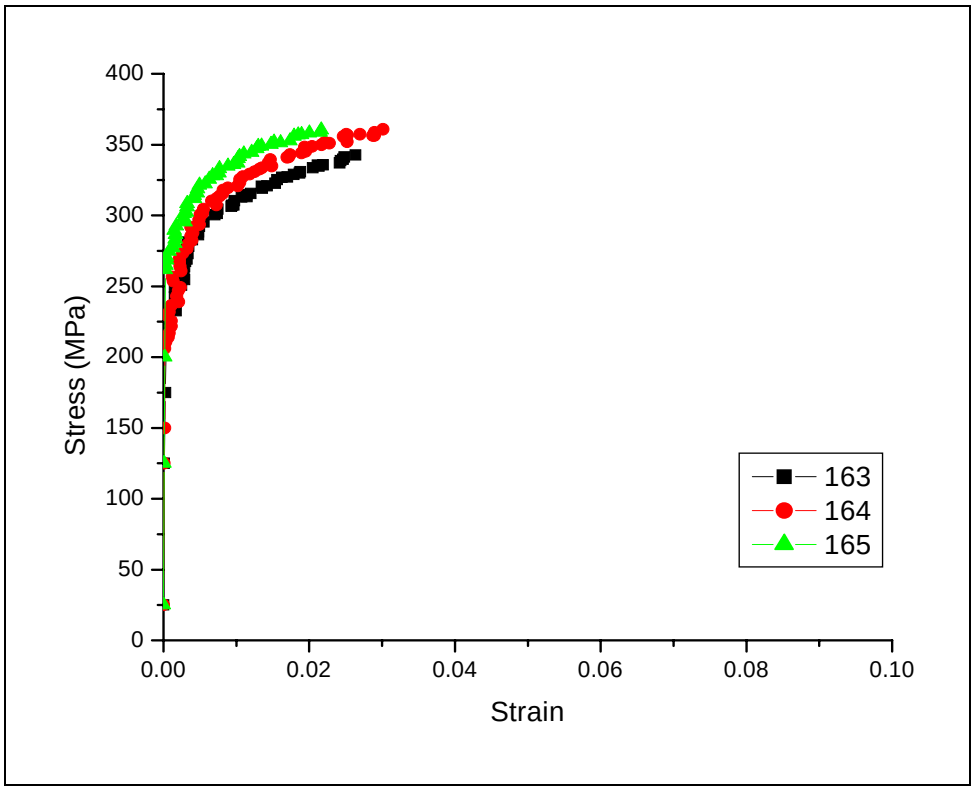

As Rcvd plate-S-T direction

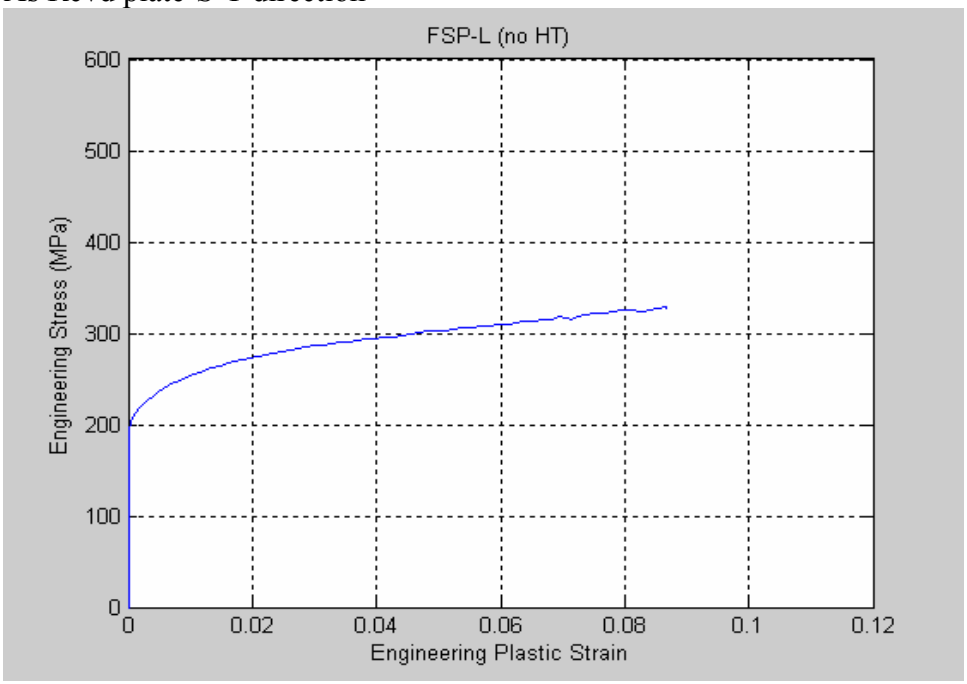

FSP plate without post heat treatment (longitudinal direction)

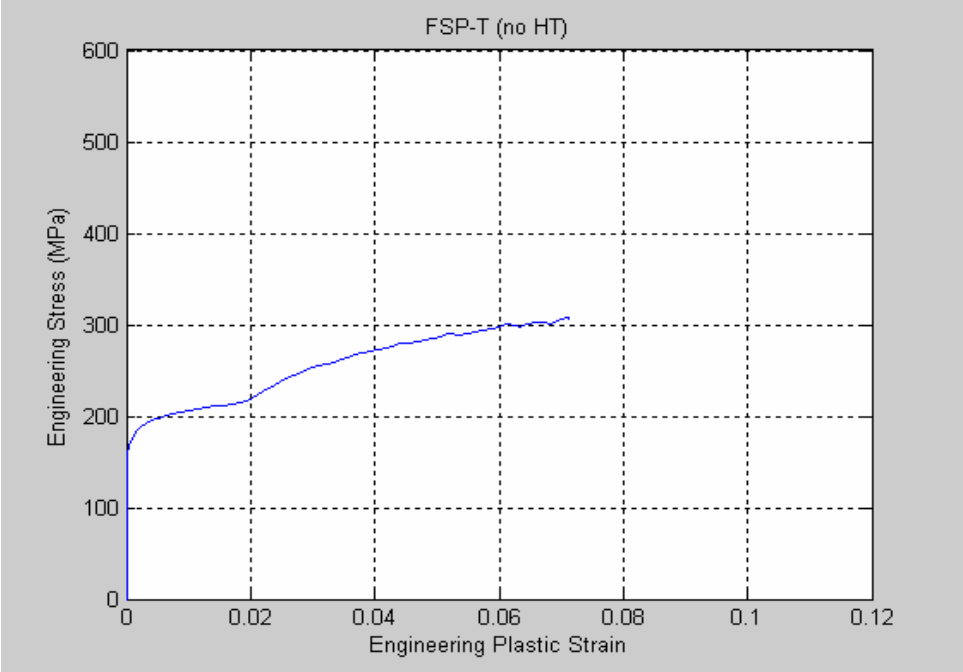

FSP plate without post heat treatment (transverse direction)

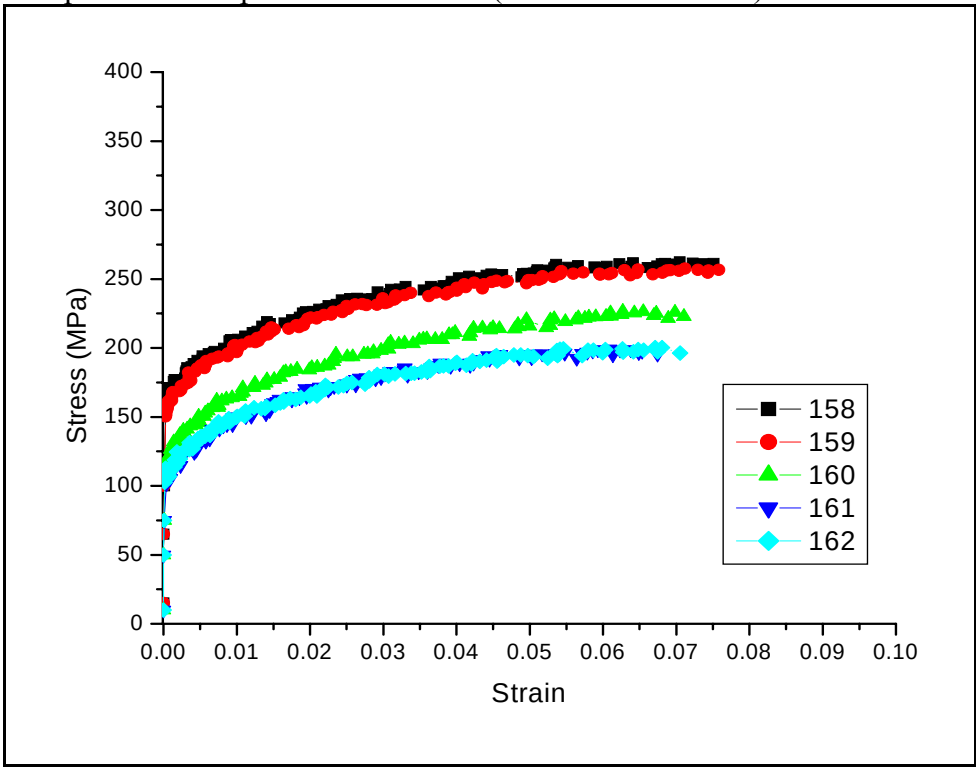

FSP plate without post heat treatment -ST direction

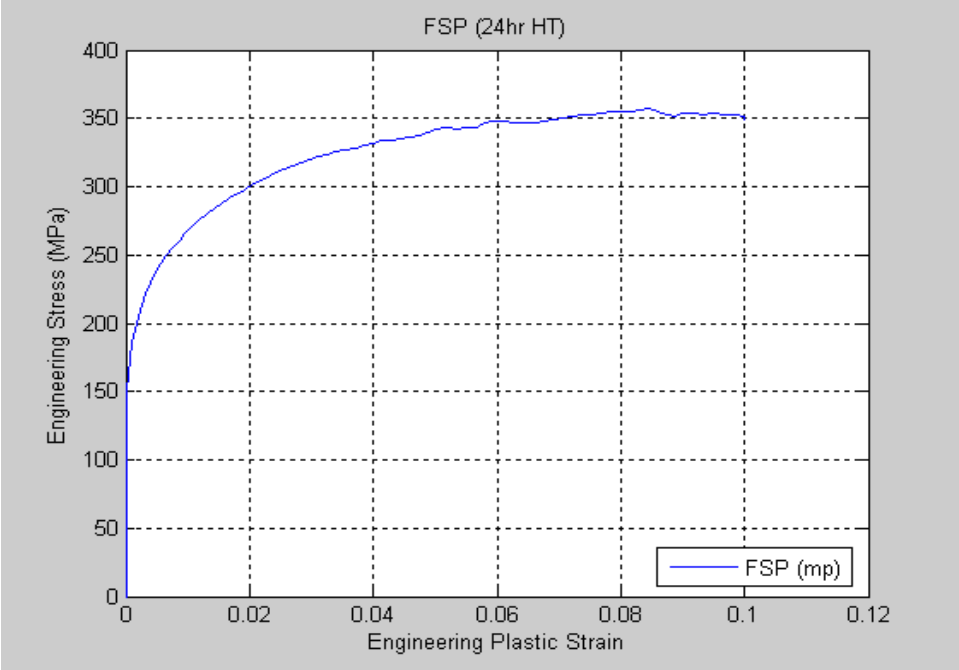

FSP plate with post heat treatment 24hrs @ 148°C (longitudinal direction)

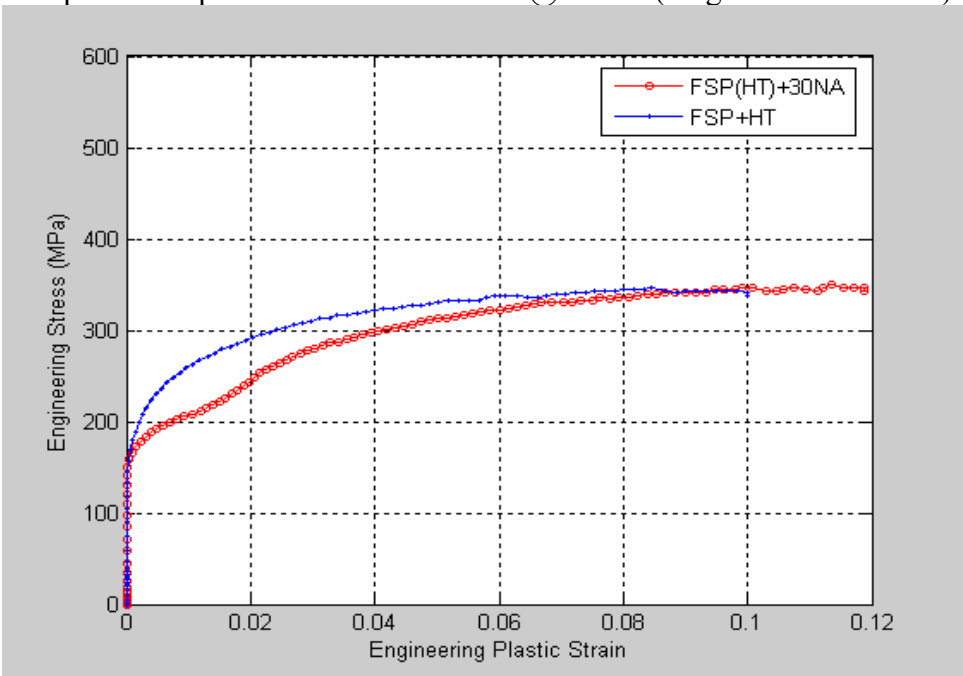

FSP plate with post heat treatment 24hrs @ 148°C (longitudinal direction); one tested following air cooling, second allowed to naturally age for 30 days prior to testing

B. HARDNESS DATA

a)

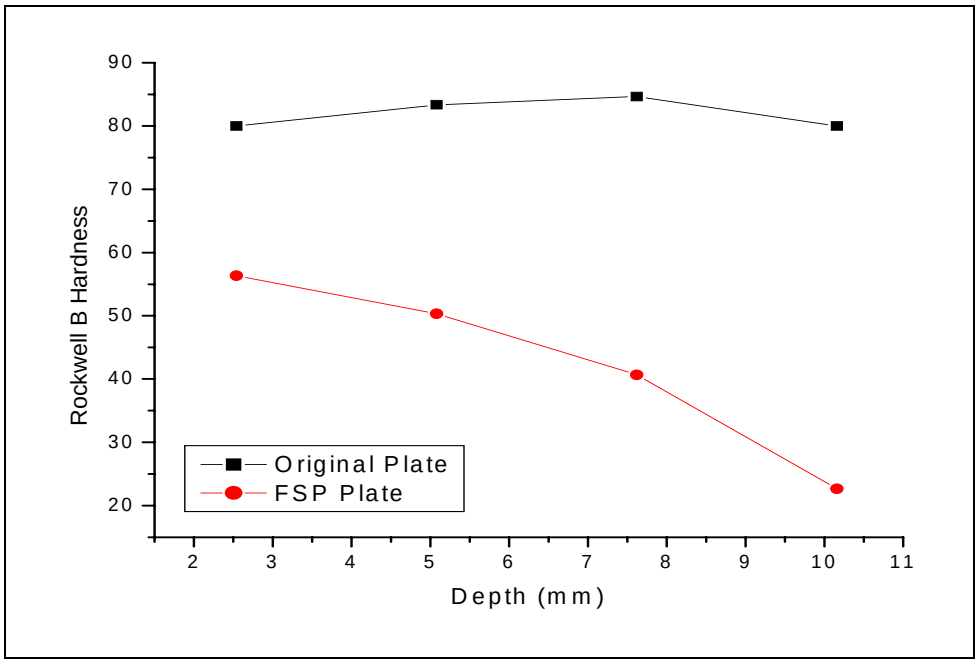

b)

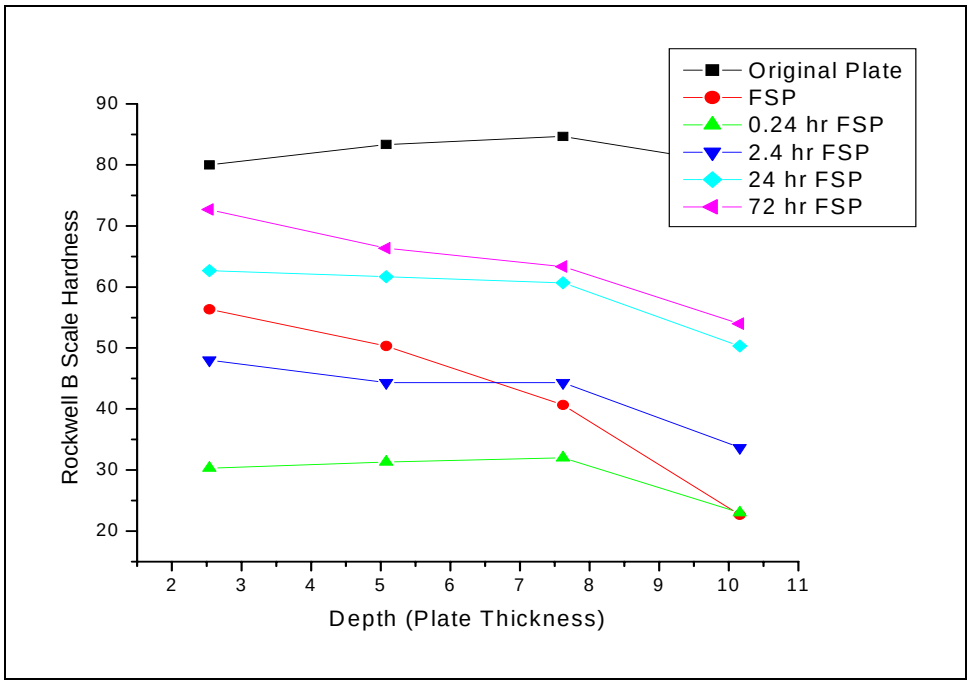

Rockwell B hardness as a function of thru-thickness depth for a) AR & FSP material b) FSP material after heat treatment for various times @ 148^{o}C

C. ANTICLASTIC TESTING

Photograph of anticlastic test specimens after failure @ various loads. From left to right, AR, FSP, and FSP+HT plate

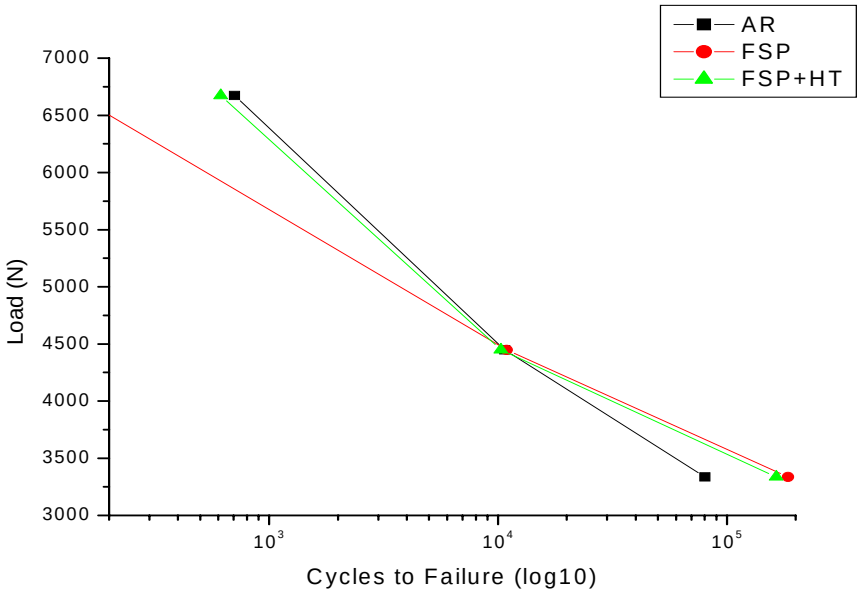

Anticlastic fatigue testing results for AR, FSP, and FSP plus 24hr heat treatment @148^{o}C

APPENDIX C. SEM FRACTOGRAPHS

A. AS RECEIVED TENSILE SAMPLES

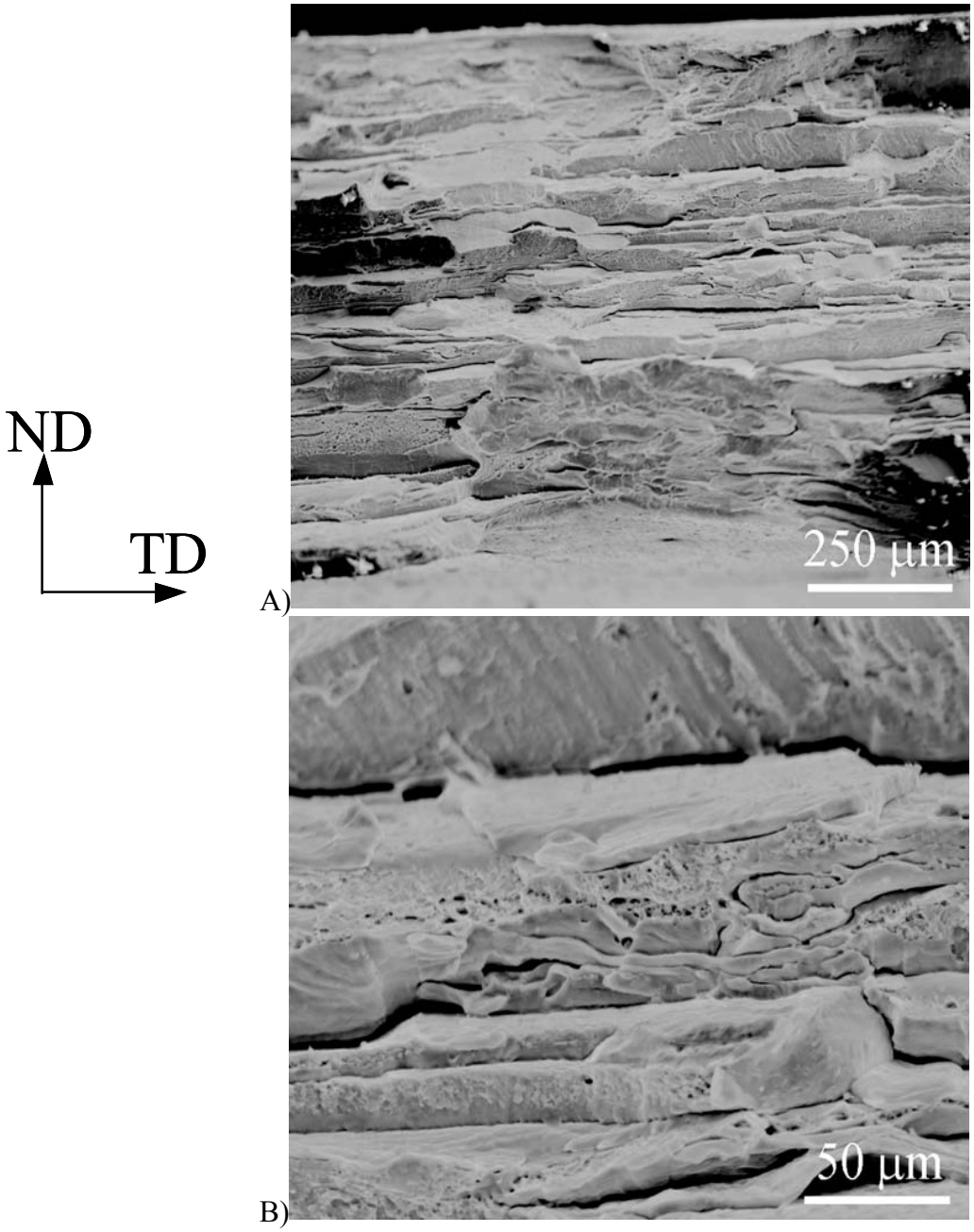

A)

B)

Longitudinal a) 130x b) 500x

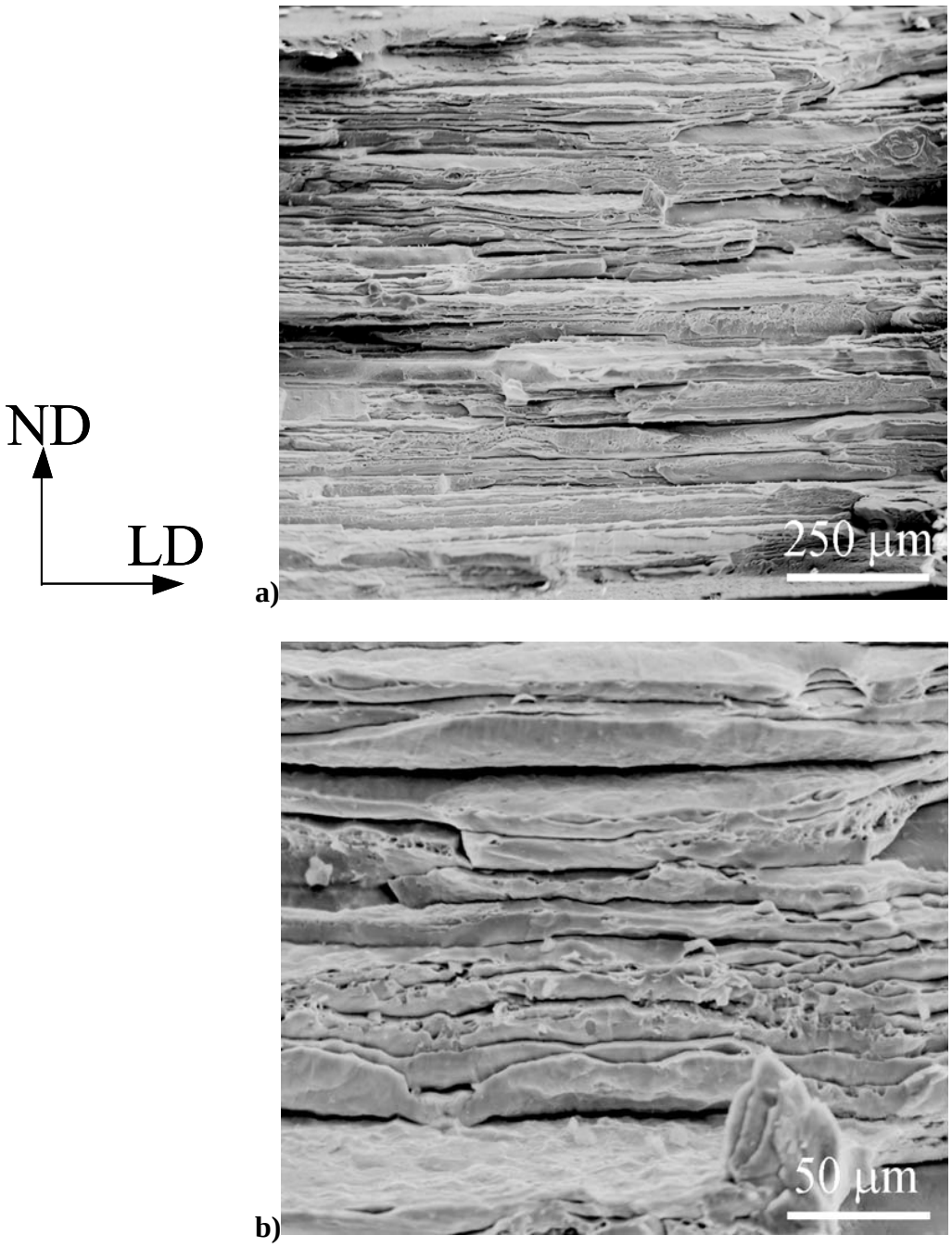

Transverse a) 130x b) 500x

B. AS RECEIVED ANTICLASTIC SPECIMENS

a)

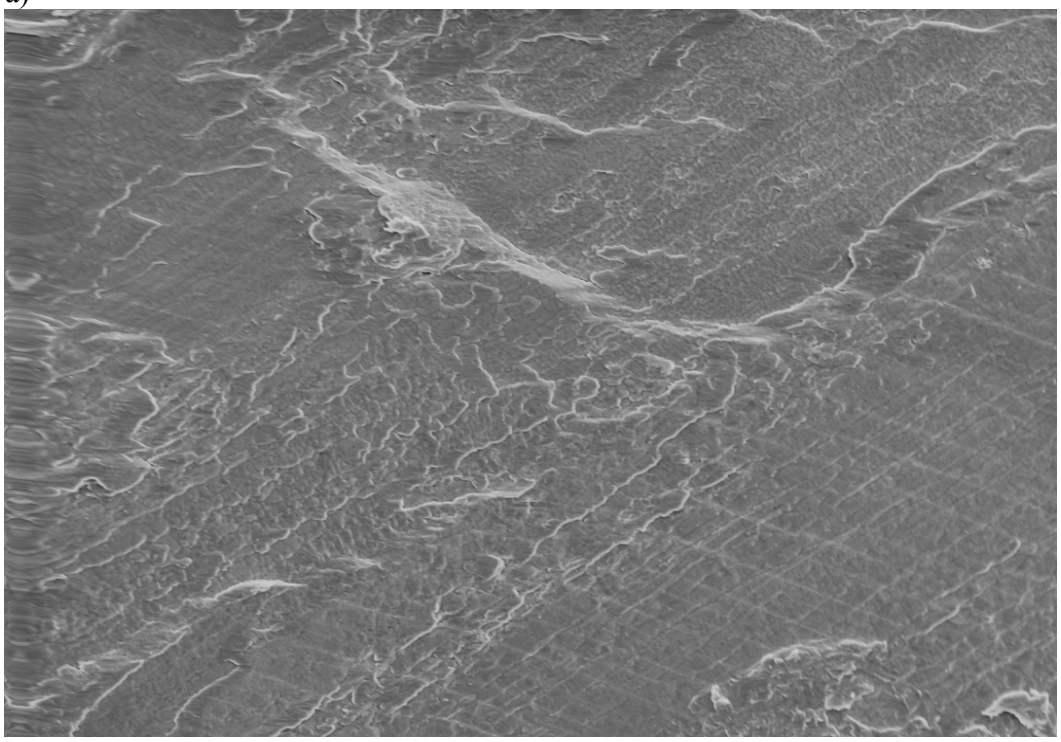

b)

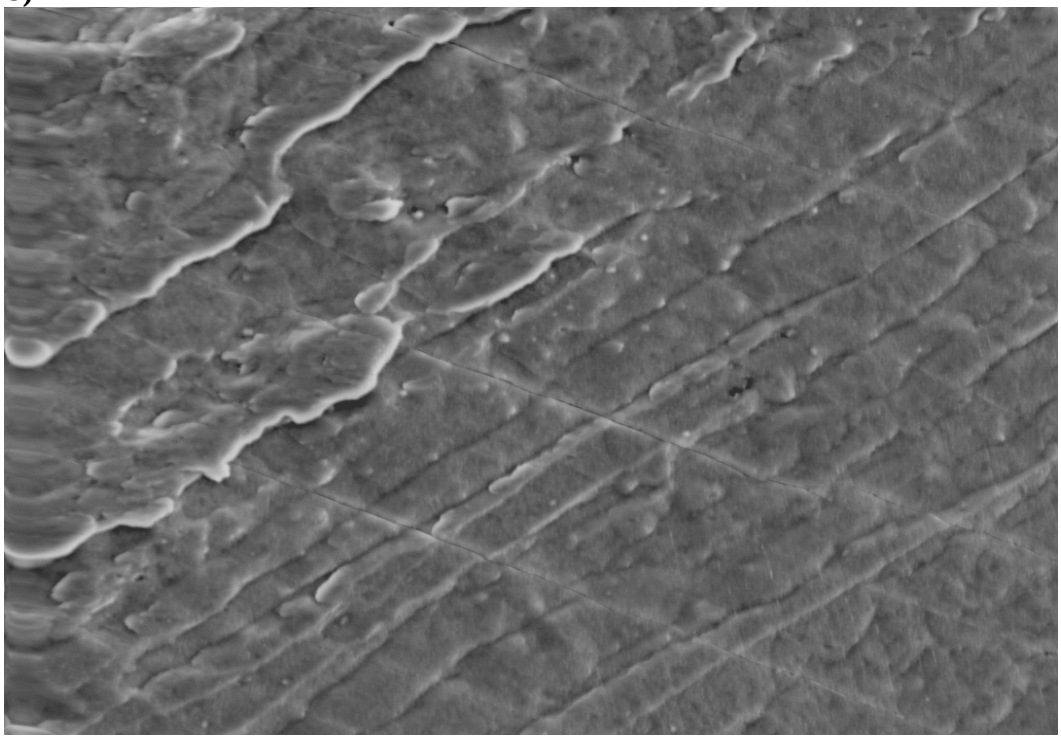

Fracture surface perpendicular to the ND direction a0 130x b) 500x

C. FRICTION STIR PROCESSED TENSILE SAMPLES

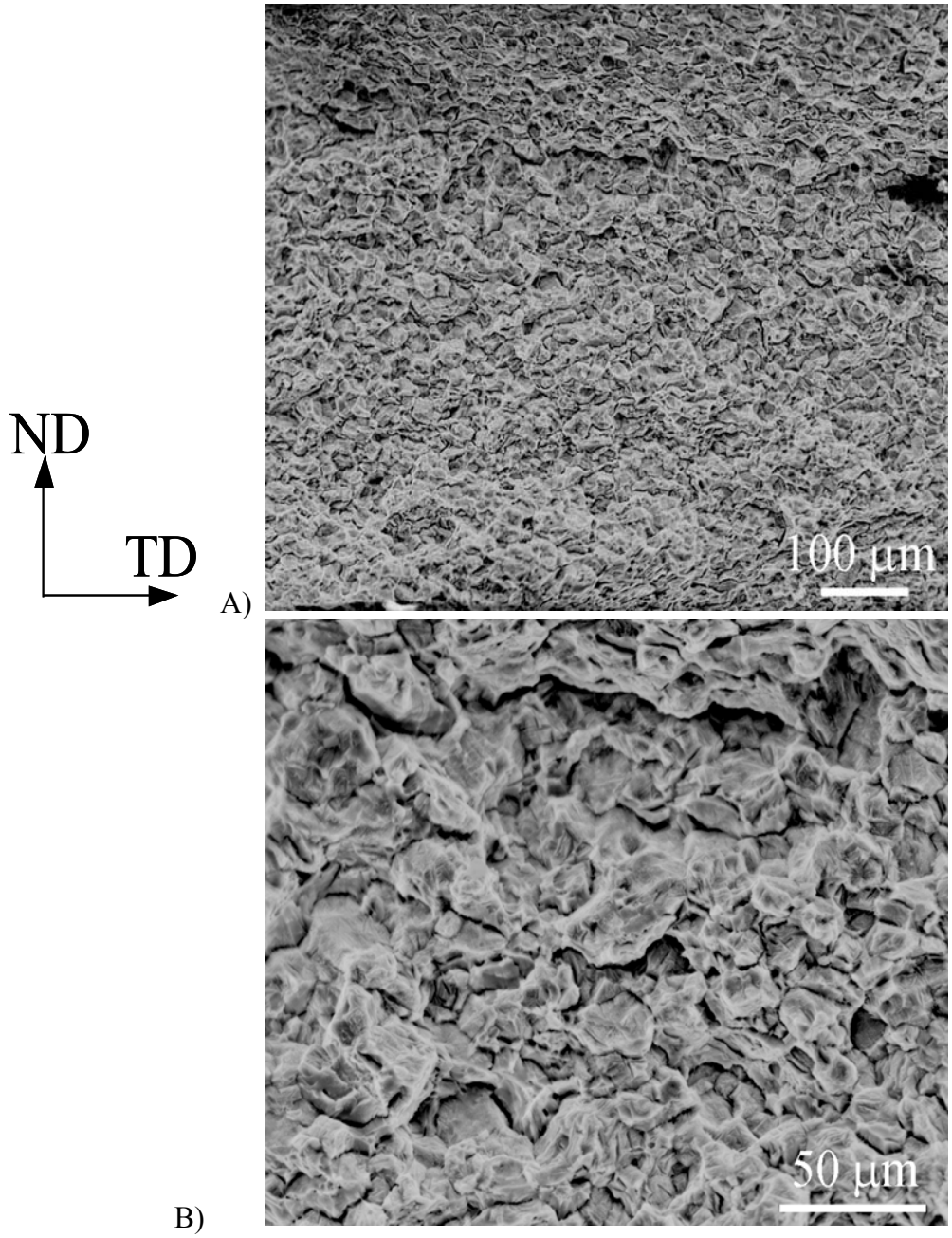

A)

B)

Longitudinal a) 130x b) 500x

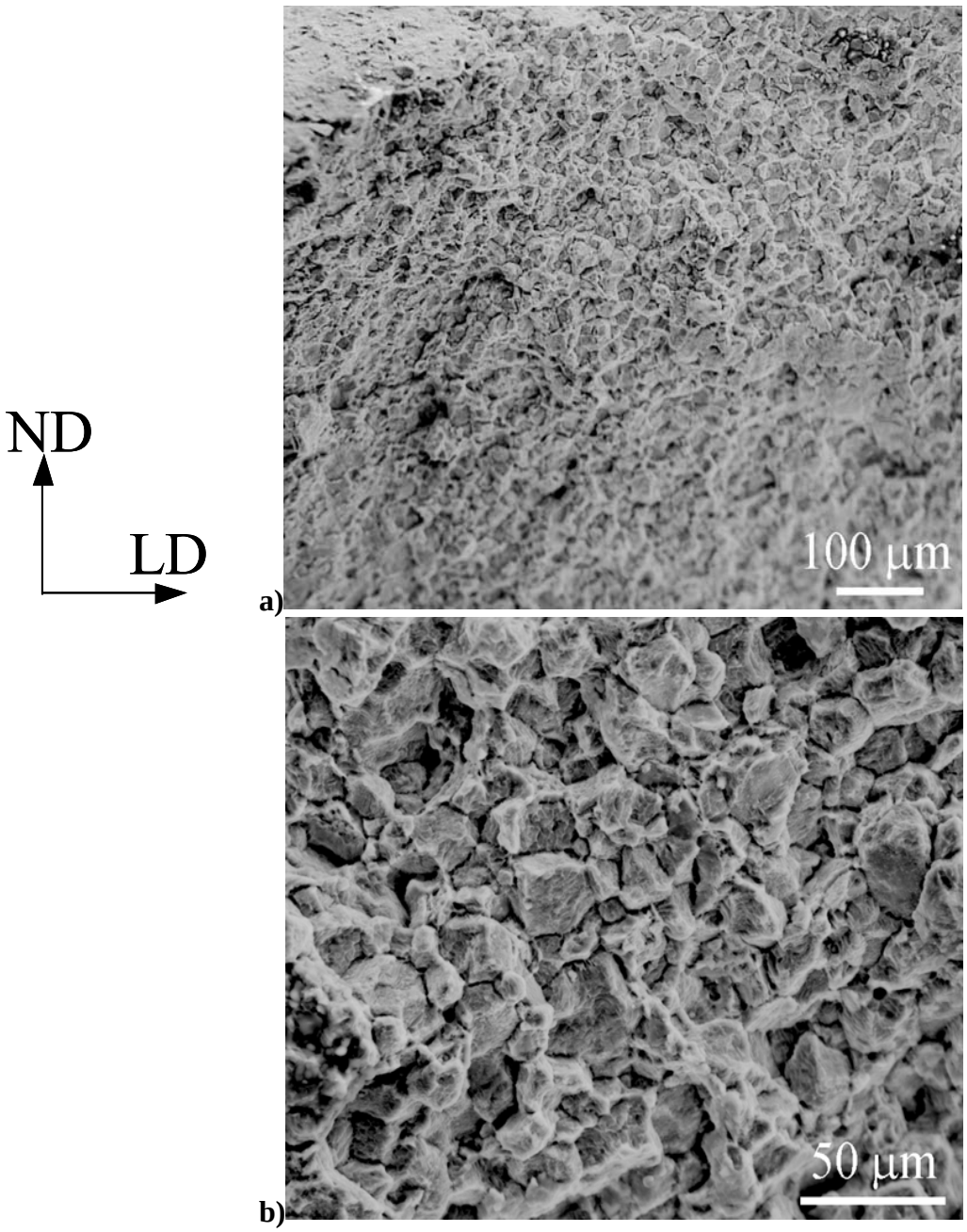

Transverse a) 130x b) 500x

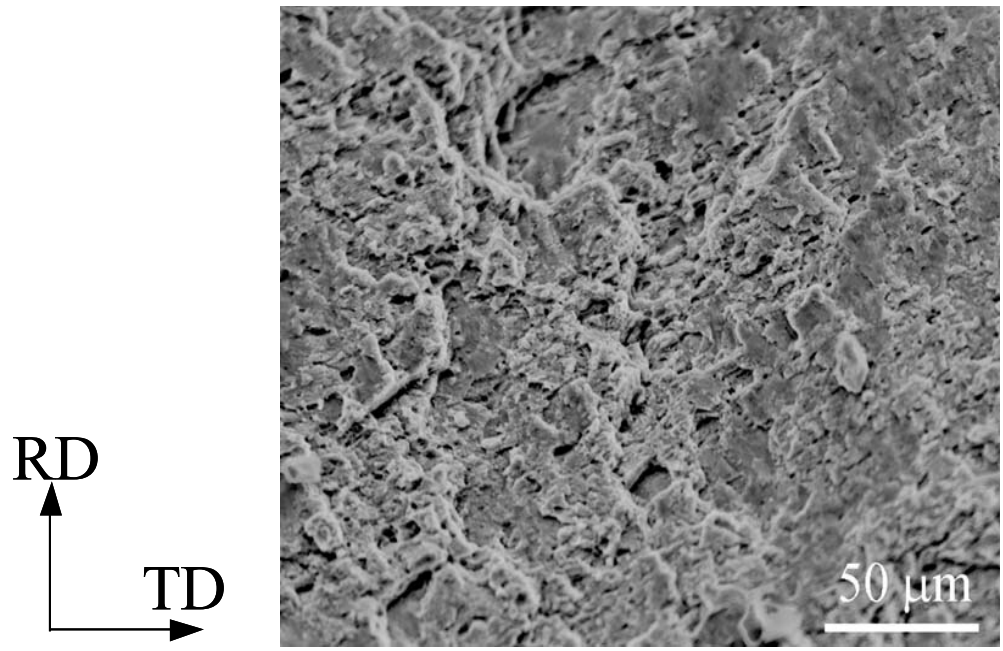

Short transverse at 500x

D. TENSILE SAMPLES OF FSP FOLLOWED BY HEAT TREATMENT

A) 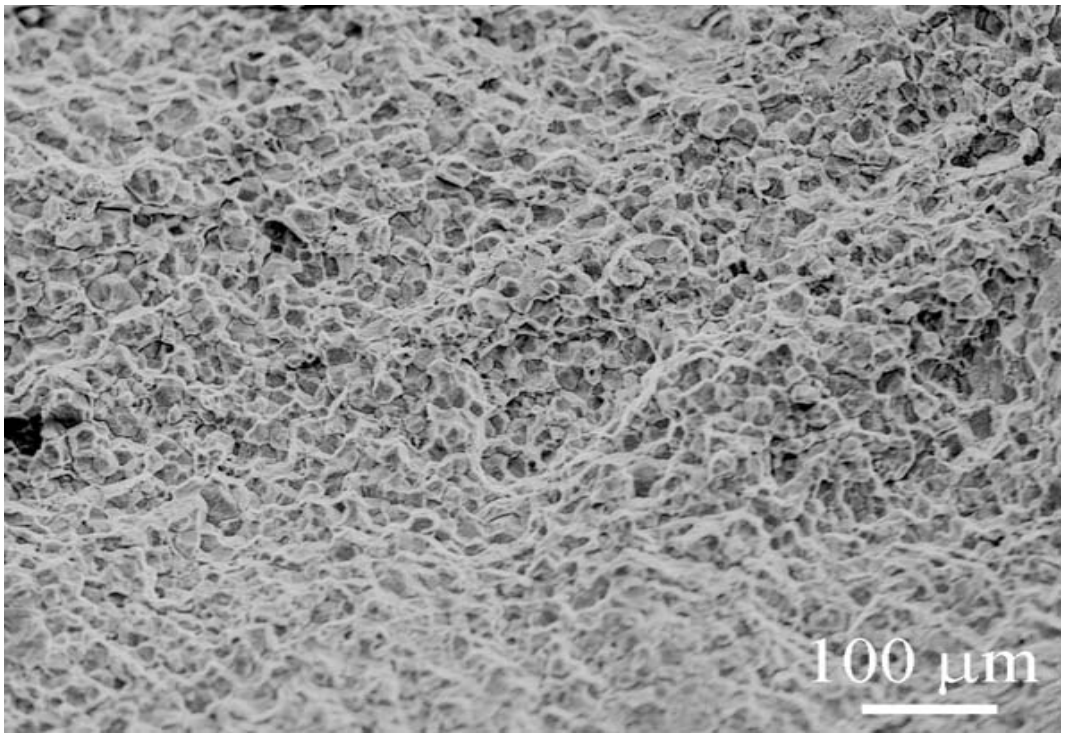

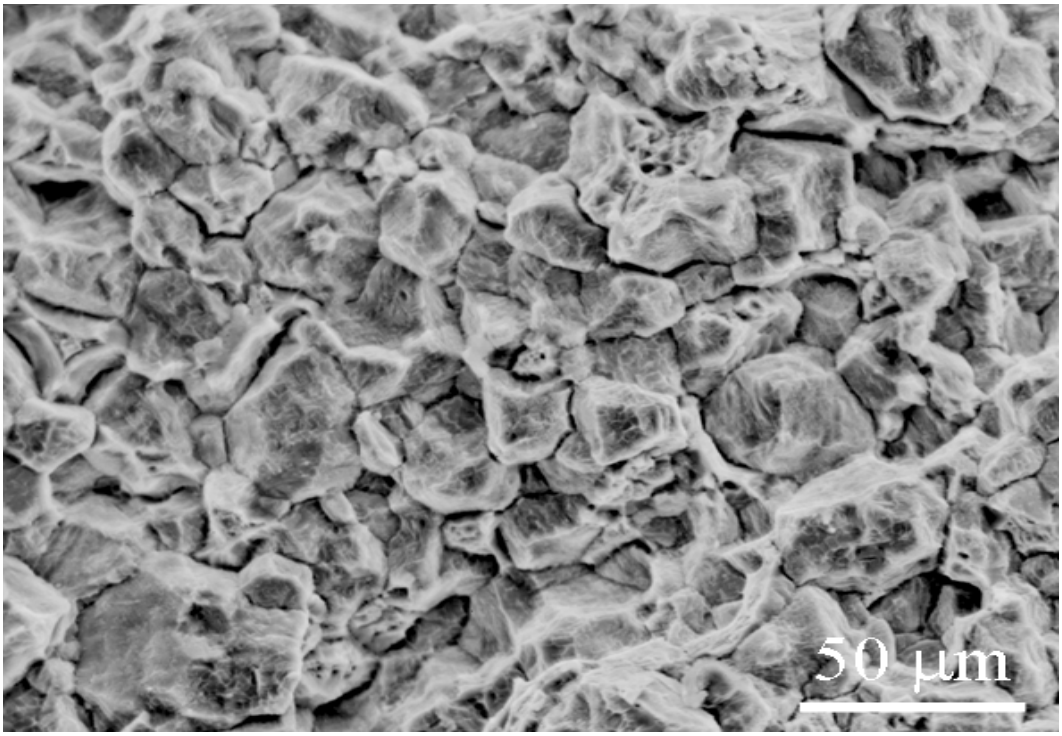

B)

Longitudinal at a) 130x b) 500x

E. ANTICLASTIC FRICTION STIR PROCESSED SPECIMENS

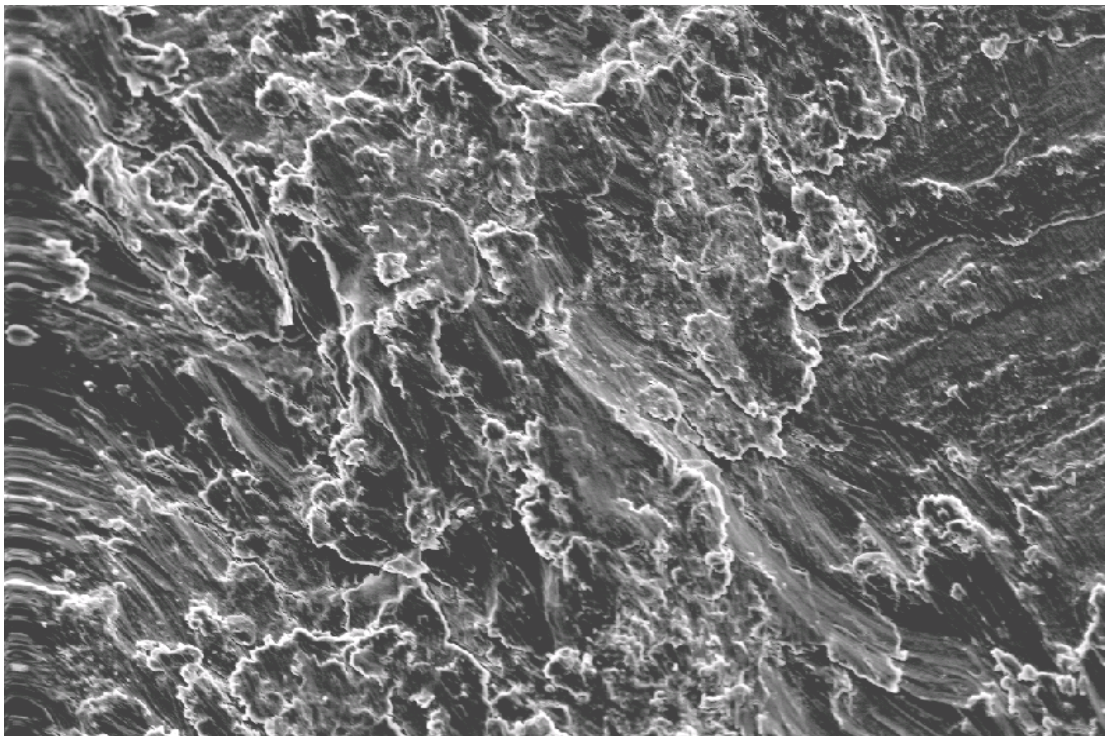

Fracture surface perpendicular to the midplane at 130x

THIS PAGE INTENTIONALLY LEFT BLANK

APPENDIX D. ANTICLASTIC BEND SPECIMEN SPECS

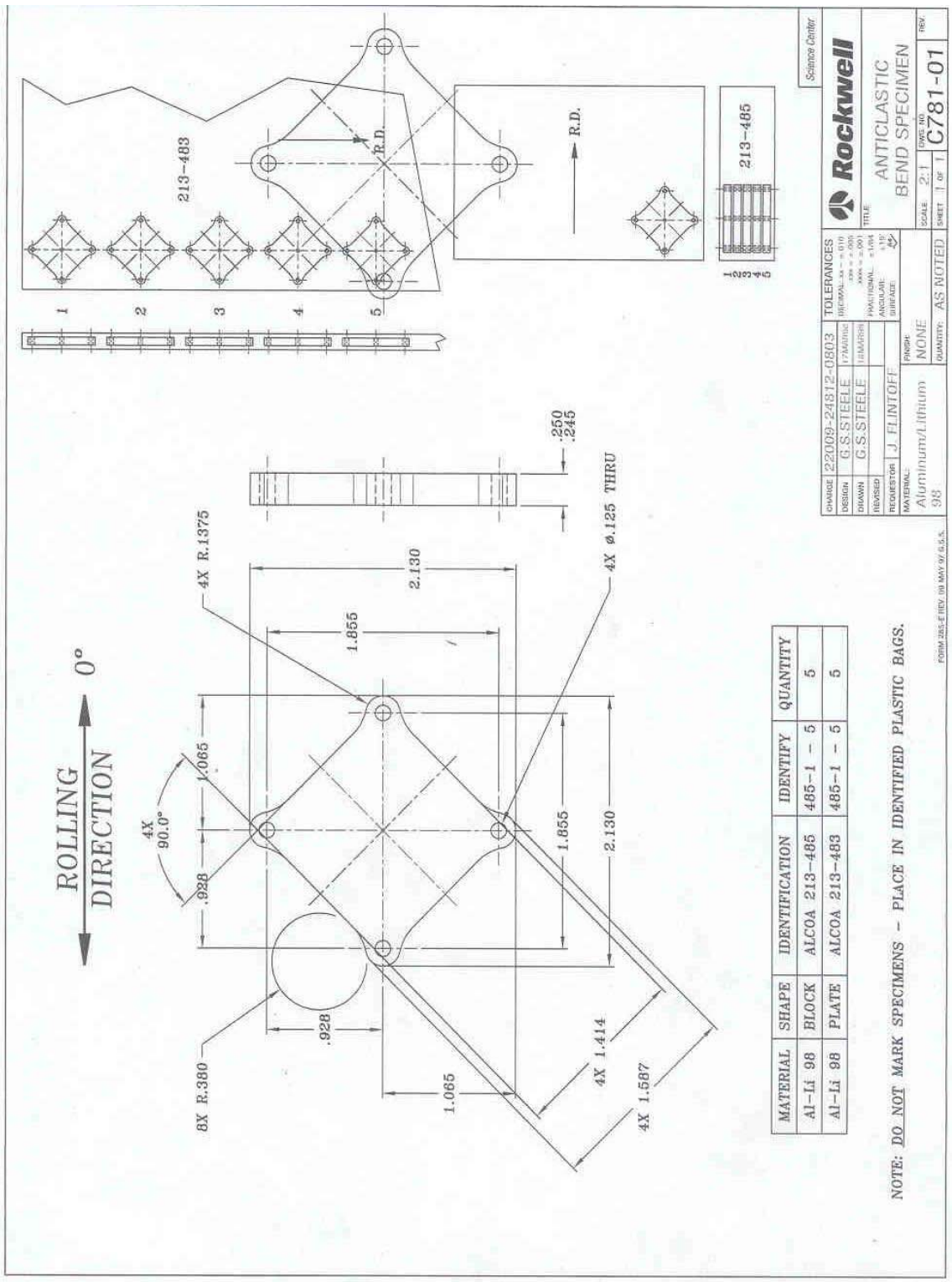

MATERIAL	SHAPE	IDENTIFICATION	IDENTIFY	QUANTITY
Al-Li 98	BLOCK	ALCOA 213-485	485-1 - 5	5
Al-Li 98	PLATE	ALCOA 213-483	485-1 - 5	5

THIS PAGE INTENTIONALLY LEFT BLANK

LIST OF REFERENCES

1. Lynch, S.P., Shekhter, A., Moutsos, S., Winkelman, G.B., "Challenges in Developing High Performance Al-Li Alloys", MAT-2003.
2. Ramesh, J., "Aluminum Lithium Alloy", ASM International Conference 1990, Aluminum Lithium Proceedings.
3. Noble, B., Bray, S.E., *Acta Mater*., vol. 46, pp. 6163-6171, 1998.
4. Flower, M.H., Gregson, P.J., *Mater. Sci. Technol.*, vol. 3, pp. 81, 1987.
5. Gable, B.M., Sontos, A.A., Starke Jr., E.A.., *J. of Light Metals*, vol. 2, pp. 65-75, 2002.
6. Williams, D.B., *Aluminum Lithium Alloys,* pp. 90-100, 1981.
7. Sanders Jr., T.H., *Aluminum Lithium Alloys,* pp. 63-67, 1981.
8. Sanders Jr., T.H., Starke Jr., E.A., *Aluminum Lithium Alloys II,* pp. 1-15, 1984.
9. Kertz, J.E., Gouma, P.I., Buchheit, R.G., *Metallurgical and Materials Trans. A*, vol. 32A, pp. 2561-2573, 2001.
10. Csontos, A.A., Starke Jr, E.A., *Metallurgical and Materials Trans. A*, vol. 31A, pp. 1965-1976, 2000.
11. Cho, K.K., Chung, Y.H., Lee, C.W., Kwun, S.I., Shin, M.C., *Scripta Mat.,* vol. 40 pp. 651-657, 1999.
12. Prasad, N.E., Prasad, K.S., Kamat, S.V., Malakondaiah, G., *Eng. Fracture Mechanics,* vol. 51, pp. 87-96, 1995.
13. Babel, H., Parrish, C., Sankaran, K.K., "Al-Li Alloys in Aerospace Products", AEROMAT 2005.
14. Jata, K.V., Semiatin, S.L., *Scripta Mater.,* vol. 43, pp. 743-749, 2000.
15. Mishra, R.S., Ma Z.Y., "Friction Stir Welding and Processing", *Materials Science and Eng. R,* [Article in Press].
16. Ohishi, K., McNelley, T.R, *Metallurgical and Materials Trans. A*, vol. 35A, pp. 2951, 2004.
17. Yoshimura, R., Konno, T.J., Abe, E., Hiraga, K, *Acta Mater.,* vol. 51, pp. 4251-4266, 2003.
18. Yoshimura, R., Konno, T.J., Abe, E., Hiraga, K, *Acta Mater.,* vol. 51, pp. 2891-2903, 2003.
19. Fonda, R.w., Bingert, J.F., Colligan, K.J., *Scripta Mater.,* vol. 51, pp. 243-248, 2004.
20. Costas, L.P., Marshall, R.P., *Trans. Metal. Soc.* AIME, vol. 224, 1962, pp. 970-974.

21. Chen, D.L, Chaturvedi, M.C., *Metal. Mater. Trans.*, vol. 32A, pp. 2729-2741, 2001.

22. Schneider, J.A., Nunes Jr, A.C., *Metallurgical and Materials Trans. B*, vol. 35B, pp. 777-783, 2004.

23. Mahoney, M.W., Rhoades C.G., Flintoff, J.G., Spurling, R.A., Bingel, W.H., *Metallurgical and Materials Trans. A*, vol. 29, pp. 1955, 1998.

24. Fonda, R.W., Bingert, J.F., *Metallurgical and Materials Trans. A*, vol. 35A, pp. 1487-1499, 2004.

25. Williams, R.A., MS Thesis, "A Microstructural and Mechanical Property Correlation of Friction Stir Processed Nickel Aluminum Bronze", Naval Postgraduate School, Monterey, CA, Sep 2004.

26. Jata, K.V., Panchanadeewaran S., Vasudevan, A.K., *Material Science and Eng.,* vol. A257, pp. 37-46, 1998.

27. Subramanian, P.R., Nirmalan, N.V., Young, L.M., Sudkamp, P., Larsen, M., Dupree, P.L., Shukla, A.K., *Friction Stir Welding and Processing II,* TMS, pp.235-242, 2003.

28. Salem, H., Reynolds, A., Lyons, J., *Lightweight Alloys for Aerospace Application,* pp. 141-150, TMS 2001.

INITIAL DISTRIBUTION LIST

1. Defense Technical Information Center
   Ft. Belvoir, VA

2. Dudley Knox Library
   Naval Postgraduate School
   Monterey, CA

3. Professor Terry McNelley
   Naval Postgraduate School
   Dept. of Mechanical and Astronautical Engineering
   Monterey, CA

4. Professor Anthony J. Healey
   Naval Postgraduate School
   Dept. of Mechanical and Astronautical Engineering
   Monterey, CA

5. CDR William Plott
   Naval Postgraduate School
   Dept. of Mechanical and Astronautical Engineering
   Monterey, CA

6. Murray W. Mahoney
   Rockwell Scientific Center
   Thousand Oaks, CA

7. LT Loan O'Brien
   U.S. Coast Guard (G-MRP-3)
   Washington D.C.